



HR Wallingford  
Working with water

UNCLASSIFIED

# Prediction of Ripple Properties in Shelf Seas

Mark 2 Predictor for Time Evolution

Final Technical Report

Prepared for

US Office of Naval Research

Contract No. N00014-04-C-0408

Report TR 154  
Release 2.0  
December 2005

R L Soulsby  
R J S Whitehouse

---

Approved for public release; distribution is unlimited

---



**UNCLASSIFIED**

## **Prediction of Ripple Properties in Shelf Seas**

**Mark 2 Predictor for Time Evolution**

**Final Technical Report**

**Prepared for**

**US Office of Naval Research**

**Contract No. N00014-04-C-0408**

**Richard L Soulsby**

**Richard J S Whitehouse**

**Report TR 154**

**Release 2.0**

**December 2005**

---

**Approved for public release; distribution is unlimited**

---



**UNCLASSIFIED**

<b>REPORT DOCUMENTATION PAGE</b>				<i>Form Approved OMB No. 0704-0188</i>	
<small>The public reporting burden for this collection of information is estimated to average 1 hour per response, including the time for reviewing instructions, searching existing data sources, gathering and maintaining the data needed, and completing and reviewing the collection of information. Send comments regarding this burden estimate or any other aspect of this collection of information, including suggestions for reducing the burden, to Department of Defense, Washington Headquarters Services, Directorate for Information Operations and Reports (0704-0188), 1215 Jefferson Davis Highway, Suite 1204, Arlington, VA 22202-4302. Respondents should be aware that notwithstanding any other provision of law, no person shall be subject to any penalty for failing to comply with a collection of information if it does not display a currently valid OMB control number.</small>					
<b>PLEASE DO NOT RETURN YOUR FORM TO THE ABOVE ADDRESS.</b>					
<b>1. REPORT DATE (DD-MM-YYYY)</b>		<b>2. REPORT TYPE</b>		<b>3. DATES COVERED (From - To)</b>	
<b>4. TITLE AND SUBTITLE</b>				<b>5a. CONTRACT NUMBER</b>	
				<b>5b. GRANT NUMBER</b>	
				<b>5c. PROGRAM ELEMENT NUMBER</b>	
<b>6. AUTHOR(S)</b>				<b>5d. PROJECT NUMBER</b>	
				<b>5e. TASK NUMBER</b>	
				<b>5f. WORK UNIT NUMBER</b>	
<b>7. PERFORMING ORGANIZATION NAME(S) AND ADDRESS(ES)</b>				<b>8. PERFORMING ORGANIZATION REPORT NUMBER</b>	
<b>9. SPONSORING/MONITORING AGENCY NAME(S) AND ADDRESS(ES)</b>				<b>10. SPONSOR/MONITOR'S ACRONYM(S)</b>	
				<b>11. SPONSOR/MONITOR'S REPORT NUMBER(S)</b>	
<b>12. DISTRIBUTION/AVAILABILITY STATEMENT</b>					
<b>13. SUPPLEMENTARY NOTES</b>					
<b>14. ABSTRACT</b>					
<b>15. SUBJECT TERMS</b>					
<b>16. SECURITY CLASSIFICATION OF:</b>			<b>17. LIMITATION OF ABSTRACT</b>	<b>18. NUMBER OF PAGES</b>	<b>19a. NAME OF RESPONSIBLE PERSON</b>
a. REPORT	b. ABSTRACT	c. THIS PAGE			<b>19b. TELEPHONE NUMBER (Include area code)</b>

## INSTRUCTIONS FOR COMPLETING SF 298

**1. REPORT DATE.** Full publication date, including day, month, if available. Must cite at least the year and be Year 2000 compliant, e.g. 30-06-1998; xx-06-1998; xx-xx-1998.

**2. REPORT TYPE.** State the type of report, such as final, technical, interim, memorandum, master's thesis, progress, quarterly, research, special, group study, etc.

**3. DATES COVERED.** Indicate the time during which the work was performed and the report was written, e.g., Jun 1997 - Jun 1998; 1-10 Jun 1996; May - Nov 1998; Nov 1998.

**4. TITLE.** Enter title and subtitle with volume number and part number, if applicable. On classified documents, enter the title classification in parentheses.

**5a. CONTRACT NUMBER.** Enter all contract numbers as they appear in the report, e.g. F33615-86-C-5169.

**5b. GRANT NUMBER.** Enter all grant numbers as they appear in the report, e.g. AFOSR-82-1234.

**5c. PROGRAM ELEMENT NUMBER.** Enter all program element numbers as they appear in the report, e.g. 61101A.

**5d. PROJECT NUMBER.** Enter all project numbers as they appear in the report, e.g. 1F665702D1257; ILIR.

**5e. TASK NUMBER.** Enter all task numbers as they appear in the report, e.g. 05; RF0330201; T4112.

**5f. WORK UNIT NUMBER.** Enter all work unit numbers as they appear in the report, e.g. 001; AFAPL30480105.

**6. AUTHOR(S).** Enter name(s) of person(s) responsible for writing the report, performing the research, or credited with the content of the report. The form of entry is the last name, first name, middle initial, and additional qualifiers separated by commas, e.g. Smith, Richard, J, Jr.

**7. PERFORMING ORGANIZATION NAME(S) AND ADDRESS(ES).** Self-explanatory.

**8. PERFORMING ORGANIZATION REPORT NUMBER.** Enter all unique alphanumeric report numbers assigned by the performing organization, e.g. BRL-1234; AFWL-TR-85-4017-Vol-21-PT-2.

**9. SPONSORING/MONITORING AGENCY NAME(S) AND ADDRESS(ES).** Enter the name and address of the organization(s) financially responsible for and monitoring the work.

**10. SPONSOR/MONITOR'S ACRONYM(S).** Enter, if available, e.g. BRL, ARDEC, NADC.

**11. SPONSOR/MONITOR'S REPORT NUMBER(S).** Enter report number as assigned by the sponsoring/monitoring agency, if available, e.g. BRL-TR-829; -215.

**12. DISTRIBUTION/AVAILABILITY STATEMENT.** Use agency-mandated availability statements to indicate the public availability or distribution limitations of the report. If additional limitations/ restrictions or special markings are indicated, follow agency authorization procedures, e.g. RD/FRD, PROPIN, ITAR, etc. Include copyright information.

**13. SUPPLEMENTARY NOTES.** Enter information not included elsewhere such as: prepared in cooperation with; translation of; report supersedes; old edition number, etc.

**14. ABSTRACT.** A brief (approximately 200 words) factual summary of the most significant information.

**15. SUBJECT TERMS.** Key words or phrases identifying major concepts in the report.

**16. SECURITY CLASSIFICATION.** Enter security classification in accordance with security classification regulations, e.g. U, C, S, etc. If this form contains classified information, stamp classification level on the top and bottom of this page.

**17. LIMITATION OF ABSTRACT.** This block must be completed to assign a distribution limitation to the abstract. Enter UU (Unclassified Unlimited) or SAR (Same as Report). An entry in this block is necessary if the abstract is to be limited.

## Document Information

<b>Project</b>	Prediction of Ripple Properties in Shelf Seas
<b>Report title</b>	Mark 2 Predictor for Time Evolution
<b>Client</b>	U.S. Office of Naval Research
<b>ONR Contract No.</b>	N00014-04-C-0408
<b>Client Representative</b>	Dr Thomas Drake
<b>Project No.</b>	CBR3689
<b>Report No.</b>	TR 154
<b>Doc. ref.</b>	TR154-Shelf Seas Mark 2 predictor_rel2-0.doc
<b>Project Manager</b>	Prof. Richard Soulsby
<b>Project Sponsor</b>	Dr Richard Whitehouse

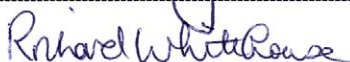
## Document History

Date	Release	Prepared	Approved	Authorised	Notes
12/12/05	1.0	rls	rjsw	kap	
11/01/06	2.0	rls	rjsw	kap	Modifications to text and tables

Prepared



Approved



Authorised



© HR Wallingford Limited  
Howbery Park  
Wallingford  
Oxon, OX10 8BA, UK

*This report is a contribution to research generally and it would be imprudent for third parties to rely on it in specific applications without first checking its suitability. Various sections of this report rely on data supplied by or drawn from third party sources. HR Wallingford accepts no liability for loss or damage suffered by the client or third parties as a result of errors or inaccuracies in such third party data. HR Wallingford will only accept responsibility for the use of its material in specific projects where it has been engaged to advise upon a specific commission and given the opportunity to express a view on the reliability of the material for the particular applications.*



# *Summary*

## Prediction of Ripple Properties in Shelf Seas

### Mark 2 Predictor for Time Evolution

R L Soulsby  
RJS Whitehouse

Report TR 154  
December 2005

The work under this contract is intended to transfer European data and thinking about sea-bed ripples into the ONR Ripples DRI project. The goal was to develop a generic predictor for bedform existence, growth/decay, height and spacing, and temporal variability at a sandy seabed location (ripples in currents, waves, and waves-plus-currents) as a function of: sediment characteristics, water depth, wave and current forcing, biological effects and time history of these processes. The work made use of existing data, through data mining and interpretation, to underpin the ongoing SAX99 and SAX04 collection of specific sediment-acoustic data within the ONR program. The present report relates to Phase 2 of the project, in which a time-evolving predictor for ripple properties generated by waves and/or currents (including bio-degradation) was developed. Information on the derivation of the predictor and some example applications are included. The Mark 2 Time-evolving Ripple Predictor is given in step-by-step algorithmic form in Appendix A. The predictor has been implemented and tested in an Excel spreadsheet “Ripple evolution waves + currents V2.0”.





## *Acknowledgements*

We gratefully acknowledge the contributions made by our European colleagues Maarten Kleinhans, Bart Grasmeijer, Carl Amos, John Harris, Leo van Rijn and Enrico Foti. Dr Maarten Kleinhans kindly made his data-set of bedform properties available to us, in the context of the EU collaborative project SANDPIT (Contract No. EVK3-2001-00056). The data-base compiled during the EU collaborative research project SEDMOC (Contract No. MAS3-CT97-0115) was also made use of. We thank Dr Tom O'Donoghue and Dr Jeff Doucette of Aberdeen University for providing their data, and for useful discussions in re-analysing their data. We gratefully acknowledge the useful discussions with colleagues in the ONR SAX04 and Ripples DRI programs during the SAX04 Workshop in Seattle (May 2005) and the Acoustics 2005 Conference in Bath, UK (September 2005). We are grateful to Dr Christine Lauchlan and Dr Sanne Niemann, both working at HR Wallingford, for undertaking part of the computational work in the present project. This work was funded by the US Office of Naval Research under Contract No. N0014-04-C-0408 within the Ripples DRI Program.



# Contents

<i>Document Information</i>	<i>i</i>
<i>Summary</i>	<i>iii</i>
<i>Acknowledgements</i>	<i>v</i>
<i>Contents</i>	<i>vii</i>

1.	Introduction .....	1
1.1	ONR BAA 04-001 .....	1
1.2	Objectives .....	1
2.	Behaviour of sea-bed ripples .....	3
2.1	Ripples and sonar propagation .....	3
2.2	Results from phase 1 .....	4
2.3	Results from phase 2 .....	4
3.	Existing ripple geometry predictors .....	7
3.1	Existing ripple predictors .....	7
3.2	Existing data-sets used to test predictors .....	7
3.3	Intercomparison of intercomparisons .....	7
3.4	Analysis of existing wave-ripple predictors .....	8
4.	New wave-only ripple geometry predictor .....	13
4.1	New wave-ripple equilibrium predictor .....	13
4.2	Time-evolution of wave-ripples .....	14
5.	New current-only ripple geometry predictor .....	17
5.1	New current-ripple equilibrium predictor .....	17
5.2	Time-evolution of current-ripples .....	19
6.	Time-stepping procedure .....	21
6.1	Aims of predictor .....	21
6.2	Basic equations .....	21
6.3	Waves versus current ripples .....	22
6.4	Bio-degradation of ripples .....	22
6.5	Solution method .....	23
7.	Tests of Mark 2 ripple predictor against data .....	25
7.1	Test with wave-ripple evolution data .....	25
7.2	Test with current-ripple “tidal” data .....	26
7.3	Test with wave-plus-current synthetic data .....	26
7.4	Test with wave-plus-current field data .....	27
8.	Conclusions .....	31
9.	References .....	33

## Contents continued

### Tables

Table 1	Ripple prediction methods and intercomparison papers
Table 2	Data-sets used in intercomparisons of methods against data
Table 3	Predictors tested in listed intercomparison papers
Table 4	Data-sets used in listed intercomparison papers
Table 5	Correspondence between predictors tested and data-sets used in listed intercomparison papers
Table 6	Prediction methods for ripple height and wavelength, and their functional dependence
Table 7	References to prediction methods in text books and comparison papers (see Table 6 for codes)

### Figures

Figure 1	Wave ripple predictors with 1000 randomly distributed input parameters, plotted against $\Delta$ . (a) height $\eta$ , (b) length $\lambda$
Figure 2	Wave ripple predictors with 1000 randomly distributed input parameters, plotted against $\Psi$ . (a) height $\eta$ , (b) length $\lambda$
Figure 3	Wave ripple predictors with 1000 randomly distributed input parameters, plotted against $\theta'_w$ . (a) height $\eta$ , (b) length $\lambda$
Figure 4	Non-dimensional ripple height $\eta/A$ from data-base plotted against (a) $\Delta$ , (b) $\Psi$ , (c) $\theta'_w$
Figure 5	Non-dimensional ripple wavelength $\lambda/A$ from data-base plotted against (a) $\Delta$ , (b) $\Psi$ , (c) $\theta'_w$
Figure 6	Test of Eq (4.2, 3) for ripple height against data-base
Figure 7	Test of Eq (4.1) for ripple wavelength against data-base
Figure 8	Comparison of new formula for equilibrium ripple height (Eq 5.6a), and B93 (modified) formula (Eq 5.4), against data from various sources
Figure 9	Comparison of new formula for equilibrium ripple wavelength (Eq 5.6b), and B93 (modified) formula (Eq 5.5), against data from various sources
Figure 10	Bedform existence plot by Van den Berg and Van Gelder (1989), with proposed wash-out and sheet-flow limits superimposed. Additional new data from B93, WMS98 and DSPW03 is included
Figure 11	Comparison of Eq (5.16) for ripple height evolution with the data of B93 for (a) $d_{50} = 0.095\text{mm}$ , (b) $d_{50} = 0.238\text{mm}$ ; and of Eq (5.17) for ripple wavelength evolution for (c) $d_{50} = 0.095\text{mm}$ , (d) $d_{50} = 0.238\text{mm}$
Figure 12	Test of wave-ripple predictor against Doucette and O'Donoghue (2005) experiments – ripple growth and decay
Figure 13	Test of wave-ripple predictor against Doucette and O'Donoghue (2005) experiments – ripple growth and further growth
Figure 14	Test of wave-ripple predictor against three (non-consecutive) Doucette and O'Donoghue (2005) experiments – slow growth; growth from specified initial height, length; decay from specified height, length
Figure 15	Test of current-ripple predictor against Whitehouse et al (1998) reversing-flume tidal experiments
Figure 16	Test of wave-plus-current ripple predictor driven by synthetic wave and current data
Figure 17	Test of wave-plus-current ripple predictor driven by field data from Teignmouth (Whitehouse, 2005)

## *Contents continued*

Figure 18 Test of wave-plus-current ripple predictor driven by Teignmouth data with doubled depths and doubled current speeds

Figure 19 Test of wave-plus-current ripple predictor driven by Teignmouth data with bio-degradation switched ON

### **Appendices**

Appendix A Algorithm for predicting the time-evolution of ripple height, wavelength and orientation in sandy sea-bed sediments under the influence of waves and currents

Appendix B Example input pages to Spreadsheet



# 1. *Introduction*

## 1.1 ONR BAA 04-001

This project has the title “Development of a new marine ripple bedform predictor for application in sandy shelf environments”. It forms part of the Department Research Initiative (DRI), ONR, on Critical Benthic Environmental Processes and Modeling at SAX04 (aka Ripples DRI). It refers to the ONR Long Range BAA 04-001, dated 10 Sep 2003.

## 1.2 OBJECTIVES

The goal was to develop a generic predictor for bedform existence, growth/decay, height and spacing, and temporal variability at a sandy seabed location (ripples in currents, ripples in waves, ripples in waves and currents) as a function of:

- sediment characteristics
- water depth
- wave and current forcing
- biological effects
- time history of the above processes

The research made use of the knowledge of marine sediment transport bedform prediction held by the PIs and accessed in the UK/European framework to the DRI program. Phase 1 of the project made use of existing data, through data mining and interpretation, to underpin the SAX99 and SAX04 collection of specific sediment-acoustic data within the ONR program. A Mark 1 version of the ripple predictor was developed initially based on this existing data. An improved Mark 2 predictor was developed in Phase 2 of the project. The resulting algorithm was delivered for use in the DRI Ripples program as Appendix A of this report.

The project provides predictive tools for the response of ripples to changes in wave and wave-current forcing, including biological degradation.

The present report relates to the Phase 2 objectives, specifically:

- Visit USA, present and discuss Mark 1 predictor, and requirements for Mark 2
- Test Mark 1 ripple predictor with existing US data (e.g. SAX99)
- Receive data from SAX04 experiment
- Test versus SAX04 data, and adapt predictor accordingly
- Add in prediction of rates of growth/decay and migration, and effects of bioturbation and “history effect”
- Delivery of Mark 2 predictor as an algorithm/subroutine
- Publication in scientific literature (subject to ONR approval)

The form of the ripple predictor should be geared to its effect on sonar performance, and written in a form that could be used to give a forecast of the spatial and temporal variations of ripple properties over a sea area, as a function of hydrodynamic and sedimentary input distributions.

There are a number of steps required to develop a ripple predictor of the kind required:

1. Choose or develop an equilibrium wave-generated ripple predictor for ripple height and length
2. Choose or develop an equilibrium current-generated ripple predictor for ripple height and length
3. Devise a method for either combining items 1 and 2, or choosing between them, for combined wave-plus-current conditions
4. Set the equilibrium orientation of the ripples (i.e. the direction of the normal to the ripple crest-lines) as being the direction of the waves or currents depending which is dominant
5. Develop a method of predicting the rate-of-change of wave-ripple geometry as a function of the wave and sediment characteristics
6. Develop an analogous method for the rate-of-change of current-ripple geometry
7. Develop a mathematical method for including biological effects on ripple geometry
8. Combine items 1 to 7 into a single algorithm
9. Test the algorithm against lab and field data.

The above steps are described in detail in Sections 3 to 7 of this report.



## 2. Behaviour of sea-bed ripples

### 2.1 RIPPLES AND SONAR PROPAGATION

The behaviour of ripples (or other types of bedform), as they might affect sonar propagation, can be considered in three stages:

1. Prediction of the *existence* of different types of bedform under different hydrodynamic conditions (waves, currents, water depths) and sedimentary conditions (characteristic grain-sizes, density, mineralogy).
2. Prediction of the characteristic descriptors of ripples *in equilibrium* with the hydrodynamic conditions (i.e. assuming that the conditions have lasted sufficiently long and been sufficiently constant that the ripples have evolved fully).
3. Prediction of the characteristic descriptors of ripples in conditions that are *not in equilibrium*, and how fast they respond (tidally varying currents, wind-driven varying currents, varying waves in storms, biological effects).

Phase 1 of the project delivered items 1 and 2, and Phase 2 delivered item 3.

The term *bedform* is used here to encompass any kind of deviation from a flat bed, of which ripples are the most prevalent, but can also include dunes, mega-ripples, hummocks and sandwaves. We distinguish *ripples* as small-scale bedforms, having spacing of order 1m and heights of order 0.1m, which enhance the penetration of sonar signals into the subsurface. Ripples (and other bedforms) may be *two-dimensional* (2D), in which case the ripple crests form straight or gently waving lines that are very much longer than the wavelength (i.e. spacing perpendicular to the crest-line), or three-dimensional (3D), in which case the shape of an individual ripple can be traced (along the crest-line) for only a short distance. Both 2D and 3D ripples (and bedforms) are encountered on the sea-bed, but their effects on sonar propagation will be different.

We consider the following properties of ripples that might affect sonar propagation:

- height (from trough to crest)
- wavelength (i.e. spacing perpendicular to the crest-lines)
- crest-length (i.e. spacing along the crest-lines)
- orientation (with respect to the North, or sonar source)
- slope with respect to horizontal (as seen by sonar source)
- shape
- grain-size.

For each of these, the effect we might expect ripples to have on sonar are as follows:

- **height:** the sonar reflection or transmission will increase with ripple height
- **spacing:** the interaction between ripples and sonar will depend on the relation between the sonar wavelength (projected onto the bed) and the spacing of the ripples, being strongest if these are matched. This interaction will be stronger if the periodicity of the ripples is “sharp” rather than diffuse
- **crest-length:** long-crested (2D) ripples will have little impact on a sonar beam directed along the crest-line, whereas short-crested (3D) ripples will impact a sonar beam even if it is directed along the (less well-defined) crest-line

- **orientation:** the strength of the interaction will be greatest if the sonar source faces the steepest slopes of the ripples directly (in azimuth), and will be progressively weaker as the ripple crest-lines form greater azimuths with the sonar direction
- **slope:** the reflection/transmission of sonar will be greatest if the face of the ripple-slopes is most nearly perpendicular to the sonar beam. Hence asymmetric current-induced ripples will have greatest interaction with a sonar beam directed towards the steeper (lee) slope, and a weaker interaction if it is directed towards the gentler (stoss) slope
- **shape:** reflection or transmission will be greater for sharp-crested (triangular) cross-section ripples than for round-crested ripples
- **grain-size:** the absorption or reflection of sonar will also depend on the grain-size of the sediment forming the ripple.

In this project the main attention was focussed on the most important geometric ripple properties: height, wavelength and orientation. We use the words ripple length, wavelength, and spacing interchangeably.

## 2.2 RESULTS FROM PHASE 1

The following tasks were achieved in Phase 1 of the Research.

HR Wallingford:

- held discussions with European (and other) ripples researchers
- compiled a digest of European source publications
- assembled a data-base of ripple geometries (height, wavelength) and driving conditions (waves, currents, sediment size)
- performed statistical analyses of ripple heights and wavelengths
- produced a graphical display in Excel of colour-coded bed elevations and cross-sections in two horizontal dimensions
- presented the results in HR Wallingford Report TR150 (Soulsby and Whitehouse, 2005).

Further details of all these results were presented in HR Wallingford Report TR150, and are not repeated here.

## 2.3 RESULTS FROM PHASE 2

At the end of Phase 2, the following tasks have been achieved.

HR Wallingford:

- devised new formulas to predict equilibrium *wave-generated* ripple heights and lengths as functions of wave and sediment properties, and tested them against the data-base
- presented results at a SAX04 workshop in Seattle (May 2005)
- submitted an abstract (now accepted) to ICCE conference, San Diego Sept 2006, on wave-generated ripple predictor (copied to ONR)
- devised alternative new formulas for predicting equilibrium *wave-generated* ripples, and used Phase 1 data-base to choose the most successful
- devised new formulas for *current-generated* ripples as functions of current speed and sediment properties, and tested against data-base

- brought together these formulas for *equilibrium* ripple heights and wavelengths (and orientations) to form the “Mark 1” ripple predictor
- assembled information about existing *intercomparisons* of ripple predictors (wave, current and combined) against existing lab and field data-sets, and summarised this in Excel spreadsheets
- produced a pro-forma spreadsheet for collecting SAX04 data from experimenters, and submitted it to ONR
- devised a new method for predicting the *time-development* of ripple heights, wavelengths and orientations
- encapsulated the equilibrium predictors in the time-development model to form the “Mark 2” ripple predictor, as algorithms and an Excel spreadsheet
- added in a term to simulate bio-degradation of ripples
- tested the time-development model for *wave-generated* ripple evolution against an existing time-series of wave data measured by University of Aberdeen (UK) in a laboratory oscillating water tunnel (effectively at full scale), and obtained good agreement
- tested the time-development model for *current-generated* ripple evolution against an existing time-series of ripple observations measured by HR Wallingford for tidally oscillating current speed in a laboratory flume (effectively at full scale), and obtained good agreement
- tested the applicability of the time-development model for *wave-plus-current-generated* ripple evolution against data measured by HR Wallingford off the UK coast (but without ripple observations).

At the end of the present contract we have developed and tested a Mark 2 predictor for the time-evolution of ripple heights, wavelengths and orientations, driven by any time-series of field inputs of waves and currents (e.g. hourly values for several weeks or months) for sand-sized sediments. This predictor has the capability to not only make reasonably accurate predictions of ripple height and wavelength under *steady* wave/current conditions, but also allows the ripples to *grow or decay* at a rate controlled by the wave and current inputs, and with the option of including biological degradation of ripples. Thus for example, if the wave/current conditions decrease below the threshold of motion, the predicted ripples become “frozen” (sometimes called relict ripples, or hysteresis), then re-adjust their height, wavelength and orientation once conditions again become intense enough. Gradual ripple washout by very intense conditions, or decay due to biological processes, are included, with subsequent re-growth when suitable conditions return. We believe this is the first ripple predictor to have all these capabilities.

However, we have not been able to test the model against SAX99 data as intended, because it proved to be unsuitable (only “frozen” ripples were observed, and the wave/current conditions forming them had not been measured). We have also not been able to test the model against the SAX04 data-set as intended, because the experimenters wish to distil and publish their own results from it before releasing it for third party use.



### 3. *Existing ripple geometry predictors*

#### 3.1 EXISTING RIPPLE PREDICTORS

Before devising new ripple predictors, a study was made to see if there were existing predictors that met all the present requirements. This was based on examination of intercomparison studies reported in the scientific literature. The statistics of the study are tabulated in Tables 1 – 5 in terms of ripple predictors and the ripple data-sets they were intercompared with. It should be noted that the predictors and data-sets listed in these tables are *only* those used in this set of intercomparison studies. They are not exhaustive, and we have made use of other data-sets in both HR report TR 150 (Soulsby and Whitehouse, 2005) and the present report.

The information contained in Tables 1 – 5 is as complete and accurate as we can make it without having read every reference. Some of the collected information on data-sets and predictors has been extracted from third party sources and we have relied on the information presented. Overall, the tables are intended to provide an indication of the situation at the present time based on our experience of the literature.

A list of existing ripple predictors has been compiled from the study of the literature. These are variously for application to height and/or wavelength of ripples, generated by waves, (W), currents (C) or both together (W+C), and for either equilibrium (E) or transient (T) conditions. The methods (and intercomparison papers), dating from 1980 up to 2005, are listed in Table 1. A code is assigned to each method (e.g. GM82 for Grant and Madsen, 1982) for use in subsequent tables and text. A total of 39 methods and intercomparisons are listed, with 28 for waves alone, 5 for currents alone, and 6 for combined waves and currents. Of the predictors, 18 are for waves alone, 5 for currents alone, and 5 for combined waves and currents. Only 4 of the methods treat the transient (time-varying) case, the remainder being for equilibrium (steady) conditions. A more detailed analysis of 9 of the wave-only predictors is given in Section 3.4.

#### 3.2 EXISTING DATA-SETS USED TO TEST PREDICTORS

A list of data-sets has been compiled based on those used to test the predictors listed in Table 1. This is not intended to be an exhaustive catalogue of ripple data-sets, but only those used for testing and intercomparison of predictors. They are categorised as generated by waves (W), currents (C) or both together (W+C); for equilibrium (E) or transient (T) conditions; and from the laboratory (L) or the field (F). The data-sets, dating from 1939 up to 2005, are listed in Table 2. As with the predictors, codes are assigned for subsequent reference. A total of 83 data-sets is listed, of which 50 are for waves alone, 22 are for currents alone, and 11 are for combined waves and currents. 75 data-sets were for equilibrium conditions and 8 for transient conditions. 71 data-sets were from the lab, and 14 from the field.

#### 3.3 INTERCOMPARISON OF INTERCOMPARISONS

A total of 24 intercomparison papers or books have been identified. These are shown in Table 3, using the codes assigned in Table 1. The predictors tested are shown with an × against each paper. The most widely tested predictors are: Nielsen (1981) [13 times], Wiberg and Harris (1994) [9 times], Grant and Madsen (1982) [7 times] and Mogridge et al (1994) [7 times], with all the others being tested 3 or less times. It is noteworthy

that the wave-only predictors have been subjected to far more testing than current-only or W+C predictors.

The most comprehensive intercomparisons in terms of number of predictors tested are those of Traykovski et al (1999), Foti and Faraci (2003), and Williams et al (2004), each testing 6 predictors. All other intercomparisons were of 5 or less predictors.

The data-sets against which intercomparisons have been made are listed in Table 4, using the codes assigned in Tables 1 and 2. The most widely used data-sets are: Inman (1957) [10 times], Carstens et al (1969) [9 times], Kennedy and Falcon (1965) [7 times], Mogridge and Kamphuis (1972) [6 times], and Dingler (1974) [5 times], with all the others being tested 4 or less times.

The most comprehensive intercomparisons in terms of number of data-sets used are those of Baas (1993) [17 data-sets], Mogridge et al (1993) [16 data-sets], ABP (2004) [13 data-sets], and Mogridge et al (1994) [13 data-sets]. All the other intercomparisons used 9 or less data-sets.

The correspondence between predictors and data-sets in intercomparisons is shown in Table 5, where all the intercomparisons are taken together. Overall, it can be seen that many of the predictors have been tested against a wide range of data-sets (taking all intercomparisons into account), although some have only been tested against the originator's own data. The predictors which have been compared with the largest number of data-sets overall are Nielsen (1981) [53 data-sets], Mogridge et al (1994) [36 data-sets] and Wiberg and Harris (1994) [24 data-sets]. All the others have been tested against 18 or less data-sets.

No attempt has been made here to rank the predictors, partly because intercomparisons rarely announce an unequivocal "winner" (unless it is their own method!), and partly because the older methods have been more frequently tested, whereas one would expect more recent methods to be better due to improvements in data and understanding.

However, individual intercomparisons have been of a relatively small sub-set of the available predictors, tested against a relatively small sub-set of the available data-sets. Furthermore, the selected sub-sets of data vary widely between the intercomparisons. A strong case could be made for a concerted effort by a group of researchers to assemble all the (easily available) data-sets, and perform a consistent and unbiased test of the available ripple predictors.

### 3.4 ANALYSIS OF EXISTING WAVE-RIPPLE PREDICTORS

As a lead-in to choosing or devising a new wave-generated ripple geometry predictor, we make a comparative review of nine existing methods for predicting the height and wavelength of wave-induced ripples which are summarised in Table 6. They are referenced and compared in the ten books and intercomparison papers listed in Table 7. Since most of the methods are given in full in either Foti and Faraci (2003) [6 methods] or Grasmeijer and Kleinhans (2004) [3 methods], the full formulae are not repeated here. Foti and Faraci (2003) additionally give Matlab codes to compute the 6 methods they reviewed.

The various methods were originally written using a wide variety of non-dimensional groupings of the input parameters. However, they can be re-cast mathematically to a smaller number, which are listed below.

### Output parameters

$\eta$  = ripple height  
 $\lambda$  = ripple wavelength

### Input parameters

$d_{50}$  = median grain diameter of sediment  
 $\rho_s$  = density of sediment  
 $\rho$  = density of water  
 $\nu$  = kinematic viscosity of water  
 $g$  = acceleration due to gravity  
 $U_w$  = amplitude of near-bed wave-induced orbital velocity  
 $T$  = wave period.

$U_w$  and  $T$  are representative of regular, sinusoidal waves. O'Donoghue et al (2005) showed from comparative laboratory tests that in regular, asymmetric waves the best representation for  $U_w$  is given by  $U_{max}$ , the maximum (usually onshore-directed) velocity (under the wave crest), and for irregular, asymmetric or symmetric waves the best representation for  $U_w$  is given by  $U_{1/10}$ , the mean of the highest one-tenth velocities. In irregular waves, the peak-period  $T_p$  gives the best representation of  $T$ .

### **Derived parameters**

$$A = U_w T / (2\pi) \quad = \text{amplitude of near-bed wave excursion} \quad (3.1)$$

$$\Delta = A / d_{50} \quad (3.2)$$

$$\Psi = \frac{U_w^2}{g(s-1)d_{50}} \quad = \text{wave mobility parameter} \quad (3.3)$$

$$\theta'_w = \frac{\frac{1}{2} f_w U_w^2}{g(s-1)d_{50}} \quad = \text{skin-friction Shields parameter} \quad (3.4)$$

$$f_w = \text{grain-related wave friction factor (function of } \Delta \text{ and } Re_w) \quad (3.5)$$

$$Re_w = \frac{U_w A}{\nu} \quad = \text{wave Reynolds number} \quad (3.6)$$

$$s = \rho_s / \rho \quad = \text{density ratio} \quad (3.7)$$

$$D_* = \left[ \frac{g(s-1)}{\nu^2} \right]^{1/3} d_{50} \quad = \text{dimensionless grain-size} \quad (3.8)$$

$$\chi = \frac{d_{50}}{g(s-1)T^2} \quad = \text{period parameter} \quad (3.9)$$

The nine methods can be re-cast to give non-dimensional expressions for the dimensionless ripple height  $\eta/A$  and wavelength  $\lambda/A$ . The non-dimensional combinations of input parameters for each method are given in Table 6. They fall into three families:

**a. Functions of  $\Delta$ .** WH94 can be re-cast to give  $\eta/A$  and  $\lambda/A$  as functions of only  $\Delta$  (Malarkey and Davies, 2003). T99 also gives functions of only  $\Delta$ . They can be regarded as “kinematic” methods, since  $\Delta$  is a ratio of lengths (or velocities), but  $g$  and  $s$  are not included. M94 gives functions containing  $\chi$  as well as  $\Delta$ , introducing a dependence on wave period combined with  $g$  and  $s$ .

**b. Functions of  $\Psi$ .** N81, VR89 and GK04 give  $\eta/A$  and  $\lambda/A$  as functions of only  $\Psi$ . FF02 gives functions containing  $\Delta$  and  $Re_w$  as well as  $\Psi$ , introducing a dependence on viscosity. They can be regarded as “semi-dynamic” methods, because they include  $g$

and  $s$ , but do not include  $f_w$  which is necessary to describe the tractive force on sediment grains.

**c. Functions of  $\theta'_w$ .** GM82 and Ma93 give  $\eta/A$  and  $\lambda/A$  as functions of  $\theta'_w$  and  $D_*$ . They can be regarded as “dynamic” methods, because the Shields parameter  $\theta'_w$  represents the ratio of forces acting on sediment grains.  $D_*$  introduces a dependence on viscosity.

Regarding the applicability of these input parameters, the following observations can be made about wave-induced ripples.

1. For very small wave-induced velocities ( $U_w$ ), the sediment is below the threshold of motion. Ripples do not form on an initially flat bed. (In the sea, “frozen” or “relict” ripples remain from previous more energetic conditions, unless biological activity has flattened them.)
2. For intermediate wave-induced velocities, ripples form. At larger velocities the ripple heights reduce.
3. For large wave-induced velocities, ripples are washed out leaving a flat bed with oscillatory sheet flow.
4. For grainsizes less than about 0.06mm, ripples are low and indistinct.
5. For grainsizes between 0.06 and about 0.7-1.0mm, ripples are well-defined.
6. For grainsizes larger than about 0.7-1.0mm ripples are either indistinct or do not form.

Since observations 1 to 3 relate to velocities, and 4 to 6 relate to grainsizes, they cannot be satisfied only by a single parameter such as  $\Delta$ ,  $\Psi$  or  $\theta'_w$ , all of which contain both velocity and grainsize. Hence it would seem to be necessary for  $\eta/A$  and  $\lambda/A$  to be formulated as independent functions of parameters such as  $\Delta$ ,  $\Psi$  or  $\theta'_w$  to satisfy observations 1 to 3, and  $D_*$  or  $\chi$  to satisfy observations 4 to 6. The methods of GM82 (containing  $\theta'_w$  and  $D_*$ ) and M94 (containing  $\Delta$  and  $\chi$ ) seem to satisfy this requirement best. The method of Ma93 superficially appears to meet the requirements but in fact is a function of only the single parameter  $(\theta'_w / D_*^{1/2})$ , so the dependencies on velocity and grainsize are linked.

All the methods are essentially empirical curves fitted to lab and field data. Hence it might be expected that, despite their dependence on different parameters, they would give similar predictions for  $\eta$  and  $\lambda$  for given input values. We have tested this by plotting all 9 methods for a wide range of inputs. We made use of the Matlab codes provided by Foti and Faraci (2003) for 6 of the methods, but with a spurious factor of  $\text{SQRT}(2)$  removed from the orbital velocities. The outputs were checked for the method WH94 against curves in the original paper, but the other methods have not been checked. The remaining 3 methods were coded in Matlab by editing the codes given by Foti and Faraci (2003).

A randomly distributed set of 1,000 inputs was generated by fixing the values  $\rho = 1027 \text{ kg m}^{-3}$ ,  $\nu = 1.36 \times 10^{-6} \text{ m}^2 \text{ s}^{-1}$  and  $\rho_s = 2650 \text{ kg m}^{-3}$  (quartz sand in sea water at 10°C, 35ppt), and randomly selecting values of the other input parameters within the ranges  $0.2 < U_w < 2.0 \text{ m.s}^{-1}$ ,  $4 < T < 16 \text{ s}$ , and  $0.06 < d_{50} < 2.0 \text{ mm}$ . The 1,000 inputs thus cover most of the conditions likely to be encountered for sand in the sea. The same 1,000 inputs were fed into the 9 prediction methods listed in Table 6, and the output values of  $\eta/A$  and  $\lambda/A$  plotted against each of the main independent variables  $\Delta$ ,  $\Psi$  and  $\theta'_w$ . Figures 1, 2 and 3 show that the 9 methods differ very widely in their predictions. The methods that depend on only  $\Delta$  plot as single curves when  $\Delta$  is the abscissa (Figure 1), as would be



expected, whereas other methods scatter widely. The same is true of the plots versus  $\Psi$  (Figure 2) and  $\theta'_w$  (Figure 3). Irrespective of whether  $\eta$  or  $\lambda$  is plotted, and whether  $\Delta$ ,  $\Psi$  or  $\theta'_w$  is the abscissa, the methods vary by factors of between 10 and 1000 in their predictions. Thus it is *not* the case that the methods give similar predictions.

Although there is already a wide selection of ripple predictors available, it is clear that they have a large measure of disagreement. Furthermore, while several intercomparisons have been made testing predictors against data, there is no consistency in either the predictors tested or the data-sets used. There is thus no predictor that is unequivocally superior to the others. For this reason, (and despite the large number already proposed) we have developed our own wave-generated ripple predictor, based partly on the data-set assembled for this project, and partly on experiences with existing predictors.



## 4. New wave-only ripple geometry predictor

### 4.1 NEW WAVE-RIPPLE EQUILIBRIUM PREDICTOR

The first question to address when devising a new predictor for wave-generated ripple geometry is which out of  $\Delta$ ,  $\psi$  and  $\theta'_w$  (or some combination of them) is the best choice of independent variable. This has been tested using the data-base assembled in Phase 1 to see which parameterisation makes the data collapse most closely onto single curves. Figures 4a, b and c show plots of  $\eta/A$  versus  $\Delta$ ,  $\psi$  and  $\theta'_w$  respectively, and Figures 5a, b and c show similar plots for  $\lambda/A$ . All the plots show considerable scatter, but the plots against  $\Delta$  appear to cluster the data more tightly than those against  $\psi$ , with the plots against  $\theta'_w$  giving the greatest scatter. On these grounds, we choose to formulate the predictors for equilibrium wave-generated ripple height and wavelength as functions of the excursion parameter  $\Delta$ .

This is the same choice as that used by Wiberg and Harris (1994), (re-stated by Malarkey and Davies (2003) in non-iterative form). An alternative case could be made for expressing the wavelength in terms of the *kinematic* ratio,  $\Delta$ , but with the ripple steepness as a function of the *dynamical* ratio  $\theta'_w$ . Dependence of steepness  $\eta/\lambda$  as a function of  $\theta'_w$  was advocated by Grant and Madsen (1982) (with additional dependence on  $D^*$ ), and by Nielsen (1992). However, on the basis of the data collapse shown in Figures 4a and 5a, we will adhere to the choice of  $\Delta$  for the functional dependence of both  $\eta$  and  $\lambda$ .

We will follow the general observations made by Wiberg and Harris (1994), who in turn followed Clifton (1976):

- For values of  $\Delta$  less than about 750,  $\lambda$  is proportioned to  $A$  (orbital ripples), with  $\lambda/A$  approximately unity
- For intermediate values of  $\Delta$ ,  $\lambda/d_{50}$  (not plotted) reaches a peak value of rather more than 1000, and then declines with increasing  $\Delta$  (sub-orbital ripples)
- For values of  $\Delta$  larger than about 3000,  $\lambda$  is proportional to  $d_{50}$  (anorbital ripples) with  $\lambda/d_{50}$  being around 500
- For values of  $\Delta$  less than about 1500, the ripple steepness  $\eta/\lambda$  is roughly constant, lying between 0.1 and 0.2
- As  $\Delta$  increases above 1500,  $\eta/\lambda$  decreases rapidly with  $\Delta$  as the ripples are washed out
- For values of  $\Delta$  greater than about 6000, ripples cannot exist and the bed is flat (or gently undulating) with sheet flow of sediment.

The following expressions (which replace those presented at the SAX04 workshop in Seattle in May 2005) for ripple wavelength and steepness follow the general principles outlined above, with values of the coefficients based on fits to the data-base and similarities with WH94:

$$\frac{\lambda}{A} = \left[ 1 + 1.87 \times 10^{-3} \cdot \Delta \left( 1 - \exp \left\{ - \left( 2.0 \times 10^{-4} \Delta \right)^{1.5} \right\} \right) \right]^{-1} \quad (4.1)$$

$$\frac{\eta}{\lambda} = 0.15 \left[ 1 - \exp \left\{ - \left( 5000 / \Delta \right)^{3.5} \right\} \right] \quad (4.2)$$

It was found that alternative expressions giving  $\eta/\lambda$  directly as a function of  $\Delta$  yielded curves of steepness  $\eta/\lambda$  versus  $\Delta$  that had unrealistic behaviour. It was therefore decided (in common with many other methods) to parameterise  $\eta/\lambda$  in terms of  $\Delta$ , and then calculate ripple height  $\eta$  from:

$$\frac{\eta}{A} = \frac{\lambda}{A} \cdot \frac{\eta}{\lambda} \quad (4.3)$$

An additional constraint is that ripples can only form and evolve if the wave-induced stress exceeds the threshold of motion of the sediment. This is expressed by comparing the actual Shields parameter  $\theta'_w$  with the threshold value  $\theta_{cr}$ . Then:

- If  $\theta'_w \leq \theta_{cr}$ , ripples take pre-existing values of  $\eta$  and  $\lambda$
- If  $\theta'_w > \theta_{cr}$ , equilibrium values of  $\eta$  and  $\lambda$  are given by Eqs (4.1), (4.2) and (4.3).

Tests of Eqs (4.2, 3) and (4.1) against lab and field data from the data-base are shown in Figures 6 and 7 respectively. In both cases, despite a large amount of scatter in the data points, the prediction curves pass through the centre of the data reasonably well. It should be borne in mind that although field data might be considered more relevant than lab data, there is always uncertainty about whether ripples in the sea are truly in equilibrium with the instantaneous wave and current conditions, and also that they are rarely due entirely to waves alone.

## 4.2 TIME-EVOLUTION OF WAVE-RIPPLES

As pointed out above, since ripples on the sea-bed are constantly varying in response to the varying wave conditions, the prediction of the rate of response of the ripples is just as important as prediction of the equilibrium geometry. Effectively, the ripples are constantly trying to catch up with the driving conditions. In addition, if the wave-induced orbital velocities fall below the threshold of sediment the pre-existing ripples remain “frozen”. The time-evolution of ripple height, wavelength and orientation all need to be considered.

Experiments on the evolution of wave-induced ripples have been performed by Doucette and O'Donoghue (2005a, 2005b) in a large oscillating water tunnel at the University of Aberdeen, UK. Smaller scale experiments were also undertaken by Smith and Sleath (2005) in an oscillating tray rig at the University of Cambridge, UK. For the present purposes, we concentrate on the large-scale experiments at Aberdeen, referred to as DO05. These were performed using sand with  $d_{50} = 0.44\text{mm}$ , and with velocities simulating the full-scale near-bed flow produced by asymmetric regular and irregular waves.

DO05 presented plots showing how ripple height and wavelength evolve with time, when steady wave conditions are applied to either an initially flat bed (ripple growth), or a rippled bed produced earlier by different wave conditions (ripple evolution). The evolution of ripples from both initially larger, and initially smaller, ripples were measured. DO05 interpreted the results by fitting an empirical relationship between a rate-of-change parameter and the wave mobility parameter  $\psi$ . Although their proposed formulation gives a good fit to their observed rates of change of ripple height, it is difficult to apply for general-purpose use in field conditions, as its extrapolated behaviour is unrealistic. In particular, extrapolation to  $\psi = 0$  (no waves) would still predict some ripple evolution, and extrapolation to large  $\psi$  predicts excessively rapid evolution. Consequently, a more suitable formulation has been developed by the

present first author (RLS) together with Dr O'Donoghue and Dr Doucette, as follows. DO05 (and Smith and Sleath, 2005) showed that the evolution of ripple height  $\eta(t)$  from an initial value of  $\eta_0$  to a new equilibrium value  $\eta_{eq}$  corresponds closely to an exponential relaxation given by:

$$\frac{\eta(t)}{\eta_{eq}} = 1 - \left\{ 1 - \frac{\eta_0}{\eta_{eq}} \right\} \exp \left\{ -\frac{\beta t}{T} \right\} \quad (4.4)$$

where  $T$  is wave period, and  $\beta$  is a coefficient that governs the rate of change (small for small waves, large for large waves). Eq (4.4) applies for a step change from one steady wave condition (or flat bed) to another steady condition. A more general expression, better suited to application to constantly varying field conditions, is given by:

$$\frac{d\eta}{dt} = \frac{\beta}{T} (\eta_{eq} - \eta) \quad (4.5)$$

Eq (4.4) is a solution of Eq (4.5) for the special case where  $\eta = \eta_0$  at  $t = 0$ , and  $\beta$ ,  $T$  and  $\eta_{eq}$  are independent of  $t$ . The method of solving the discretised form of Eq (4.5) is described in Section 6. The following expression for  $\beta$  gives a good fit to the DO05 data, and has the plausible asymmetry behaviour of tending to zero for zero waves, and tending to a (large) constant for very large waves:

$$\beta = 2.996\psi^{1.07}/(21700 + \psi^{1.07}) \quad (4.6)$$

The application of Eqs (4.5) and (4.6) to predict the varying ripple height  $\eta(t)$  for time-varying wave inputs is described in Section 6. DO05 did not present similar data for the rate of change of wavelength, although they remarked that the ripple length reached equilibrium at about the same time as the ripple height. On this basis, we will take an analogous equation for wavelengths,  $\lambda$ , to that given for heights in Eq (4.5), and use the same Eq (4.6) for the rate of change of wavelength. By analogy, but without justification due to lack of data, we will use analogous equations for the variation of ripple orientation in response to changes in wave direction.



## 5. *New current-only ripple geometry predictor*

### 5.1 NEW CURRENT-RIPPLE EQUILIBRIUM PREDICTOR

As shown in Section 3, there are far fewer current-generated than wave-generated ripple predictors, and there have not been definitive intercomparison tests of them. We therefore again developed a new predictor for this project.

In developing a new current-ripple predictor we draw heavily on laboratory experiments by Baas (1993), Whitehouse et al (1998) and Damgaard et al (2003).

The PhD thesis of Baas (1993) [B93] describes an extensive series of laboratory experiments in a continuously-circulating race-track flume at the University of Utrecht, the Netherlands. Two sediments were used: a very fine sand with  $d_{50} = 0.095\text{mm}$ , and a fine sand with  $d_{50} = 0.238\text{mm}$ . The experiments were run for sufficiently long durations that both the evolution of the ripples and their equilibrium form could be studied with confidence. A wide range of current speeds was used. A comprehensive compilation of data from previous researchers was also made, and used to assist interpretation of the experimental results.

Whitehouse et al (1998) [WMS98] performed experiments in a reversing flume at HR Wallingford, UK. A single sediment was used with  $d_{50} = 0.510\text{mm}$ . Initial experiments were conducted with steady currents, with step changes between current speeds, to investigate the equilibrium ripple geometry, and the evolution from a plane bed. Subsequent experiments were performed with a flow that reversed sinusoidally with a period of 12.5 hours for three tidal periods. This was regarded as a direct full-scale simulation of the bottom 0.1m or so of a full-scale tidal flow in the sea. The aim was to investigate tidal variations in ripple geometry.

Damgaard et al (2003) [DSPW03] performed experiments in a sloping sediment duct at HR Wallingford, UK. Two sediments were used: a well-sorted fine sand with  $d_{50} = 0.237\text{mm}$  and  $d_{90}/d_{10} = 2.4$ , and a widely-graded fine sand with  $d_{50} = 0.231\text{mm}$  and  $d_{90}/d_{10} = 4.2$ . The main aim was to investigate the effect of steep slopes (up to  $20^\circ$ ) on sediment transport rates, but the ripple properties were also measured. Only the tests with a horizontal bed were used for the present purposes.

WMS98 and DSPW03 do not appear in Tables 1 to 7, because they have not been used in existing intercomparisons.

B93 presented convincing evidence for his hypothesis that, within the rippled-bed regime (i.e. for all current speeds greater than the threshold of motion but less than the start of wash-out), a given grain-size will develop ripples of a constant height and wavelength provided that the current speed is maintained for a long enough time. This is contrary to most earlier interpretations, in which ripple height was assumed to increase with increasing current speed to a certain point, then decrease due to wash-out. B93 also found that current speeds greater than a certain value led to a flat bed with sheet flow (upper stage plane bed) for very fine sand with  $d_{50} = 0.095\text{mm}$ , but led to a transition to dunes of greater height and wavelength than the ripples for fine sand with  $d_{50} = 0.238\text{mm}$ . B93 proposed expressions, based on his own data and that from other sources, for the maximum ripple height and wavelength,

$$\eta_{\max} = 3.4 \log_{10}(d_{50}) + 18 \quad (5.1)$$

$$\lambda_{\max} = 75.4 \log_{10}(d_{50}) + 197 \quad (5.2)$$

where  $\eta_{\max}$ ,  $\lambda_{\max}$  and  $d_{50}$  are all in mm. These dimensionally inhomogeneous equations can be re-cast in homogeneous form if it is assumed that (a) the length-scale determining  $\eta_{\max}$  and  $\lambda_{\max}$  is  $d_{50}$ , (b) that the remaining influence of  $d_{50}$  is expressed by the commonly-used dimensionless grainsize  $D_*$ , where

$$D_* = \left[ \frac{g(s-1)}{v^2} \right]^{1/3} d_{50} \quad (5.3)$$

Equations (5.1) and (5.2) can then be written as:

$$\frac{\eta_{\max}}{d_{50}} = \frac{1}{D_*} [31.1 \ln(D_*) + 285] \quad (5.4)$$

$$\frac{\lambda_{\max}}{d_{50}} = \frac{1}{D_*} [700 \ln(D_*) + 2023] \quad (5.5)$$

where  $\ln$  is the natural logarithm.

However, these expressions do not fit closely to the measurements of WMS98 and DSPW03. Instead, the following expressions are proposed here, which fit closely to the data of B93, WMS98 and DSPW03, and reasonably well to the other data collated by B93:

$$\eta_{\max} = d_{50} \cdot 202 D_*^{-0.554} \quad , \text{ for } 1.2 < D_* < 14 \quad (5.6a)$$

$$\lambda_{\max} = d_{50} (500 + 1881 D_*^{-1.5}) \quad , \text{ for } 1.2 < D_* < 14 \quad (5.6b)$$

For  $D_* > 14$  ( $d_{50} \geq 0.7\text{mm}$ ) ripples are indistinct or do not form.

The prediction curves and all the data mentioned above are plotted in Figures 8 and 9. The equations were fitted exactly to the very-fine-sand data of B93 and the coarse-sand data of WMS98. They fit quite closely to the fine-sand data of B93 and DSPW03, and reasonably well to the other data.

The effect of wash-out at large current speeds is included by again using the data of B93, WMS98 and DSPW03 together with a plot by Van den Berg and Van Gelder (1989) reproduced by Van Rijn (1993). All these are shown in Figure 10, with lines added as an approximation to the start of wash-out and the completion of wash-out and the start of sheet-flow (with or without dunes). The lines are given in terms of the skin-friction Shields parameter  $\theta'_c$  as a function of  $D_*$ . For present purposes,  $\theta'_c$  is defined by:

$$\theta'_c = \frac{C_D \bar{U}^2}{g(s-1)d_{50}} \quad (5.7a)$$

$$C_D = \left[ \frac{0.40}{\ln(h/z_0) - 1} \right]^2 \quad (5.7b)$$

$$z_0 = d_{50} / 12 \quad (5.7c)$$



although the plot by Van den Berg and Van Gelder used  $z_0 = d_{90}/10$  (the differences are not great). Here  $\bar{U}$  is depth-averaged current speed,  $C_D$  is drag coefficient, and  $z_0$  is grain-related bed roughness length.

The proposed limits of wash-out and sheet-flow are:

$$\theta'_{wo} = 1.66 D_*^{-1.3} \quad \text{for } D_* > 1.58 \quad (5.8a)$$

$$\theta'_{sf} = 2.26 D_*^{-1.3} \quad \text{for } D_* > 1.58 \quad (5.8b)$$

$$\theta'_{wo} = 0.916 \text{ and } \theta'_{sf} = 1.25 \quad \text{for } D_* \leq 1.58 \quad (5.8c)$$

Applying a linear reduction in ripple height with  $\theta'_c$ , the expression for equilibrium ripple height including wash-out is:

$$\eta_{eq} = \text{pre-existing value} \quad \text{for } 0 \leq \theta'_c \leq \theta_{cr} \quad (5.9a)$$

$$\eta_{eq} = \eta_{max} \quad \text{for } \theta_{cr} < \theta'_c \leq \theta'_{wo} \quad (5.9b)$$

$$\eta_{eq} = \eta_{max} \left( \frac{\theta'_{sf} - \theta'_c}{\theta'_{sf} - \theta'_{wo}} \right) \quad \text{for } \theta'_{wo} < \theta'_c \leq \theta'_{sf} \quad (5.9c)$$

$$\eta_{eq} = 0 \quad \text{for } \theta'_c > \theta'_{sf} \quad (5.9d)$$

The wavelength is assumed to be unaffected by wash-out (i.e. only the ripple steepness declines) and is given by:

$$\lambda_{eq} = \lambda_{max} \quad (5.10)$$

No account is taken here of the lengthening of  $\lambda$  on transition to dunes for fine and medium sands. The expressions for  $\eta_{max}$ ,  $\lambda_{max}$ ,  $\theta'_{wo}$  and  $\theta'_{sf}$  are given by Eqs (5.6a), (5.6b), (5.8a, c) and (5.8b, c) respectively.

## 5.2 TIME-EVOLUTION OF CURRENT-RIPPLES

As with wave-ripples, current-ripples alter their height, wavelength and orientation with changing current speed and direction. (They also alter their asymmetry, but that is not considered here.) The speed of ripple evolution decreases as the current speed decreases, and is zero for currents below the threshold of motion of sediment (frozen ripples).

By analogy with the approach used for wave-ripples in Section 4.2 (c.f. Eq 4.5), the rates of change of ripple height and wavelength are given by:

$$\frac{d\eta}{dt} = \frac{\beta_\eta}{T_c} (\eta_{eq} - \eta) \quad (5.11)$$

$$\frac{d\lambda}{dt} = \frac{\beta_\lambda}{T_c} (\lambda_{eq} - \lambda) \quad (5.12)$$

where  $\eta_{eq}$  is given by (5.9a-d), and  $\lambda_{eq}$  is given by Eq (5.10). B93 found that the ripple height evolved faster than the wavelength, and hence two different parameters,  $\beta_\eta$  and  $\beta_\lambda$ , are employed. The basic time-scale  $T_c$  is less easy to identify for currents than it was for waves, where wave period  $T$  was the natural choice. Here we take  $T_c$  to be related to the time taken for the volume of a ripple per unit width (proportional to  $\eta_{max} \cdot \lambda_{max}$ ) to be delivered by the bedload transport rate,  $q_b$ . The bedload transport can be written in the form (Soulsby, 1997, p. 158):

$$\Phi = \frac{q_b}{[g(s-1)d_{50}^3]^{1/2}} = \text{func}(\theta'_c, \theta_{cr}) \quad (5.13)$$

The adaptation time in Eqs (5.11) and (5.12) can then be written as:

$$\begin{aligned} \frac{T_c}{\beta_x} &= \frac{\eta_{max} \cdot \lambda_{max}}{q_b} \\ &= \frac{\eta_{max} \cdot \lambda_{max}}{[g(s-1)d_{50}^3]^{1/2}} \cdot \frac{1}{\text{func}(\theta'_c, \theta_{cr})} \end{aligned} \quad (5.14)$$

from which the time-scale  $T_c$  and rate-coefficient  $\beta_x$  (where  $x = \eta$  or  $\lambda$ ) can be separated as:

$$T_c = \frac{\eta_{max} \cdot \lambda_{max}}{[g(s-1)d_{50}^3]^{1/2}} \quad (5.15)$$

and  $\beta_x = \text{func}(\theta'_c, \theta_{cr})$ , where  $x = \eta$  or  $\lambda$ , and  $\beta_\eta$  and  $\beta_\lambda$  are different functions of  $\theta'_c, \theta_{cr}$ .

B93 tabulated data from his experiments for the time taken for ripples to achieve 99% of their final height or wavelength. These data have been used here to devise and calibrate expressions for  $\beta_\eta$  and  $\beta_\lambda$ :

$$\beta_\eta = \frac{20(\theta'_c - \theta_{cr})^{1.5}}{2.5 + (\theta'_c - \theta_{cr})^{1.5}} \quad (5.16)$$

$$\beta_\lambda = \frac{12(\theta'_c - \theta_{cr})^{1.5}}{2.5 + (\theta'_c - \theta_{cr})^{1.5}} \quad (5.17)$$

These curves are shown in Figures 11a – d, together with the data from B93, and give a reasonably good fit.

In the absence of data, the orientation  $\phi$  of the ripples is assumed to change at the same rate as the wavelength. Thus the evolution is taken to be given by:

$$\frac{d\phi}{dt} = \frac{\beta_\lambda}{T_c} (\phi_{eq} - \phi) \quad (5.18)$$

where  $\phi_{eq}$  is the direction of the instantaneous current.

## 6. *Time-stepping procedure*

### 6.1 AIMS OF PREDICTOR

The aim is to develop a ripple predictor that predicts: time-varying ripple heights, lengths and orientations, for any sandy sediment, driven by any time-series of: water depths, wave heights, periods and directions, and current speeds and directions. It must take account of: evolution (“history”), threshold-of-motion, and wash-out effects, as well as bio-degradation of ripples. It must cover both wave-generated and current-generated ripples, switching between them (in an evolving sense) depending on which forcing is dominant.

### 6.2 BASIC EQUATIONS

The full predictor is based on the methods and equations derived in Sections 4 (for waves) and 5 (for currents). It is set out in step-by-step algorithmic form in Appendix A.

The equilibrium height and wavelength for *wave-generated* ripples are given by Eqs (4.1) – (4.3), with the threshold constraint given after Eq (4.3).

The equilibrium height and wavelength for current-generated ripples are given by Eqs (5.6) – (5.10), with the threshold constraint given by Eq (5.9a).

These methods include both threshold-of-motion and wash-out effects. The differential equations expressing the evolution of ripple height  $\eta(t)$ , length  $\lambda(t)$  and orientation  $\phi(t)$  are given by Eq (4.5) for wave-generated ripple height, with analogous equations for length and orientation; and by Eqs (5.11), (5.12) and (5.18) respectively for current-generated ripples.

The rate-of-change parameters in these equations are:  $\beta/T$  for wave-generated ripple height, length and orientation; and  $\beta_\eta/T_c$ ,  $\beta_\lambda/T_c$  and  $\beta_\phi/T_c$  respectively for current-generated ripple height, length and orientation. In these:

- $\beta$  is given by Eq (4.6), where  $\psi$  is given by Eq (3.3)
- $T$  is wave period (see discussion in Section 3.4 on selection of  $T$ )
- $\beta_\eta$  is given by Eq (5.16), where  $\theta'_c$  is given by Eqs (5.7a) to (5.7c)
- $\beta_\lambda$  is given by Eq (5.17)
- $T_c$  is given by Eq (5.15), where  $\eta_{\max}$  and  $\lambda_{\max}$  are given by Eqs (5.6a) and (5.6b).

The differential equations for ripple orientation  $\phi$  (= direction of normal to ripple crests) are **an interim approximation only**. They do not behave correctly when  $\phi$  passes anticlockwise through  $0^\circ\text{N}$ ; for example, if  $\phi_{\text{eq}}$  makes a step change from  $10^\circ\text{N}$  to  $350^\circ\text{N}$ ,  $\phi(t)$  rotates clockwise via South instead of anticlockwise through North. An alternative approach, expressing wavelength  $\lambda$  as a vector  $(\lambda_x, \lambda_y)$  was not an improvement. In fact, any such approach with a single ripple train is unrealistic, because a spatially extended ripple field cannot swing around as a whole when the wave (or current) direction changes. The present approach should therefore be used with caution, and preferably only for wave (or current) directions within a  $180^\circ$  sector that excludes  $0^\circ$ . It is hoped to devise a more robust method in the future.

### 6.3 WAVES VERSUS CURRENT RIPPLES

The present version of the time-stepping procedure adopts a bi-polar approach to the relative effects of waves and currents in generating ripples. This amounts to a switch from the wave-only to the current-only expressions, and vice versa, depending on the dominant value of Shields parameter. A similar approach was used by Lyne et al (1990) based on the ratio of current speed to wave orbital velocity. However, the present approach is proposed on the stronger basis that bedload sediment transport rates (which are the driving mechanism for ripple orientation) depend directly on Shields parameter.

Thus, comparing  $\theta'_w$  for waves (Section 4) with  $\theta'_c$  for currents (Section 5):

- if  $\theta'_w \geq \theta'_c$ , the wave-generated expressions summarised in Section 6.2 are used
- if  $\theta'_c > \theta'_w$ , the current-generated expressions summarised in Section 6.2 are used where  $\theta'_w$  is given by Eq (3.4) and  $\theta'_c$  by Eq (5.7a, b, c).

Li and Amos (1998) proposed expressions for ripple geometry due to combined waves and currents, and gave a three-fold categorisation of the relative effects based on the ratio  $\theta'_w/\theta'_c$ . Neither Lyne et al (1990) nor Li and Amos (1998) used a time-evolving predictor; they just assumed that the ripple geometry was always in equilibrium with the instantaneous hydrodynamic conditions.

### 6.4 BIO-DEGRADATION OF RIPPLES

Marine creatures burrowing in the sea-bed sediments can cause a ripple field to flatten. This is especially noticeable at slack water for (tidal) current-generated ripples, or under calm conditions for wave-generated ripples. Amos et al (1988) observed at a depth of 22m on the Scotian shelf that re-working by burrowing organisms could mix the top 10cm or so of the sea-bed within 4 to 6 hours, thereby flattening current-formed ripple patterns in periods when both tidal flow and wave activity were sub-threshold. Baas (1993) described video observations of the bottom of a subtidal channel in the Dutch Wadden Sea in which intensive bioturbation obliterated ripples formed during one tide. He also reported geological evidence of current ripples in turbidite beds found in the Pyrenees Mountains (Spain), many of which showed evidence of bioturbation. In the SAX04 experiment, fish were observed to pock-mark the sea-bed sediments, disturbing the ripple pattern. Wheatcroft (1994) observed the bottom roughness of a silt bed in 90m of water on the central California shelf. The rms heights of the bottom roughness were found to vary over short periods of time (12 hours). In general, all physical bedforms could be destroyed by bioturbation processes in periods of hours to days. Marine creatures can also *create* bed topography. For example, the dominant bed roughness in the intertidal Eden estuary in eastern Scotland is caused by a pattern of the eroded worm-casts of burrowing marine worms (personal observation).

The detailed effects of bioturbation depend on the organism involved. However, a simple method is proposed here for simulating the effects of both ripple flattening and residual biologically-induced bed roughness. The reduction in height of ripples is expressed by a biological half-life  $T_{1/2,b}$  representing the time taken for biological activity to reduce the ripple height to one half of its initial value in conditions when waves and currents are below the threshold of motion. The residual bio-roughness is expressed by  $\eta_b$ , representing the average “trough to crest” height of the biologically induced bed features.

These are implemented as follows:

1. A switch  $Sw_b$  is given the value 1 if bio-degradation is included, and 0 if it is not
2. Equation (4.5) is modified to:  

$$\frac{d\eta}{dt} = \frac{\beta}{T}(\eta_{eq} - \eta) - \frac{\eta}{T_b} \cdot Sw_b \quad (6.1)$$

where  $T_b = T_{1/2,b}/\ln(2) = 1.443 T_{1/2,b}$
3. The ripple height  $\eta(t)$  is set to the maximum of  $\eta_b$  or the value derived from integration of Eq (6.1).
4. The same rules are applied to Eq (5.11) if the ripples are current-generated.

The biological term in Eq (6.1) causes the ripple height to decrease exponentially with time. The ripple length and orientation are not modified by biological effects in the present treatment.

The choice of values for  $T_{1/2,b}$  and  $\eta_b$  must be made using knowledge about the biological activity of the study site. At present, it is not easy to recommend values, but ultimately this might be possible by examining evidence from a number of representative sites.

## 6.5 SOLUTION METHOD

The various differential equations for the evolution of ripple height, wavelength and orientation, produced by waves or by currents, can all be written in the general form:

$$\frac{dx}{dt} = a(t) - b(t) \cdot x(t) \quad (6.2)$$

where  $x$  represents either height, wavelength or orientation. The time-varying coefficients  $a(t)$  and  $b(t)$  are related to the time-varying inputs of wave heights and periods, water depths, and current speeds. For example, taking Eq (6.1) where  $x \equiv \eta$ , the coefficients are:

$$a(t) = \frac{\beta}{T} \cdot \eta_{eq} \quad (6.3)$$

$$b(t) = \frac{\beta}{T} + \frac{1}{T_b} \cdot Sw_b \quad (6.4)$$

and  $\beta$ ,  $T$  and  $\eta_{eq}$  are all time-varying with the wave conditions. The observed values of the wave and current conditions are usually recorded at discrete intervals of time,  $\Delta t$ , in lab and field measurements, where  $\Delta t$  may or may not be constant throughout the experiment. The simplest approach to implementing Eq (6.2) is to treat the coefficients  $a$  and  $b$  as being fixed at their value  $a(t)$  and  $b(t)$  over the time interval  $t$  to  $t + \Delta t$ . Eq (6.2) then has the analytical solution:

$$x_{i+1} = x_i + \left( \frac{a_i}{b_i} - x_i \right) (1 - \exp(-b_i \Delta t)) \quad (6.5)$$

where  $x_i = x(t)$ ,  $x_{i+1} = x(t + \Delta t)$ ,  $a_i = a(t)$  and  $b_i = b(t)$ . Similar approaches to Eq (6.5) were used by Baas (1993) for current-induced ripples, Wilbers (2004) for sub-aqueous dunes, and ABP (2004) for ripples under random waves. However, this approach

neglects the changes in  $a$  and  $b$  during the time interval  $\Delta t$ , and hence is not accurate if  $a$  or  $b$  changes significantly in time  $\Delta t$ .

The improved approach adopted here is to solve Eq (6.2) for  $a$  and  $b$  varying linearly with time from  $a_i$  to  $a_{i+1}$ , and  $b_i$  to  $b_{i+1}$ . This does not, in the general case, have an analytical integral analogous to Eq (6.5). Various solution schemes were tried, including an explicit forward-stepping (Euler) scheme, two implicit schemes, and a standard Runge-Kutta integration scheme. All of these became unstable if  $(b\Delta t)$  became too large. The solution adopted was a Runge-Kutta integration with an “over-ride” if  $b\Delta t > 1.6$ . In the latter case, the analytical solution Eq (6.5) is applied. However, it was found in the tests with lab and field data-sets described in Section 7 that the “over-ride” only takes effect for a very small proportion of the time. The adopted scheme (Runge-Kutta with over-ride) appears to be stable for all inputs tested. Details are given in algorithmic form in Appendix A.

The time-stepping procedure thus has the following elements at each point in time  $t_i$ :

- calculate equilibrium ripple height, wavelength and orientation due to *wave* forcing, together with  $\beta$  and  $\theta'_w$
- calculate equilibrium ripple height, wavelength and orientation due to *current* forcing, together with  $\beta_\eta$ ,  $\beta_\lambda$  and  $\theta'_c$
- decide wave or current dominance, depending on  $\theta'_w >$  or  $< \theta'_c$
- set values of coefficients of  $a_i$  and  $b_i$  for time-step  $t_i$ , based on wave or current dominance
- calculate  $x_{i+1}$  from Eq (6.2) using Runge-Kutta integration (with over-ride using Eq (6.5) if  $b\Delta t > 1.6$ ) for each of ripple height, wavelength and orientation
- move to next time-step ( $t_{i+1}$ ).

To test the algorithm, and act as a demonstrator, the above procedure (as detailed in Appendix A) has been implemented in an Excel spreadsheet. It would be a straightforward matter to implement the procedure as a FORTRAN subroutine (or other preferred computer language). The Excel spreadsheet has the title “Ripple evolution waves and currents V2.0”. The first worksheet gives instructions on its use. Examples of the input sheets are given in Appendix B. Because field and lab data-sets are so very varied (different recording intervals, durations, measures of wave heights, period or orbital velocity, depth-averaged or point current measurements) it is expected that a user will need to tailor the format of the inputs, and the scales etc. of output plots, to specific applications. **It is research-level, not operational, software.**

## 7. Tests of Mark 2 ripple predictor against data

### 7.1 TEST WITH WAVE-RIPPLE EVOLUTION DATA

The time-evolving wave-ripple predictor has been tested against the detailed time-series of ripple height and wavelength in response to step-changes in wave conditions measured by DO05 (kindly provided by Drs Doucette and O'Donoghue). In the predictor, the values of "wave height" used as input were selected to match the orbital diameters ( $D = 2A$ ) produced in the Oscillating Water Tunnel and tabulated by DO05. The periods were set to the values tabulated by DO05, and the sediment  $d_{50}$  was as reported by DO05. All the experiments used in these tests were for regular asymmetric waves.

Figure 12 shows an experiment with ripple growth, followed by decay under reduced wave conditions. The bed was initially flat, and oscillatory velocities with period  $T = 5s$  and  $D = 0.99m$  were imposed for 40 minutes. At this time the velocities were changed to  $T = 4s$  and  $D = 0.48m$ , and imposed for a further 77 minutes. The predictor simulates the rate of growth in ripple height and wavelength reasonably well, but slightly underestimates the ultimate (equilibrium) values. It also simulates the rate of decrease reasonably well after the change in inputs, this time slightly overestimating the final values.

Figure 13 shows an experiment with ripple growth followed by further growth under increased wave conditions. The bed was initially flat, and oscillatory velocities with  $T = 2s$  and  $D = 0.24m$  were imposed for 42 minutes, after which time the ripples had attained equilibrium. At this time the velocities were changed to  $T = 4s$  and  $D = 0.48m$ , and imposed for a further 67 minutes. The rather weak wave action at the start did not start to form vortex ripples in the flattened bed for the first 15 minutes. The ripple predictor was "switched off" during this period when rolling-grain ripples were present (a common feature at the start of laboratory experiments with flattened beds). The predictor simulates the rate of growth reasonably well, but slightly over-predicts the ultimate height and wavelength after 42 minutes. The predictor also simulates the renewed growth after the change in wave conditions reasonably well, and predicts both the final height and wavelength reasonably accurately.

Figure 14 shows three separate experiments separated on the plots by gaps (for ease of plotting, these are not consecutive experiments). The first shows growth from an initially flat bed for wave inputs of  $T = 6s$  and  $D = 0.57m$ . The growth is very slow under these weak wave conditions, starting with about 40 minutes before vortex ripples begin to form on the flattened bed, during which time the ripple predictor was "switched off". After 40 minutes, the predictor accurately simulates both the growth rates and the final height and wavelength over the next 160 minutes. The second experiment is the one used in the latter part of Figure 13, but with the starting ripple height and wavelength set in the predictor to the *observed* initial values. Likewise, the third experiment is the same as the latter part of Figure 12, with the predictor started from *observed* values. The correspondence of the predictions and observations are improved in these cases compared with Figures 13 and 12, where the predictor used its own *predicted* initial values from the end of the prior experiments.

The performance of the time-evolving wave-ripple predictor is thus reasonably good. It predicts the rate of change quite accurately (although the tests are for the data-set against which it was calibrated). It also gives acceptably good predictions of the

equilibrium ripple height and wavelength. Some of the deviations may be due to the orbital velocities in the experiments being strongly asymmetrical, which the predictor was not specifically designed for.

## 7.2 TEST WITH CURRENT-RIPPLE “TIDAL” DATA

The expressions for ripple evolution were derived in Section 5.2 using only the data of Baas (1993) for the growth of ripples from an initially flat bed. It has been tested against the more realistic case of the evolution of ripples under continuously changing currents, using an independent data-set from the tidally reversing flume experiments of Whitehouse et al (1998). These started with an initially flat bed, and measured the ripple development over three tidal cycles (37.5 hours). The six half-cycles are denoted as 1 to 6 in the commentary on the results given below. Here we have used the current speed measured at a height of 0.10m in the flume to drive the current-induced ripple predictor. The equilibrium height and wavelength are given by Eqs (5.9a-d) and (5.10). The time evolution is obtained by a time-stepping integration of Eqs (5.11) and (5.12), in which  $T_c$  is given by Eq (5.15), and  $\beta_\eta$  and  $\beta_\lambda$  by Eqs (5.16) and (5.17) respectively.

It is seen in Figure 15 that the time-evolving ripple predictor manages to predict many of the features seen in the data: the growth from a flat bed, the effects of a slight asymmetry in the tidal cycle, and the partial wash-out that occurs at the peak of the negative (stronger) half-cycles. The following features can be seen. In the first half-cycle, the model starts to form ripples from an initially flat bed at about the right time. The predicted growth rate for ripple height is a bit too fast, but is about right for ripple length. The slight washout at maximum velocity, which briefly halts the growth, is predicted correctly. The slack-water dwell between the first and second half-cycles (when velocity is below threshold) occurs for about the right time, although the height and length are slightly over-estimated. The similar dwells at subsequent slack waters are predicted quite accurately for both height and length. After the first half-cycle, the predicted ripple height continues to grow slowly, in line with the observations, attaining almost the equilibrium value towards the end of the second, fourth and sixth half-cycles. The ripples start to wash out near the maximum velocity in half-cycles 1, 3 and 5, because the velocity is slightly larger than in half-cycles 2, 4 and 6. The model correctly predicts the reductions in height, but does not predict the increases in wavelength at these times (this is probably the start of a transition to dunes, which is not included in the model). At 25 hours the flume was switched off for over a month, during which time the ripple height slumped by about 6mm due to artificial disturbance. The standard run of the model does not (of course) reflect this, but in a test in which the height was re-set at 25.5 hours to the slumped value, the model re-built the height very much as observed. Thus the model reproduces most of the features seen in the observations. The predicted ripple heights are nearly always within 5mm of the observed values, and the wavelength generally within about 5cm. The predictor does not capture the increase in wavelength at peak flows, as this is associated with dune development, which the predictor is not designed to include.

Overall, the performance of the predictor is seen to be good. In fact, it even elucidates aspects of the measurements that were not apparent from the data alone.

## 7.3 TEST WITH WAVE-PLUS-CURRENT SYNTHETIC DATA

A test was made of the full wave-plus-current predictor to check that it can predict the features intended, such as ripple growth and decay, wash-out, frozen ripples, and



switching from wave-dominated to current-dominated conditions (and vice versa). A time-series of waves and currents was synthesised in which:

- Sediment  $d_{50} = 0.2\text{mm}$
- Water depth = 10m (constant)
- Wave heights vary sinusoidally between 0m (calm) and 2m (storm) with a period of 120 hours (5 days) between storms
- Wave period varies sinusoidally between 4s and 8s in line with heights
- Wave direction varies sinusoidally between  $80^\circ\text{N}$  and  $140^\circ\text{N}$  in line with heights
- Current speed varies sinusoidally with amplitude  $0.8\text{ms}^{-1}$  and reverses rectilinearly between  $90^\circ\text{N}$  and  $270^\circ\text{N}$ , with period 12 hours (tidal)
- Bio-degradation switched OFF
- Initial values of ripple height, wavelength and orientation are set to 0.02m, 0.2m and  $100^\circ\text{N}$ .

The resulting ripple evolution repeats with a 5-day period (Fig 16). The following features can be seen. After an initial rapid transient at the start of Day 0, ripples of height 0.017m, wavelength 0.13m and tidally oscillating orientation are formed under the current-dominant conditions while the waves are weak. At the peak velocity of each tidal half-cycle, the ripple height reduces to 0.008m due to partial wash-out, then recovers back to 0.017m as the current speed drops. This behaviour repeats for four tidal half-cycles until the wave heights pick up at the start of Day 1.

From Day 1.0 to Day 1.5, there are alternating periods of wave dominance and current dominance, with the ripple height, wavelength and orientation all varying accordingly. At about Day 1.5 the waves assert their dominance, creating ripples of height 0.032m, wavelength 0.22m and orientation  $110^\circ\text{N}$ . As the waves become larger (increasing storm), the ripples progressively start to wash out, reducing the height to 0.015m and the wavelength to 0.15m. At the same time, the orientation of the ripples swings round from  $110^\circ\text{N}$  to  $140^\circ\text{N}$ , following the wave direction. As the waves then decrease (waning storm), the ripple height and wavelength recover to 0.032m and 0.22m, and the orientation swings back from  $140^\circ\text{N}$  to  $110^\circ\text{N}$ , again following the wave direction. At Day 3.5, another period of alternating wave and current dominance ensues, until from Day 4.0 to 5.0 the current takes charge and the ripples behave in the same way as at the start. From Day 5 to Day 10 the pattern repeats.

All the changes take place relatively quickly, because the maximum wave and current conditions are both strong. Tests with other values of the inputs show different behaviour (not illustrated). For example, reducing the peak wave height to 0.5m makes the ripples mainly current-dominated, with waves only taking over around their maximum heights. Reducing the peak current to  $0.5\text{ms}^{-1}$  (with maximum  $H = 2\text{m}$ ) gives a largely wave-dominated picture with no current-induced wash-out. Setting peak current to  $0.41\text{ms}^{-1}$  and peak wave height to 0.5m (both just above threshold) gives a very slowly changing pattern, sometimes current-dominated and sometimes wave-dominated, and not fully established by the end of 5 days, so the second 5-day cycle looks very different from the first. All the tests resulted in the behaviour expected.

## 7.4 TEST WITH WAVE-PLUS-CURRENT FIELD DATA

It was originally intended that the full Mark 2 Ripple Predictor would be tested, and if necessary re-calibrated, against data obtained from the ONR field programs SAX99 and SAX04. It subsequently transpired that the SAX99 data comprised only “frozen ripples”, for which the wave and current conditions at the time of their formation

occurred before the measurement period. Although this demonstrates the importance of ripple predictors including the “frozen ripples” effect, it was not possible to test the predictor without knowing the foregoing conditions. The SAX04 data appear to be eminently suitable for test purposes, but were not at a stage to be made available within the present contract.

Instead, as a substitute, a set of measurements at hourly intervals for 11 months of waves, currents and water depths recorded on a sea-bed instrumented frame at a site off Teignmouth on the south coast of England has been used. This was measured by HR Wallingford as part of the EU collaborative research project COAST3D, and is described fully in Whitehouse (2004). However, the ripple geometries at the recording station were not measured, so the data can only be used to test whether the predictor gives plausible results. An approximately two-month section of data from 8 July to 9 September 1999 has been selected as a test-case, which includes two storms with calm periods in between, and four spring-neap cycles of water levels and tidal currents. The inputs are:

- Sediment  $d_{50} = 0.145\text{mm}$
- Water depth varying tidally (and with spring-neap variation) between about 3m and 7m
- Wave height ( $H_{1/10}$ ) reaching about 2m in two storms each of duration about 5 days, and reaching 0.5m to 1.1m in four minor storms, with  $H_{1/10} < 0.5\text{m}$  in the rest of the time
- Wave period ( $T_{1/10}$ ) generally between 4s and 10s, but occasionally reaching 14s
- Wave direction from offshore sector, generally between East and South-east ( $90^\circ\text{N}$  to  $135^\circ\text{N}$ )
- Current speed varying tidally up to about  $0.3\text{m.s}^{-1}$ , occasionally reaching  $0.4\text{m.s}^{-1}$  when wind-assisted
- Current direction generally rotating clockwise
- There is a break at Day 227 for servicing of instruments
- Days are counted from 1 January 1999.

Bio-degradation was switched OFF in the predictions, and initial ripple heights, length and orientation were set to 0.02m, 0.2m and  $100^\circ\text{N}$ . The resulting predictions (Figure 17) demonstrate a number of features. The ripples are almost entirely wave-generated. On the few occasions that the current dominates, it is so weak that it has little or no effect on the pre-existing ripples. Small waves in days 189 to 206 produce ripples with heights between 0.014 and 0.023m, wavelengths between 0.09 and 0.16m and orientations between  $90^\circ$  and  $150^\circ\text{N}$ . There are long periods of frozen ripples, when neither the waves nor the current exceed the threshold of motion. The first storm, starting day 206, initially builds ripples, but then partially washes them out, with some periods of recovery near low water when the wave heights are reduced. As the storm wanes, the ripple height and length grow to about 0.023m and 0.15m respectively. From days 210 to 232 the ripples respond to minor storms. The second major storm (days 233 to 237) partially washes out the ripples, which recover by day 235, and the ripples re-grow during the waning storm. From days 239 to 245 neither the waves nor the currents are strong enough to alter the ripples, which remain frozen. Minor storms in the last 6 days re-activate the ripples. The main features expected of wave-generated ripples thus appear to be (at least qualitatively) predicted correctly.

Further tests have been made by scaling the measured Teignmouth inputs.

*Stronger currents and weaker waves (Figure 18).* The depths were doubled (weakening the wave orbital velocities) and the current speeds were also doubled. Most of the time the ripples are current-generated (and without any wash-out), giving constant height = 0.015m, constant length = 0.12m, and alternating orientations. During the two major storms, and to a lesser extent the minor storms, the ripple height, length and orientation become wave-related.

*Biodegradation switched ON (Figure 19).* The biodegradation half-life  $T_{b,1/2}$  was set to 50 hours (corresponding to  $T_b = 72$  hours), and the residual bio-roughness was set to 5mm. Whenever the physical ripple growth is small or zero, the pre-existing ripple height decays due to biological activity. The “ripple height” does not decrease below 5mm, because of the residual bio-roughness. The predicted length and orientation are not affected in these periods.



## 8. *Conclusions*

A time-evolving sea-bed ripple predictor has been developed, based on a mixture of European and North American data and understanding. It predicts the time-varying ripple heights, lengths and orientations in sandy sediments under the action of waves and currents. It takes account of evolution (history effect), threshold-of-motion effects (frozen ripples), wash-out effects (leading to flat bed), and biological effects (bio-degradation).

Detailed achievements are:

- Digest of source publications (Report TR 150, Soulsby and Whitehouse, 2005)
- Data-base of ripple geometries and driving conditions (Report TR 150)
- Statistical analyses of ripple heights and wavelengths (Report TR 150)
- Made an “Intercomparison of intercomparisons” – 24 intercomparison papers were analysed, which overall compared 28 ripple prediction methods (for wave and/or current-generated ripples) with (subsets of) 84 data-sets. There is a need to make a definitive test of all predictors against all data
- Devised Mark 1 Ripple Predictor for equilibrium ripples under (a) waves, (b) currents
- Devised Mark 2 Ripple Predictor for the time-evolution of ripples
- Tested Mark 2 Ripple Predictor against laboratory and field data-sets.

The Mark 2 Ripple Predictor gave good agreement with quasi-full-scale laboratory measurements of ripple growth and decay due to (a) changing wave conditions, (b) changing current conditions. The tests against field data were only qualitative, and tests against field data with time-series of ripple measurements were not possible. Tests against SAX04 data await the release of that data in the future. The data used to derive and test the predictor covered sediments in the range of sizes  $0.095\text{mm} \leq d_{50} \leq 0.51\text{mm}$ . The predictor is, by extension, expected to give realistic results in the grain-size range 0.062mm to 0.7mm. Finer sediments will increasingly feel the effects of electro-chemical cohesion, which will limit ripple formation. Sediments coarser than about 0.7mm do not usually form ripples. No limits need to be imposed on water depths (on the continental shelf), wave conditions or current conditions, since the predictor is designed to cope with all values. The method used for predicting ripple orientation is an interim approach, limited in general to wave and current directions that do not pass anticlockwise through  $0^\circ\text{N}$ .

The Mark 2 Ripple Predictor is presented as a step-by-step algorithm in Appendix A, suitable for coding as a computer subroutine or program (not done in present work) in any preferred language and for interfacing to other (e.g. acoustic propagation) software packages.

An Excel spreadsheet has been created to test and demonstrate the predictor. It can be tailored to data-sets in different forms to the ones tested, but is not intended as an operational tool. Individual results can be fed into the Excel ripple visualiser developed in Phase 1 (Report TR 150).



## 9. *References*

- ABP (2004). Modelling moveable seabed roughness under random waves, Report R.1092 for Defra (UK) funded project EstProc ([www.estproc.net](http://www.estproc.net)).
- Ackers, P. (1964). Experiments on small streams in alluvium, Journal of Hydraulics Division, American Society of Civil Engineers 90, 1-37.
- Alexander, L.J.D. (1980). On the geometry of ripples generated by unidirectional open channel flows, Master's Thesis, Queens University, Kingston, Ontario, Canada, pp. 108.
- Allen, J.R.L. (1971). A theoretical and experimental study of climbing-ripple cross-lamination, with a field application to the Uppsala esker, Geogr. Annlr., A53, 157-187.
- Amos, C.L., Bowen, A.J., Huntley, D.A. and Lewis, C.F.M. (1988). Ripple generation under the combined influences of waves and currents on the Canadian continental shelf, Continental Shelf Research 8 (10), 1129-1153.
- Baas, J.H., (1993). Dimensional analysis of current ripples in recent and ancient depositional environments. PhD Thesis, University of Utrecht, The Netherlands, 199pp.
- Bagnold, R.A. (1946). Motion of waves in shallow water: Interactions between waves and sand bottoms, Proceedings of the Royal Society of London, Series A, 187, 1-15.
- Banks, N.L. and Collinson, J.D. (1975). The size and shape of small-scale current ripples: an experimental study using medium sand, Sedimentology, 22, 583-599.
- Barton, J.R. and Lin, P.N. (1955). A study of the sediment transport in alluvial channels, Civil Engineering Department, Report No. 55JRBZ, Colorado College, Fort Collins, USA.
- Carstens, M.R., Neilson, F.M. and Altinbilek, H.D. (1969). Bed forms generated in the laboratory under an oscillatory flow: Analytical and experimental study, US Army Corps of Engineers, Coastal Engineering Research Centre, Technical Memo. 28.
- Clifton, H.E. (1976). Wave-formed sedimentary structures: A conceptual model, in Beach and Nearshore Sedimentation, edited by Davies, R.A. and Ethington, R.L., Special Publication SEPM Society of Sedimentary Geology, 24, 126-148.
- Clifton, H.E. and Dingler, J.R. (1984). Wave-formed sedimentary structures and paleoenvironmental reconstruction, Marine Geology, 60, 165-198.
- Costello, W.R. and Southard, J.B. (1981). Flume experiments on lower-flow-regime bedforms in coarse sand, Journal of Sedimentary Petrology, 51, 849-864.
- Damgaard, J.S., Soulsby, R.L., Peet, A. and Wright, S. (2003). Sand transport on steeply sloping plane and rippled beds, Journal Hyd. Eng., ASCE, Vol.129, 706-719.
- Davies, T.R. (1971). Summary of experimental data for flume tests over fine sand, University of Southampton, Department of Civil Engineering, Report, CE/3/71, pp. 2.

- Dingler, J.R. (1974). Wave-formed ripples in nearshore sands, Ph.D. thesis, University of California, San Diego, pp. 136.
- Dingler, J.R. and Inman, D.L. (1976). Wave-formed ripples in near-shore sands, Proc. 15<sup>th</sup> Conference of Coastal Engineers, American Society of Civil Engineers, Honolulu, Hawaii.
- Doucette, J.S. (2002). Ripple grain size sorting and geometry prediction on low-energy sandy beaches, *Sedimentology*, 49, 483-503.
- Doucette, J.S. and O'Donoghue, T. (2005a). Transient ripple dynamics in oscillatory flows, Paper X in: "SANDPIT: Sand Transport and Morphology of Offshore Mining Pits", eds. Van Rijn, Soulsby, Hoekstra and Davies. Aqua Publications, The Netherlands. ISBN 90-800356-7-X.
- Doucette, J.S. and O'Donoghue, T. (2005b). Response of sand ripples to change in oscillatory flow, *Sedimentology* (in press).
- Du Toit, C.G. (1980). Velocities close to a bed of sand in oscillatory flow. D.Phil Thesis, University of Cambridge, 183 pp.
- Du Toit, C.G. and Sleath, J.F.A. (1981). Velocity measurements close to rippled beds in oscillatory flow, *Journal of Fluid Mechanics*, 112, 71-96.
- Engel, P. (1981). Length of flow separation over dunes, *Journal of Hydraulic Engineering*, American Society of Civil Engineers, 107, (HY10), 1133-1143.
- Faraci, C. and Foti, E. (2002). Geometry, migration and evolution of small-scale bedforms generated by regular and irregular waves, *Coastal Engineering*, 47, 35-52.
- Fok, A.T.K. (1975). On the development of ripples by an open channel flow, Master's thesis, Queens University, Kingston, Ontario, Canada, pp. 73.
- Foti, E. and Faraci, C. (2003). Sea bed roughness variability in presence of a rippled bed. Report to EC collaborative research project SANDPIT (unpublished).
- Fredsøe, J. and Deigaard, R. (1992). *Mechanics of Coastal Sediment Transport*. World Scientific Publishing.
- Grant, W.D. and Madsen, O.S. (1982). Movable bed roughness in unsteady oscillatory flow, *Journal of Geophysical Research*, 87(C1), 469-481.
- Grasmeijer, B., (2002). Process-based cross-shore modelling of barred beaches, *Netherlands Geographical Studies* 302, Utrecht, The Netherlands, pp. 251.
- Grasmeijer, B.T. and Van Rijn, L.C. (1999). Transport of fine sands by currents and waves: III. Breaking waves over barred profile with ripples, *Journal of Waterway, Port, Coastal and Ocean Engineering*, 125 (2), 71-79.
- Grasmeijer, B.T., Kleinhans, M.G. (2004). Observed and predicted bed forms and their effect on suspended sand concentrations, *Coastal Engineering*, 51, 351-371.



Guy, H.P., Simons, D.B., and Richardson, E.V. (1966). Summary of alluvial channel data from flume experiments 1959-61, US Geological Survey Professional Paper 462-1.

Hanes, D.M., Alymov, V., Chang, Y.S. (2001). Wave-formed ripples at Duck, North Carolina, *Journal of Geophysical Research*, 106 (C10), 22575-22592.

Hayakawa, N., Tsujimoto, G. and Hashimoto, H. (1983). Velocity distribution and suspended sediment concentration over large scale ripples, *Coastal Engineering in Japan*, 26.

Horikawa, K. and Watanabe, A. (1967). A study on sand movement due to wave action, *Coastal Engineering in Japan*, 10, 39-57.

Horikawa, K. and Watanabe, A. (1968). Laboratory study on oscillatory boundary layer flow, *Coastal Engineering in Japan*, 11, 13-28.

Hume, T.M., Green, M.O. and Oldman, J.W. (1999). What happens at the seabed off a headland during a tropical cyclone, paper presented at Coastal Sediments '99, American Society of Civil Engineering, Reston, Va.

Inman, D.L. (1957). Wave-generated ripples in nearshore sands, US Army Corps of Engineers, Beach Erosion Board, Technical Memo 100.

Inman, D.L. and Bowen, A.J. (1963). Flume experiments on sand transport by waves and currents, in *Coastal Engineering, Proceedings of the 8<sup>th</sup> Conference*, American Society of Civil Engineering, New York, pp. 137-150.

Jopling, A. and Forbes, D.L. (1979). Flume study of silt transportation and deposition, *Geogr. Annlr.*, 61A, 67-85.

Kennedy, J.F. (1961). Further laboratory studies of the roughness and suspended load of alluvial streams, California Institute of Technology, Pasadena, Report No. KH-4-3, pp. 36.

Kennedy, J.F. and Falcon, M. (1965). Wave-generated sediment ripples, Report 86, Massachusetts Institute of Technology, Massachusetts, pp. 55.

Khelifa, A. and Ouellet, Y. (2000). Prediction of sand ripple geometry under waves and currents, *Journal of Waterway, Port, Coastal and Ocean Engineering*, 126 (1), 14-22.

Kos'yan, R.D. (1988). On the dimensions of passive ripple marks in the nearshore zone, *Marine Geology*, 80, 149-153.

Lambie, J.M. (1984). An experimental study of the stability of oscillatory flow bed configurations, M.Sc. thesis, Massachusetts Institute of Technology, Cambridge, Massachusetts.

Lauchlan, C.S. (2004). Experimental investigation of bed-load and suspended-load transport over weirs, *Journal of Hydraulic Research*, Vol. 42 (5), pp549-555.

Laursen, E.M. (1958). The total sediment load of streams, *Journal of the Hydraulics Division, American Society of Civil Engineers*, 84, 1-36.

- Li, M.Z. and Amos, C.L. (1998). Predicting ripple geometry and bed roughness under combined waves and currents in a continental shelf environment, *Continental Shelf Research*, 18, 941-970.
- Li, M.Z., Wright, L.D. and Amos, C.L. (1996). Predicting ripple roughness and sand re-suspension under combined flows in a shoreface environment, *Marine Geology*, 130, 139-161.
- Lofquist, K.E.B., (1978). Sand ripple growth in an oscillatory flow water tunnel, US Army Corps of Engineers, Coastal Engineering Research Centre, Technical Paper No. 78-5.
- Lyne, V.D., Butman, B. and Grant, W. (1990). Sediment movement along the U.S. east coast continental shelf – I. Estimates of bottom stress using the Grant-Madsen model and near-bottom wave and current measurements, *Continental Shelf Research*, 10 (5), 397-428.
- Madsen, O.S. (1993). Sediment transport on the shelf, Parsons Lab., Massachusetts Institute of Technology, Massachusetts.
- Malarkey J. and Davies, A.G. (2003). A non-iterative procedure for the Wiberg and Harris (1994) oscillatory sand ripple predictor, *Journal of Coastal Research*, 19 (3), 738-739.
- Manohar, M. (1955). Mechanics of bottom sediment movement due to wave action, US Army Corps of Engineers, Beach Erosion Board, Technical Memorandum No. 75, pp. 121.
- Mantz, P.A. (1983). Semi-empirical correlations for fine and coarse cohesionless sediment transport, *Proceedings of the Institution of Civil Engineers, London*, Part 2, 1-33.
- Mathisen, P.P. (1989). Experimental study on the response of fine sediments to wave agitation and associated wave attenuation, M.Sc. thesis, Massachusetts Institute of Technology, Cambridge, Massachusetts.
- McLean, S.R. and Smith, J.D. (1986). A model for flow over two-dimensional bedforms, *Journal of Hydraulic Engineering*, 112, 300-317.
- Miller, M.C. and Komar, P.D. (1980). Oscillation sand ripples generated by laboratory apparatus, *Journal of Sedimentary Petrology*, 50 (1), 183-192.
- Mogridge, G.R. and Kamphuis, J.W. (1972). Experiments on bed form generation by wave action, *Proceedings 13<sup>th</sup> Coastal Engineering Conference*, American Society of Civil Engineers, Vancouver B.C., Canada, Vol II, pp. 1123-1142.
- Mogridge, G.R., Willis, D.H. and Davies, M.H. (1993). Wave-generated bedform geometry and prediction methods, National Research Council Canada, Technical Report 03.
- Mogridge, G.R., Davies, M.H. and Willis, D.H. (1994). Geometry prediction for wave-generated bedforms, *Coastal Engineering*, 22, 255-286.

- Nelson, J.M. and Smith, J.D. (1989). Mechanics of flow over ripples and dunes, *Journal of Geophysical Research*, 94 (C6), 8146-8162.
- Nielsen, P. (1979). Some basic concepts of wave sediment transport, Technical University of Denmark, Institute of Hydrodynamics and Hydraulic Engineering, Series Paper No. 20, pp. 160.
- Nielsen, P. (1981). Dynamics and geometry of wave-generated ripples, *Journal of Geophysical Research*, 86(C7), 6467-6472.
- Nielsen, P. (1992). Coastal bottom boundary layers and sediment transport, *Advanced Series on Ocean Engineering* 4, World Scientific, Singapore, 324.
- Nieuwjaar, M. and Kaay, Th. van der. (1987). Sediment Concentrations and Sediment Transport in case of Irregular Non-Breaking Waves with a Current, Delft University, Civil Engineering, Delft, The Netherlands.
- O'Donoghue, T. and Clubb, G.S., (2001). Sand ripples generated by regular oscillatory flow, *Coastal Engineering*, 44, 101-115.
- O'Donoghue, T., Doucette, J.S., van der Weerf, J.J. and Ribberink, J.S. (2005). Flow tunnel measurements of full-scale ripples in oscillatory flow, Paper V in: "SANDPIT: Sand Transport and Morphology of Offshore Mining Pits", eds. Van Rijn, Soulsby, Hoekstra and Davies. Aqua Publications, The Netherlands. ISBN 90-800356-7-X.
- Pratt, C.J. and Smith, K.V.H. (1972). Ripple and dune phases in a narrowly graded sand, *Journal of Hydraulics Division, American Society of Civil Engineers*, 98, 859-874.
- Ribberink, J. and Van Rijn, L.C. (1987). Influence of wave-asymmetry and wave-irregularity on time and bed averaged sediment conditions, Delft Hydraulics, Report H186-00-1, Delft, The Netherlands.
- Ribberink, J.S. and Al-Salem, A.A. (1994). Sediment transport in oscillatory boundary layers in cases of rippled beds and sheet flow, *Journal of Geophysical Research*, 99(C6), 12707-12727.
- Rosengaus, M. (1987). Experimental study on wave generated bedforms and resulting wave attenuation, Ph.D. thesis, Massachusetts Institute of Technology, Cambridge, Massachusetts.
- Sakakiyama, T., Shimizu, T., Kajima, R., Saito, S. and Maruyama, K. (1985). Sand ripples generated by prototype waves in a large wave flume, *Coastal Engineering in Japan*, 28.
- Shibayama, T. (1984). Sediment transport mechanism and two-dimensional beach transformation due to waves, D. Eng. Thesis, University of Tokyo, pp.159.
- Skafel, M.G. and Krishnappan, B.G. (1984). Suspended sediment distribution in wave field, *Journal of Waterway, Port, Coastal and Ocean Engineering*, 110 (2), 215-230.
- Sleath, J.F.A. (1976). On rolling-grain ripples, *Journal of Hydraulic Research*, 14 (1), 69-81.

- Sleath, J.F.A., (1984). *Sea Bed Mechanics*. Wiley, New York.
- Smith, D. and Sleath, J.F.A. (2005). Transient ripples in oscillatory flows, *Continental Shelf Research*, 25, 485-501.
- Soulsby, R.L. (1997). *Dynamics of Marine Sands – a Manual for Practical Applications*. Thomas Telford Publications, London, United Kingdom. ISBN 0 7277 2584 X.
- Soulsby, R.L. and Whitehouse, R.J.S. (2005). Prediction of ripple properties in shelf seas. Mark 1 Predictor. HR Wallingford Report TR150, February, 2005.
- Southard, J.B., Lambie, J.M., Federico, D.C., Pile, H.T. and Weidman, C.R. (1990). Experiments on bed configurations in fine sands under bidirectional purely oscillatory flow, and the origin of hummocky cross-stratification, *Journal of Sedimentary Petrology*, 60, 1-17.
- Steetzel, H.J. (1984). Sediment suspension in an oscillating water motion close to the sand bed (in Dutch), Coastal Engineering Department, Delft University of Technology, Delft, The Netherlands.
- Straub, L.G. (1939). Laboratory investigation of flume traction and transportation: A discussion, *Transactions of the American Society of Civil Engineers*, 65.
- Tanaka, H. and Dang, V.T. (1996). Geometry of sand ripples due to combined wave-current flows, *Journal of Waterway, Port, Coastal and Ocean Engineering*, 122 (6), 298-300.
- Tanaka, H. and Shuto, N. (1984). Sand movement due to wave-current combined motion, *Coastal Engineering in Japan*, 27, 179-191.
- Thorne, P.D. and Bell, P.S. (2002). Acoustic measurements of suspended sediments and bedform morphology during the main Egmond experiment, Paper G in Van Rijn *et al* (2002).
- Traykovski, P., Hay, A.E., Irish, J.D. and Lynch, J.F. (1999). Geometry, migration, and evolution of wave orbital ripples at LEO-15, *Journal of Geophysical Research*, 104 (C1), 1505-1524.
- Van den Berg, J.H. and Van Gelder, A. (1989). Scour and fill sequences in flows over very fine sand and silt, *Proceedings of the 4<sup>th</sup> International Conference on Fluvial Sedimentology*, Barcelona, Spain.
- Van Rijn, L.C. (1987). Mathematical modelling of morphological processes in the case of suspended sediment transport, Doc. Thesis, Delft University of Technology, Delft, The Netherlands.
- Van Rijn, L.C. (1989). *Handbook of Sediment Transport by Currents and Waves*, Delft Hydraulics, Delft, The Netherlands.
- Van Rijn L.C. (1993). *Principles of Sediment Transport in Rivers, Estuaries and Coastal Seas*. Aqua Publications, Amsterdam.

- Van Rijn, L.C. and HAVINGA, F.J. (1995). Transport of fine sands by currents and waves, *Journal of Waterway, Port, Coastal and Ocean Engineering*, 121 (2), 123-133.
- Van Rijn, L.C., Nieuwjaar, M.W.C., Van der Kaay, T., Nap, E. and Van Kampen, A. (1993). Transport of fine sands by currents and waves, *Journal of Waterway, Port, Coastal and Ocean Engineering*, 119 (2), 123-143.
- Van Rijn, L.C., Ruessink, B.G. and Mulder, J.P.M. (2002). COAST3D-Egmond. The behaviour of a straight sandy coast on the time scale of storms and seasons. End document. EC MAST project No MAS3-CT97-0086.
- Vanoni, V.A. and Brooks, N.H. (1957). Laboratory studies of roughness and suspended load of alluvial streams, California Institute of Technology, Sedimentation Laboratory, Report E-68, pp. 121.
- Vanoni, V.A. and Hwang, L.-S. (1967). Relation between bed forms and friction in streams, *Journal of Hydraulics Division, American Society of Civil Engineers*, 93, 121-144.
- Villaret, C. (1994). Ripples development and equivalent roughness measurements in unsteady flow conditions, Laboratoire National D'Hydraulique, Chatou, France. Report HE-42/94/16.
- Villaret, C. and Latteux, B. (1994). Étude expérimentale du transport de sable fin en suspension sous l'action de la houle et du courant, *La Houille Blanche*, Grenoble, France, 4, 35-40.
- Vongvisessomjai, S. (1984). Oscillatory ripple geometry, *Journal of Hydraulic Engineering*, 110 (3), 247-266.
- Vongvisessomjai, S., Munasinghe, L.C.J. and Gunaratna, P.P. (1987). Transient ripple formation and sediment transport. In: *Coastal Engng., Proc. 20<sup>th</sup> Int. Conf. Coastal Engng.*, (ed) Edge, B.L., Taipei, Taiwan, 9-14 Nov. 1986, Vol. 2, Chap. 120, ASCE, New York, pp. 1638-1652.
- Wheatcroft, R.A. (1994). Temporal variation in bed configuration and one-dimensional bottom roughness at the mid-shelf STRESS site, *Continental Shelf Research*, 14 (10/11), 1617-1190.
- Whitehouse, R.J.S. (2004). (Editor). Special Issue: Sediment Transport and Morphodynamics on a Complex Coastline, *Continental Shelf Research*, 24 (11).
- Whitehouse, R.J.S., Mitchener, H.J. and Soulsby, R.L. (1998). Laboratory experiments on ripple development and bed roughness in tidal flow. Data Report. Report TR66, October 1988, HR Wallingford, UK.
- Wiberg, P.L. and Nelson, J.M. (1992). Unidirectional flow over asymmetric and symmetric ripples, *Journal of Geophysical Research*, 97 (C8), 12,745-12,761.
- Wiberg, P.L. and Harris, C.K., (1994). Ripple geometry in wave-dominated environments, *Journal of Geophysical Research*, 99 (C1), 775-789.

Wilbers, A., (2004). The development and hydraulic roughness of subaqueous dunes. Netherlands Geographical Studies 323 (PhD-thesis), The Royal Dutch Geographical Society, Faculty of Geosciences, Utrecht University, The Netherlands, 227 pages.

Williams, J.J., Bell, P.S., Coates, L.E., Davies, A.G., Hardcastle, J.D., Humphrey, J.D., Moores, S.P., Van Rijn, L.C., Thorne, P.D. and Trouw, J. (1999). Laboratory evaluation of instrumentation used in field studies of wave-sediment interactions, in Coastal Engineering, Proceedings of the 26<sup>th</sup> International Conference on Coastal Engineering, ed. Edge, B.L., Copenhagen, Denmark, 1998, Vol. 3, ASCE, New York, 2423-2434.

Williams, J.J., Bell, P.S., Thorne, P.D., Trouw, K., Hardcastle, P.J. and Humphrey, J.D. (2000). Observed and predicted vertical suspended sediment concentration profiles and bedforms in oscillatory-only flow, Journal of Coastal Research 16 (3), 698-708.

Williams, J.J., Bell, P.S., Thorne, P.D., Metje, N. and Coates, L.E. (2004). Measurement and prediction of wave-generated suborbital ripples, Journal of Geophysical Research, 109, (Part 2, Sect. 3): article no. C02004.

Williams, J.J., Bell, P.S. and Thorne, P.D., (2005). Unifying large and small wave-generated ripples, Journal of Geophysical Research, 110, C02008.

Willis, D.H., Davies, M.H. and Mogridge, G.R. (1993). Laboratory observations of bedforms under directional irregular waves, Canadian Journal of Civil Engineering, accepted for publication in August 1993.

Yalin, M.S. (1985). On the determination of ripple geometry, Journal of Hydraulic Engineering, 111, 1148-1155.

Yalin, M.S. and Russell, R.C.H. (1962). Similarity in sediment transport due to waves, paper presented at 8<sup>th</sup> Coastal Engineering Conference, American Society of Civil Engineers, Mexico City.

Yalin, M.S. and Karahan, E. (1978). On the geometry of ripples due to waves, Proceedings of the 16<sup>th</sup> Coastal Engineering Conference, Hamburg, Vol II, 1776-1786.

*Tables*





**Table 1 Ripple prediction methods and intercomparison papers**

Predictor/Intercomparison	Code	Wave (W), Current (C) or both (W+C)	Equilibrium (E) or transient (T)	Predictor	Inter- comparison
Miller & Komar 1980	MK80	W	E	P	
Nielsen 1981	N81	W	E	P	
Grant & Madsen 1982	GM82	W	E	P	
Clifton & Dingler 1984	CD84	W	E	P	
Tanaka & Shuto 1984	TS84	W+C	E	P	I
Vongvisessomjai 1984	V84	W	E	P	I
Yalin 1985	Y85	C	E	P	I
McLean & Smith 1986	MS86	C	E	P	
Vongvisessomjai 1987	V87	W	T	P	
Nelson & Smith 1989	NS89	C	E	P	
Van Rijn 1989	VR89	W	E	P	
Lyne <i>et al</i> 1990	L90	W+C	E	P	I
Nielsen 1992	N92	W	E	P	I
Wiberg & Nelson 1992	WN92	C	E	P	I
Baas 1993	B93	C	E	P	I
Madsen 1993	Ma93	W	E	P	
Mogridge <i>et al</i> 1993	M93	W	E	P	I
van Rijn 1993	VRN93	W	E		I
van Rijn <i>et al</i> 1993	VR93	W	E	P	
Mogridge <i>et al</i> 1994	M94	W	E	P	I
Wiberg & Harris 1994	WH94	W	E	P	I
Li <i>et al</i> 1996	L96	W+C	E	P	
Tanaka & Dang 1996	TD96	W+C	E	P	
Li & Amos 1998	LA98	W+C	E		I
Traykovski <i>et al</i> 1999	T99	W	E		I
Khelifa & Ouellet 2000	KO00	W+C	E	P	I
Hanes <i>et al</i> 2001	H01	W	E		I
O'Donoghue & Clubb 2001	ODC01	W	E		I
Faraci & Foti 2002	FF02	W	E	P	I
Grasmeijer 2002	G02	W	E	P	
Foti & Faraci 2003	FF03	W	E		I
ABP 2004	ABP04	W	T	P	I
Grasmeijer & Kleinhans 2004	GK04	W	E		I
Williams <i>et al</i> 2004	W04	W	E		I
Doucette & O'Donoghue 2005a,b	DO05	W	T	P	I
O'Donoghue <i>et al</i> 2005	OD05	W	E		I
Smith & Sleath 2005	SS05	W	T	P	
van Rijn 2005	vR05	W	E		
Williams <i>et al</i> 2005	W05	W	E		I
Total Wave		28			
Total Current		5			
Total W+C		6			
Total Equilibrium			35		
Total Transient			4		
Total Predictors				28	
Total Intercomparisons					24

**Table 2 Data-sets used in intercomparisons of methods against data**

<b>Data-set</b>	<b>Code</b>	<b>Wave (W), Current (C) Or both (W+C)</b>	<b>Equilibrium (E) or transient (T)</b>	<b>Lab (L) or field (F)</b>
Straub 1939	S39	C	E	L
Bagnold 1946	B46	W	E	L
Barton & Lin 1955	BL55	C	E	L
Manohar 1955	M55	W	E	L
Inman 1957	I57	W	E	F
Vanoni & Brooks 1957	VB57	C	E	L
Laursen 1958	L58	C	E	L
Kennedy 1961	K61	C	E	L
Yalin & Russell 1962	YR62	W	E	L
Inman & Bowen 1963	IB63	W+C	E	L
Ackers 1964	A64	C	E	L
Kennedy & Falcon 1965	KF65	W	E	L
Guy <i>et al</i> 1966	G66	C	E	L
Horikawa & Watanabe 1967	HW67	W	E	L
Vanoni & Hwang 1967	VH67	C	E	L
Horikawa & Watanabe 1968	HW68	W	E	L
Carstens <i>et al</i> 1969	C69	W	E	L
Allen 1971	A71	C	E	L
Davies 1971	D71	C	E	L
Mogridge & Kamphuis 1972	MK72	W	E	L
Pratt & Smith 1972	PS72	C	E	L
Dingler 1974	D74	W	E	F
Banks & Collinson 1975	BC75	C	E	L
Fok 1975	F75	C	T	L
Dingler & Inman 1976	DI76	W	E	F
Sleath 1976	S76	W	E	L
Lofquist 1978	L78	W	E	L
Yalin & Karahan 1978	YK78	W	E	L
Jopling & Forbes 1979	JF79	C	E	L
Nielsen 1979	N79	W	E	L
Alexander 1980	A80	C	E	L
Du Toit 1980	DT80	W	E	L
Miller & Komar 1980	MK80	W	E	L
Costello & Southard 1981	CS81	C	T	L
Du Toit <i>et al</i> 1981	DT81	W	E	L
Engel 1981	E81	C	E	L
Nielsen 1981	N81	W	E	F
Hayakawa <i>et al</i> 1983	H83	W	E	L
Mantz 1983	M83	C	E	L
Lambie 1984	L84	W	E	L
Shibayama 1984	S84	W	E	L
Skafel & Krishnappan 1984	SK84	W	E	L
Steetzel 1984	SZ84	W	E	L
Tanaka & Shuto 1984	TS84	W+C	E	F + L
Vongvisessomjai 1984	V84	W	E	L
Sakakiyama <i>et al</i> 1985	S85	W	E	L
Yalin 1985	Y85	C	E	L

**Table 2 Data-sets used in intercomparisons of methods against data (continued)**

<b>Data-set</b>	<b>Code</b>	<b>Wave (W), Current (C) Or both (W+C)</b>	<b>Equilibrium (E) or transient (T)</b>	<b>Lab (L) or field (F)</b>
Nieuwjaar <i>et al</i> 1987	N87	W+C	E	L
Ribberink <i>et al</i> 1987	RB87	W	E	L
Rosengaus 1987	R87	W	E	L
van Rijn 1987	VR87	W	E	L
Vongvisessomjai 1987	V87	W	T	L
Kos'yan 1988	K88	W	E	F + L
Mathisen 1989	M89	W	E	L
Nelson & Smith 1989	NS89	C	E	L
Lyne <i>et al</i> 1990	L90	W+C	T	F
Southard <i>et al</i> 1990	S90	W	E	L
Nielsen 1992	N92	W	E	L
Wiberg & Nelson 1992	WN92	C	E	L
Baas 1993	B93	C	T	L
van Rijn <i>et al</i> 1993	vR93	W+C	E	L
Willis <i>et al</i> 1993	W93	W	E	L
Ribberink & Al-Salem 1994	RAS94	W	E	L
Villaret & Latteux 1994	VL94	W+C	E	L
Van Rijn & Havinga 1995	VRH95	W+C	E	L
Li & Amos 1998	LA98	W+C	E	F
Grasmeijer & Van Rijn 1999	GVR99	W	E	L
Hume <i>et al</i> 1999	H99	W	E	F
Traykovski <i>et al</i> 1999	T99	W+C	E	F
Williams <i>et al</i> 1999	W99	W	E	L
Khelifa & Ouellet 2000	KO00	W+C	E	L
Williams <i>et al</i> 2000	W00	W	E	L
Hanes <i>et al</i> 2001	H01	W	E	F
O'Donoghue & Clubb 2001	ODC01	W	E	L
Doucette 2002	D02	W	E	F
Faraci & Foti 2002	FF02	W	T	L
Thorne & Bell 2002	T02	W	E	L
Grasmeijer & Kleinhans 2004	GK04	W	E	F
Williams <i>et al</i> 2004	W04	W	E	L
Doucette & O'Donoghue 2005	DO05	W	T	L
O'Donoghue <i>et al</i> 2005	OD05	W	E	L
Smith & Sleath 2005	SS05	W	T	L
Williams <i>et al</i> 2005	W05	W+C	E	F
Total Wave		50		
Total Current		22		
Total W+C		11		
Total papers		83		
Total Equilibrium			75	
Total Transient			8	
Total Lab				71
Total Field				14

**Table 3 Predictors tested in listed intercomparison papers**

Predictor	MK80	N81	GM82	CD84	TS84	V84	Y84	Y85	MS86	NS89	VR89	N92	WN92	B93	M93	Ma93	VR93	M94	WH94	L96	TD96	KO00	FF02	G02	ABP04	DO05	Totals
Inter-comparison																											
TS84					x																						1
V84						x																					1
Y85							x																				1
L90							x																				2
N92		x																									1
WN92									x				x														3
B93								x						x													2
M93		x				x									x												3
VRN93		x									x																2
M94																		x									1
WH94		x																	x								3
LA98		x	x																x	x	x						4
T99	x	x	x	x								x								x							6
KO00	x	x																x			x	x					5
H01		x																	x								2
ODC01		x				x												x	x	x							4
FF02																							x				1
FF03												x					x		x	x			x	x			6
ABP04		x																x	x	x				x			4
GK04																	x										3
W04	x	x	x								x							x	x	x							6
DO05																										x	1
OD05		x																x	x								3
W05		x	x								x																3
Totals	3	13	7	1	1	3	3	1	1	1	3	3	1	1	1	1	1	7	9	1	1	1	2	1	1	1	

**Table 4 Data-sets used in listed intercomparison papers**

Dataset	S39	B46	BL55	M55	I57	VB57	L58	K61	YR62	IB63	A64	KF65	G66	HW67	VH67	HW68	C69	A71	D71	MK72	PS72	D74	BC75	F75	DI76	S76	
Inter-comparison																											
TS84																											
V84					x					x								x			x						
Y85			x			x																					
L90																											
N92					x				x								x										
WN92																											
B93	x					x	x	x			x		x		x				x		x						
M93		x		x					x			x		x				x								x	
VRN93					x													x									
M94		x		x					x			x		x				x			x					x	
WH94												x						x			x						
LA98																											
T99																											
KO00										x																	
H01					x																						
ODC01																											
FF02																											
ABP04																											
GK04																											
W04																											
DO05																											
OD05																											
SS05																											
W05																											
Totals	1	2	1	2	10	2	1	1	3	3	1	7	1	2	2	1	9	1	1	1	6	1	5	1	1	2	2

**Table 4 Data-sets used in listed intercomparison papers (continued)**

Dataset	L78	YK78	JF79	N79	A80	DT80	MK80	CS81	DT81	E81	N81	H83	M83	L84	S84	SK84	SZ84	TS84	V84	S85	Y85	N87	R87	vR87	K88	M89
Inter-comparison																										
TS84							x											x								
V84	x			x																						
Y85																					x					
L90																										
N92				x			x																			
WN92										x																
B93					x			x					x													
M93		x					x				x								x						x	
VRN93									x			x										x				
M94		x					x																		x	
WH94																										
LA98																										
T99																										
KO00				x													x									
H01											x															
ODC01																										
FF02																										
ABP04	x			x		x								x	x							x				x
GK04																										
W04																										
DO05																										
OD05																										
SS05																										
W05																										
Totals	2	2	1	4	1	1	4	1	1	1	2	1	1	1	1	1	1	1	1	1	1	1	1	1	2	1

**Table 4 Data-sets used in listed intercomparison papers (continued)**

Dataset	NS89	L90	S90	N92	WN92	B93	vR93	W93	RAS94	VL94	vRH95	LA98	GvR99	H99	T99	W99	KO00	W00	H01	ODC01	D02	FF02	T02	GK04
Inter-comparison																								
TS84																								
V84																								
Y85																								
L90		x																						
N92				x																				
WN92	x				x																			
B93						x																		
M93								x																
VRN93																								
M94																								
WH94			x																					
LA98												x												
T99															x									
KO00							x	x		x	x						x							
H01																			x					
ODC01																				x				
FF02																					x			
ABP04																x							x	
GK04							x				x		x						x					x
W04																								
DO05																								
OD05																								
SS05																								
W05																								
Totals	1	1	1	1	1	1	2	2	1	1	2	1	1	2	1	1	1	1	3	1	1	1	1	1

**Table 4 Data-sets used in listed intercomparison papers (continued)**

Dataset	W04	DO05	OD05	SS05	W05	Totals
Inter-comparison						
TS84						4
V84						8
Y85						4
L90						1
N92						9
WN92						3
B93						17
M93						16
VRN93						9
M94						13
WH94						6
LA98						1
T99						1
KO00						8
H01						4
ODC01						1
FF02						
ABP04						13
GK04						6
W04	x					4
DO05		x				1
OD05			x			1
SS05				x		1
W05					x	6
Totals	1	1	1	1	1	



**Table 5** Correspondence between predictors tested and data-sets used in listed intercomparison papers

Predictor	Dataset	MK80	N81	GM82	CD84	TS84	V84	Y85	MS86	NS89	vR89	L90	N92	WN92	B93	M93	vR93	M94	WH94	L96	TD96	KO00	FF02	ABP04	DO05	Totals
S39								x							x											2
B46		x					x									x										4
BL55								x																		1
M55		x					x									x										4
I57	x	x	x	x			x						x			x	x	x	x							10
VB57								x							x											2
K61								x							x											2
YR62		x					x									x										4
IB63	x	x				x	x											x								7
A64								x							x											2
KF65		x					x								x	x		x	x				x			7
G66								x							x											2
HW67		x					x									x										4
VH67								x																		1
HW68		x																								1
C69		x					x									x		x	x				x			8
A71								x							x											2
D71								x							x											2
MK72	x	x	x	x			x								x	x		x	x					x		9
PS72								x							x											2
D74		x					x													x						4
BC75								x							x											2
F75								x							x											2
DI76		x					x									x		x								4
S76		x					x									x		x								4
L78		x					x											x	x					x		5
YK78		x					x									x		x	x							4
JF79								x							x											2
N79	x	x					x											x	x					x		9
A80								x							x											2

**Table 5** Correspondence between predictors tested and data-sets used in listed intercomparison papers (continued)

Predictor	MK80	N81	GM82	CD84	TS84	V84	Y85	MS86	NS89	VR89	L90	N92	WN92	B93	M93	VR93	M94	WH94	L96	TD96	KO00	FF02	ABP04	DO05	Totals
DT80		x															x	x					x		4
MK80		x		x		x										x	x								5
CS81							x								x										2
DT81		x								x															2
E81								x					x												3
N81		x				x									x			x							4
H83		x							x																2
M83							x								x										2
L84		x															x	x					x		4
S84		x															x	x					x		4
SK84	x	x		x													x			x					6
SZ84		x								x															2
TS84				x																					1
V84		x				x									x										3
S85		x								x															2
Y85							x																		1
N87		x																							2
R87		x								x							x	x					x		4
RB87		x								x															2
VR87		x								x															2
K88		x				x									x		x								4
M89		x															x	x					x		4
NS89								x					x												3
L90			x								x														2
S90																		x							1
N92		x																							1
WN92								x					x												3
B93							x							x											2
VR93	x	x	x	x								x				x	x			x	x				9
W93	x	x		x	x	x									x		x			x	x				8
RAS94		x															x	x					x		4

**Table 5** Correspondence between predictors tested and data-sets used in listed intercomparison papers (continued)

Predictor	MK80	N81	GM82	CD84	TS84	V84	Y85	MS86	NS89	VR89	L90	N92	WN92	B93	M93	VR93	M94	WH94	L96	TD96	KO00	FF02	ABP04	DO05	Totals
VL94	x	x			x												x			x	x				6
VRH95	x	x	x		x							x					x			x	x				9
LA98		x	x															x	x						4
GvR99			x									x					x								3
H99	x	x	x							x							x	x							6
T99	x	x	x	x								x						x							6
W99		x															x	x					x		4
KO00	x	x			x												x			x	x				6
W00		x	x							x															3
H01		x	x							x		x						x							6
ODC01		x				x											x	x							4
D02		x	x							x															3
FF02		x			x												x			x	x				6
T02		x															x	x					x		4
GK04			x									x													3
W04	x	x	x							x							x	x							6
DO05																								x	1
OD05		x															x	x							3
W05		x			x												x			x	x				6
Totals	13	53	14	1	13	21	18	3	3	15	1	7	3	15	16	6	36	24	1	10	10	4	13	1	301

**Table 6 Prediction methods for ripple height and wavelength, and their functional dependence**

Method	Code	$\eta/\Lambda$ and $\lambda/\Lambda$ are functions of:
Nielsen (1981)	N81	$\Psi$
Grant and Madsen (1982)	GM82	$\theta'_w, D_*$
Van Rijn (1989)	VR89	$\Psi$
Madsen (1993)	Ma93	$(\theta'_w / D_*^{3/2})$
Mogridge <i>et al</i> (1994)	M94	$\Delta, \chi$
Wiberg and Harris (1994)	WH94	$\Delta$
Traykovski <i>et al</i> (1999)	T99	$\Delta$
Faraci and Foti (2002)	FF02	$\Psi, Re_w, \Delta$
Grasmeijer and Kleinhans (2004)	GK04	$\Psi$

**Table 7 References to prediction methods in text books and comparison papers (see Table 6 for codes)**

Reference source	N81	GM82	VR89	Ma93	M94	WH94	T99	FF02	GK04
<i>Text books</i>									
Sleath (1984)	×								
Nielsen (1992)	×								
Fredsøe and Deigaard (1992)	×								
Van Rijn (1993)	×		×						
Soulsby (1997)	×	×							
<i>Intercomparisons</i>									
Wiberg and Harris (1994)	×	×				×			
Traykovski <i>et al</i> (1999)	×					×	×		
Foti and Faraci (2003)	×			×	×	×		×	×
Grasmeijer and Kleinhans (2004)	×	×	×						
O'Donoghue <i>et al</i> (2005)	×				×	×			

## *Figures*



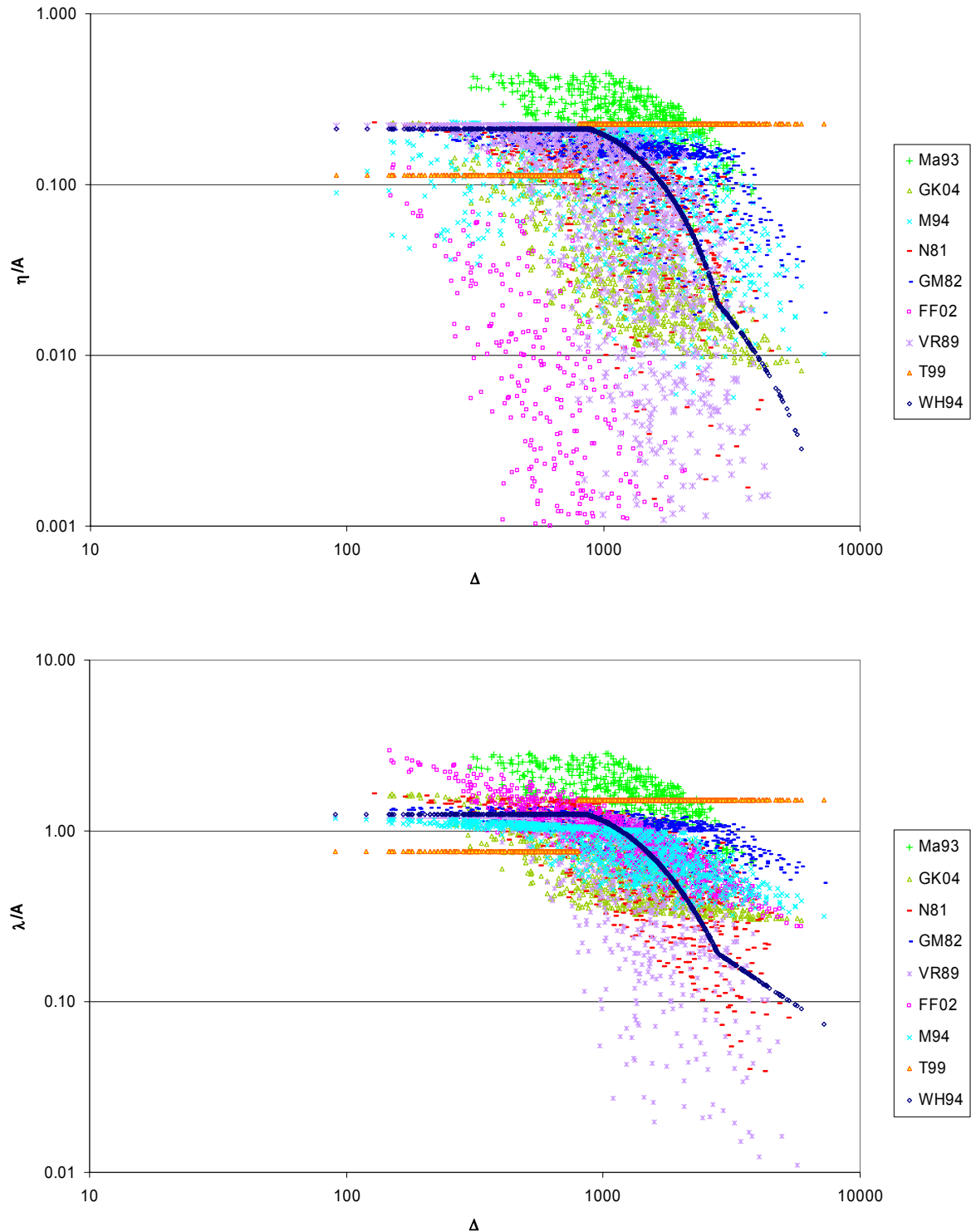


**Figure 1** *Wave ripple predictors with 1000 randomly distributed input parameters, plotted against  $\Delta$ . (a) height  $\eta$ , (b) length  $\lambda$*

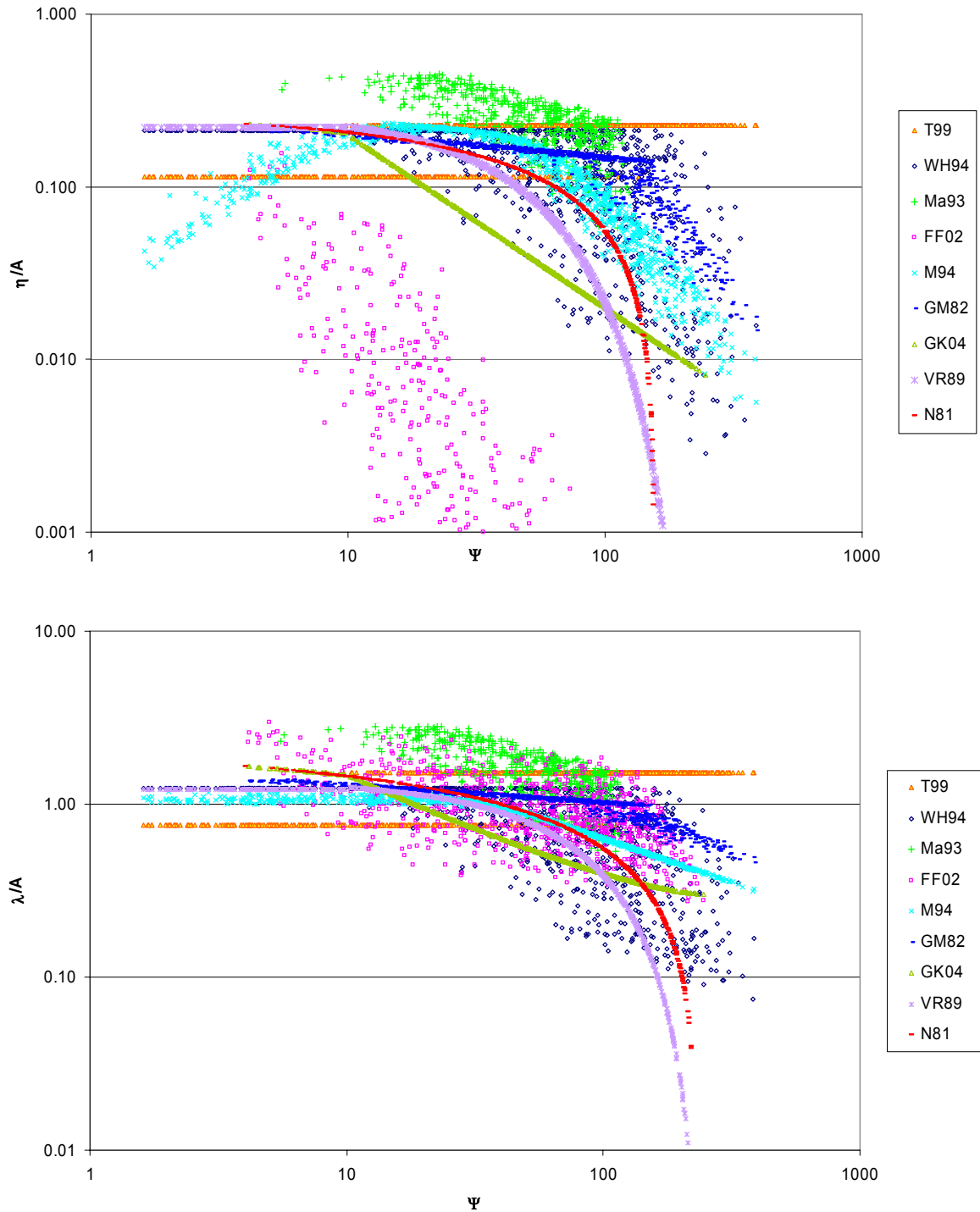


**Figure 2** *Wave ripple predictors with 1000 randomly distributed input parameters, plotted against  $\Psi$ . (a) height  $\eta$ , (b) length  $\lambda$*



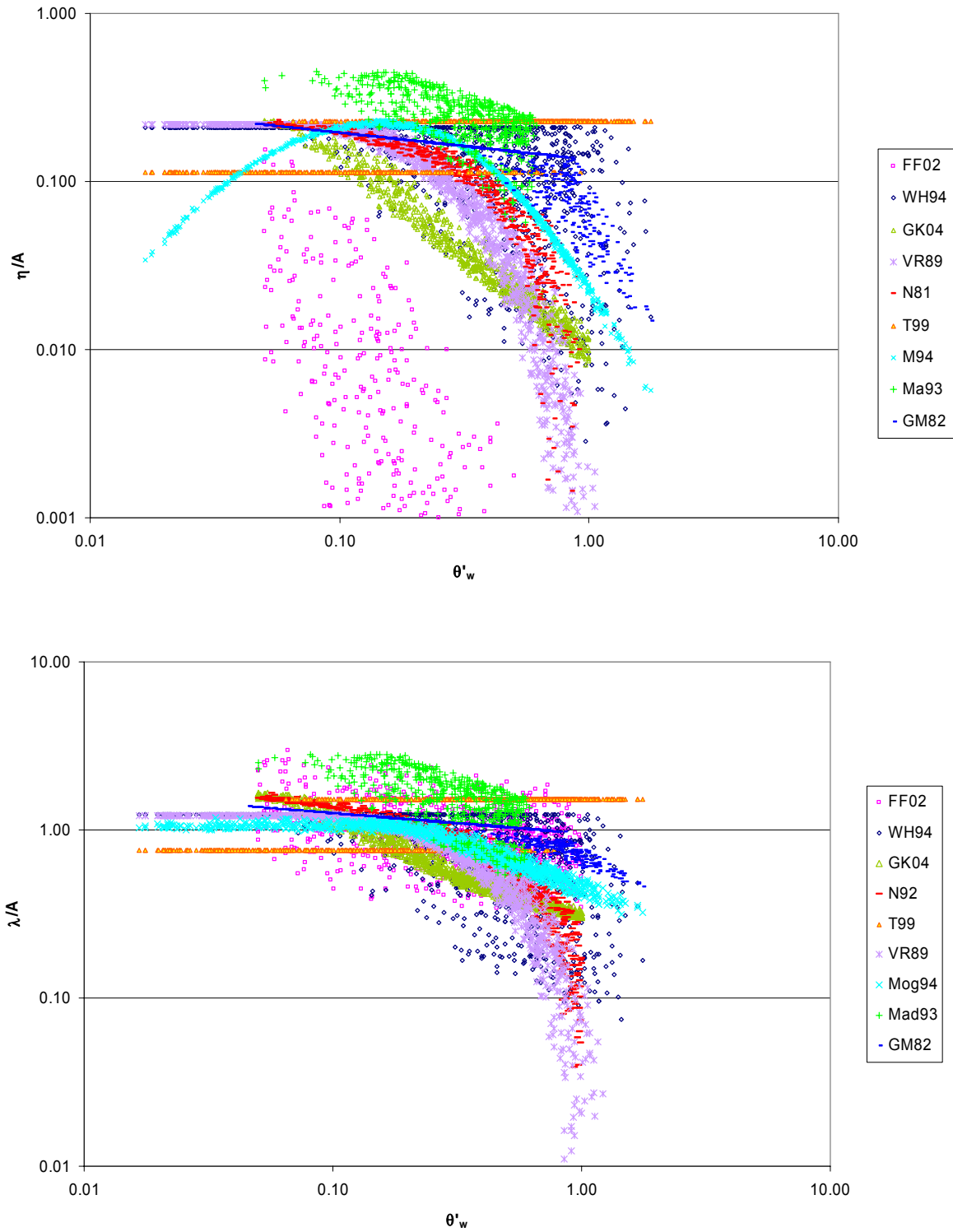


**Figure 3** *Wave ripple predictors with 1000 randomly distributed input parameters, plotted against  $\theta'_w$ . (a) height  $\eta$ , (b) length  $\lambda$*

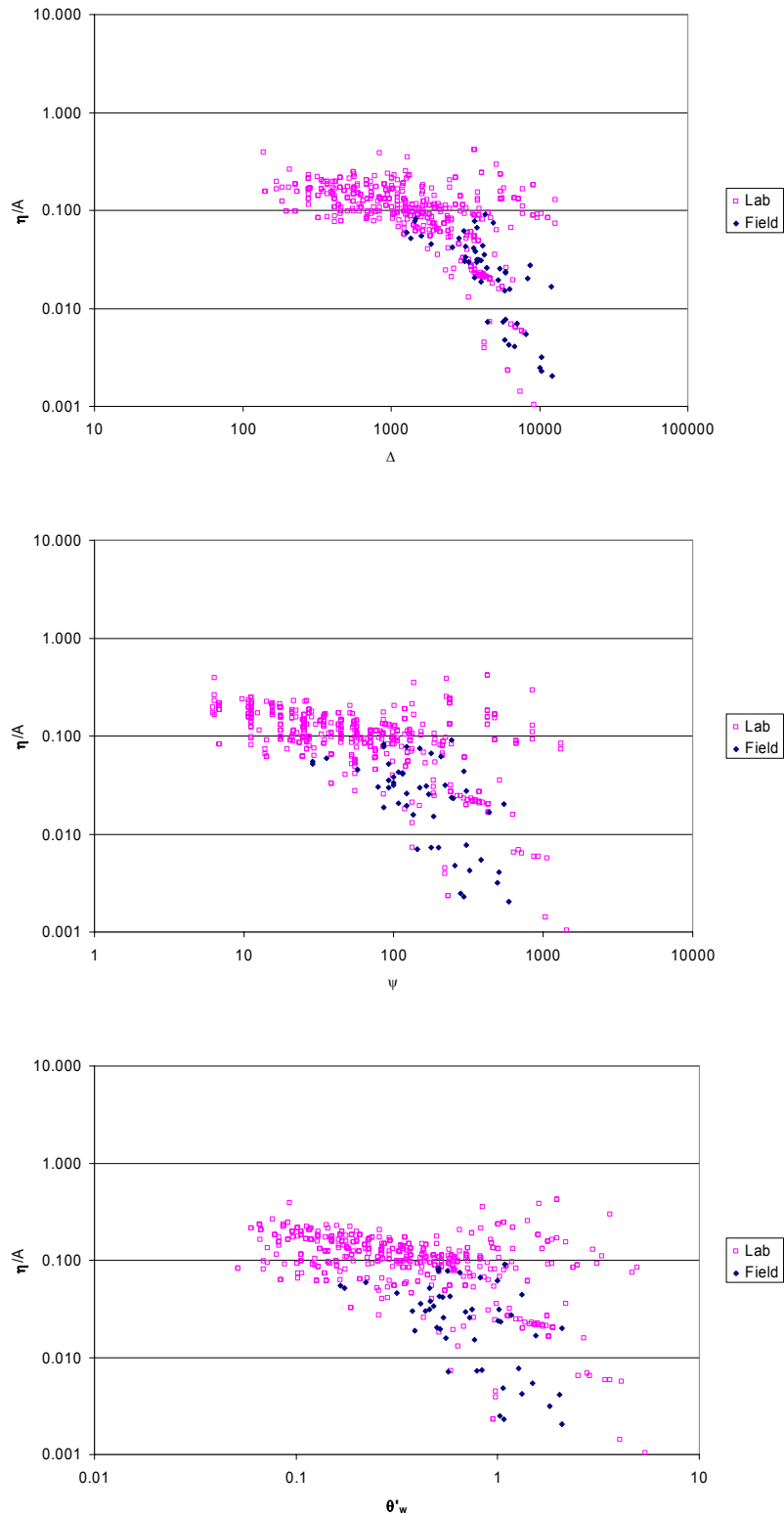


**Figure 4** *Non-dimensional ripple height  $\eta/A$  from data-base plotted against (a)  $\Delta$ , (b)  $\Psi$ , (c)  $\theta'_w$*

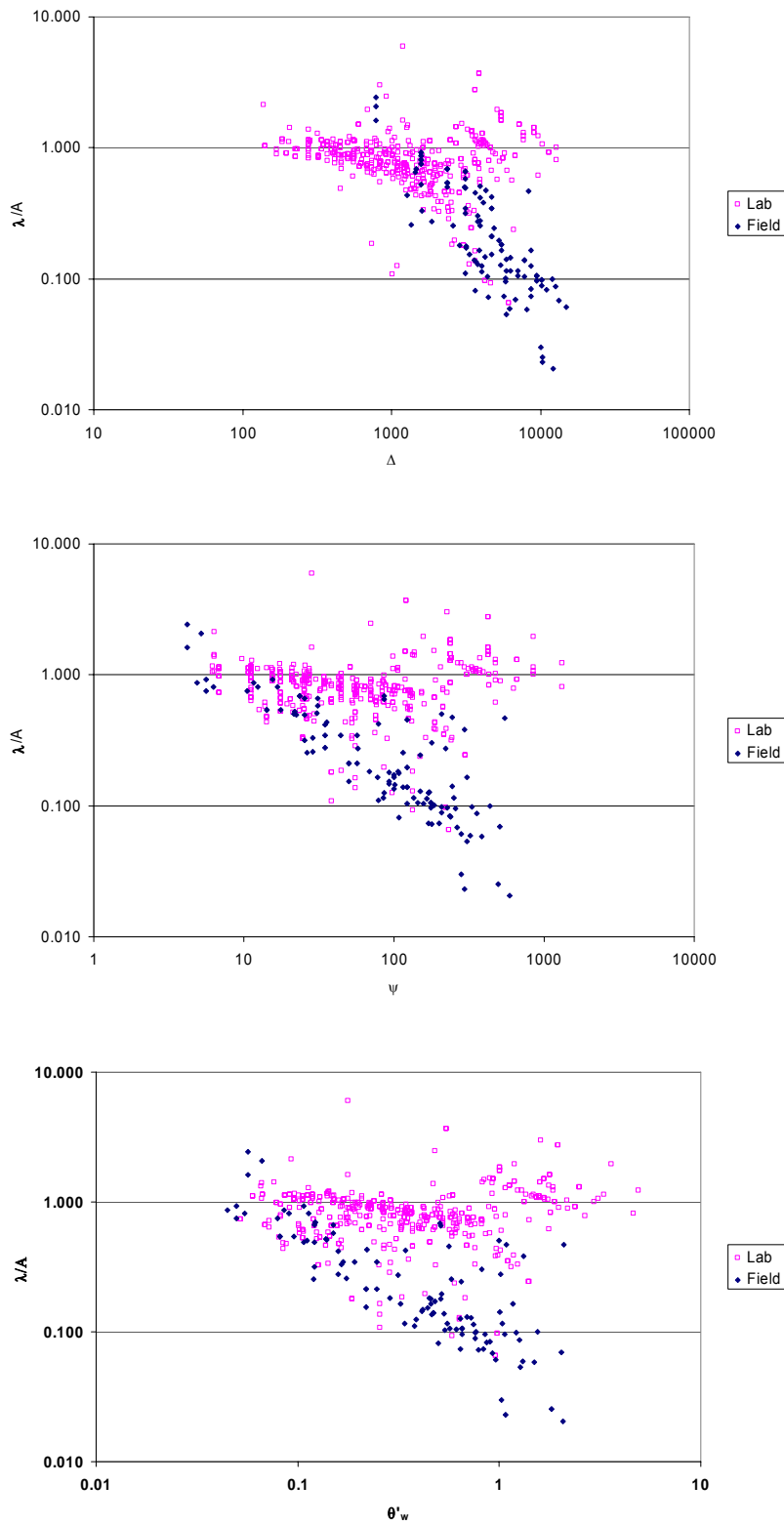


**Figure 5** *Non-dimensional ripple wavelength  $\lambda/A$  from data-base plotted against (a)  $\Delta$ , (b)  $\Psi$ , (c)  $\theta'_w$*

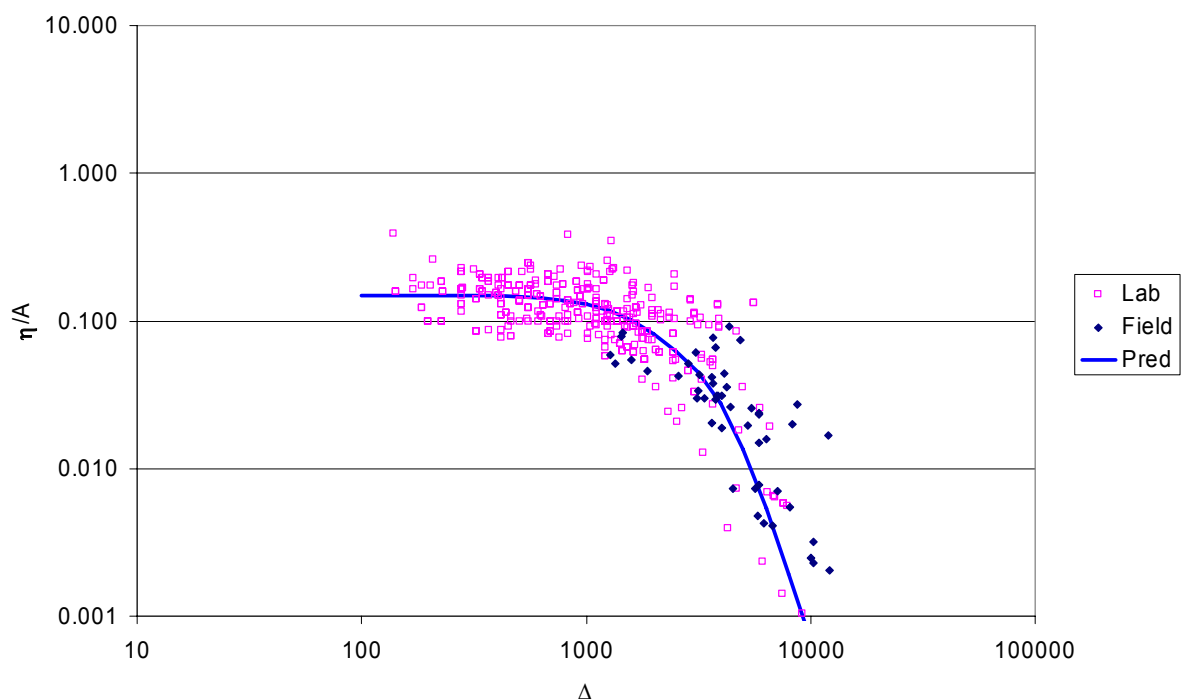


**Figure 6** *Test of Eq (4.2, 3) for ripple height against data-base*

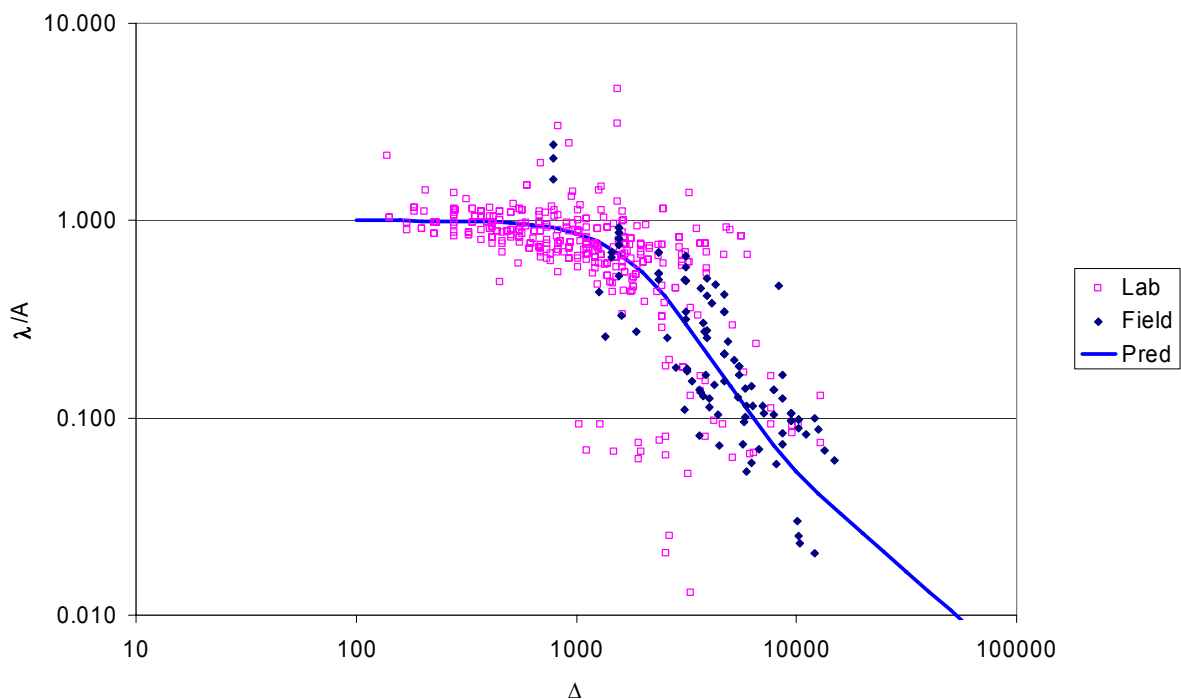


**Figure 7** *Test of Eq (4.1) for ripple wavelength against data-base*

## Ripple heights

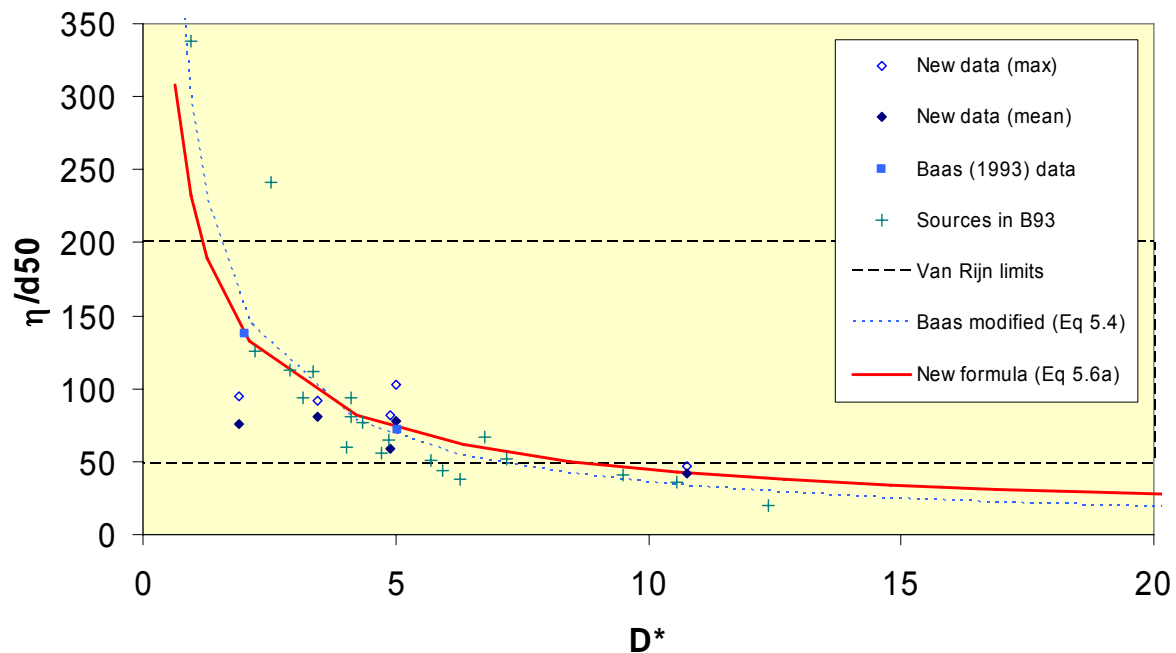


**Figure 8** Comparison of new formula for equilibrium ripple height (Eq 5.6a), and B93 (modified) formula (Eq 5.4), against data from various sources

New data is from Whitehouse et al (1998), Damgaard et al (2003), Lauchlan (2004) and Villaret (1994)

## Ripple lengths

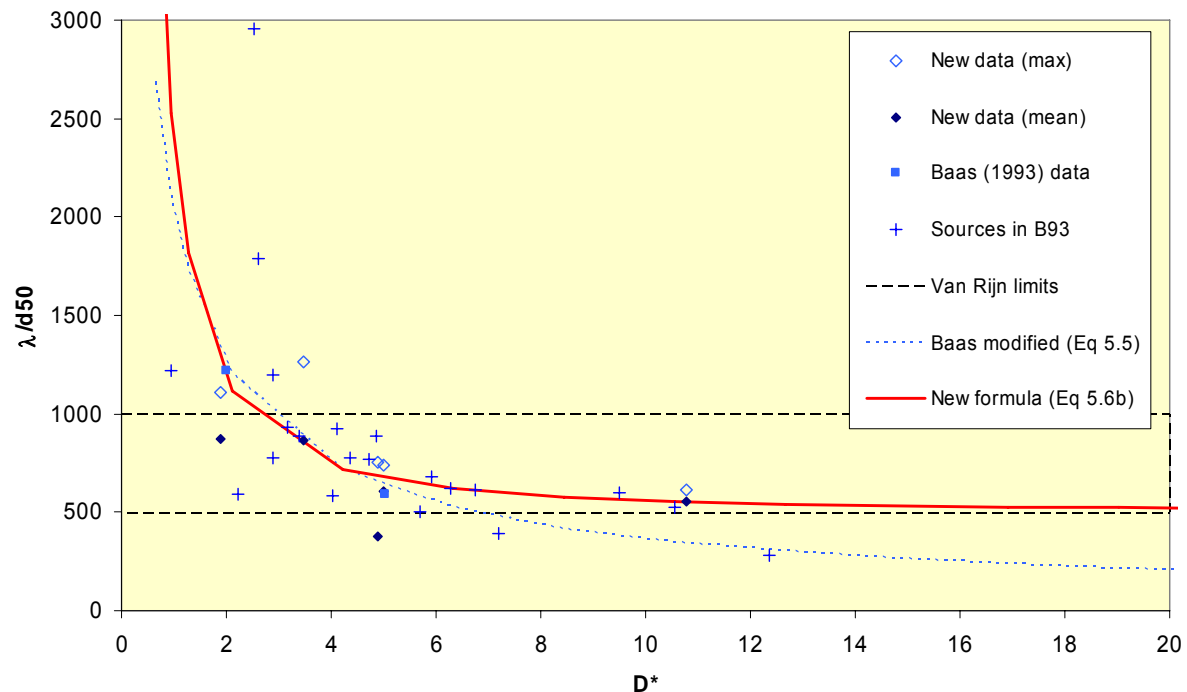


**Figure 9** Comparison of new formula for equilibrium ripple wavelength (Eq 5.6b), and B93 (modified) formula (Eq 5.5), against data from various sources

New data is from Whitehouse et al (1998), Damgaard et al (2003), Lauchlan (2004) and Villaret (1994)

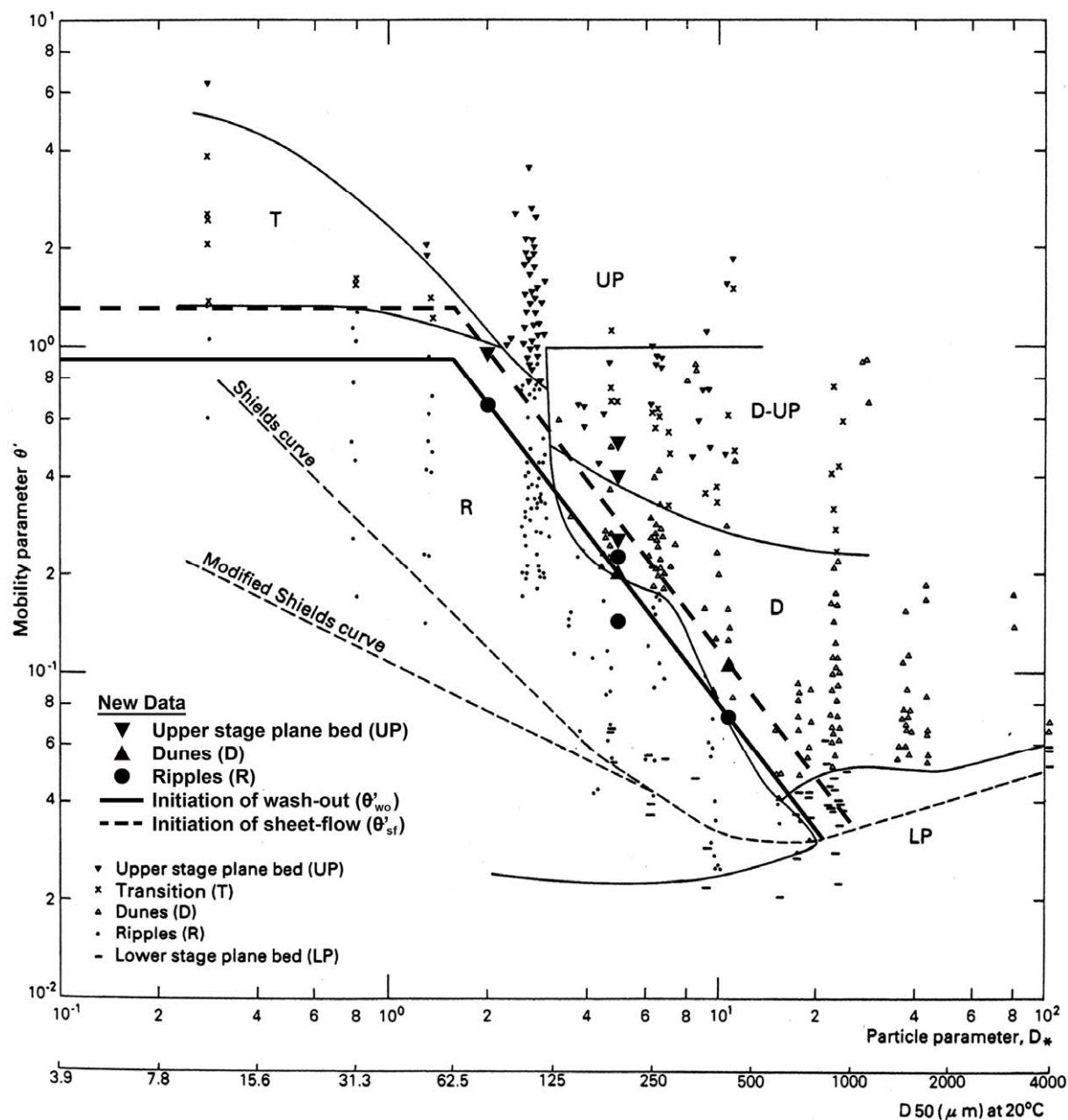


**Figure 10** *Bedform existence plot by Van den Berg and Van Gelder (1989), with proposed wash-out and sheet-flow limits superimposed. Additional new data from B93, WMS98 and DSPW03 is included*

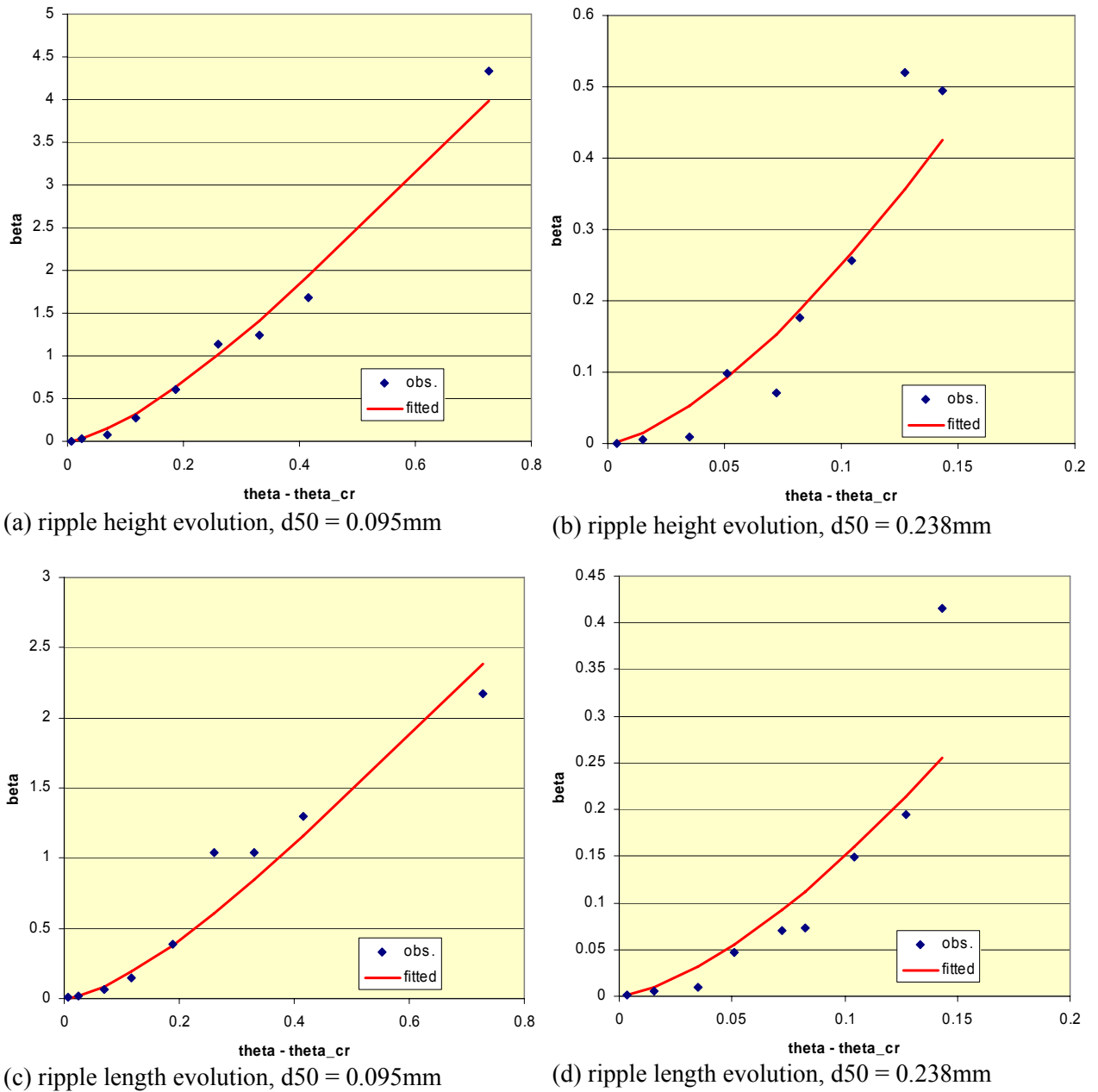


**Figure 11** Comparison of Eq (5.16) for ripple height evolution with the data of B93 for (a)  $d_{50} = 0.095\text{mm}$ , (b)  $d_{50} = 0.238\text{mm}$ ; and of Eq (5.17) for ripple wavelength evolution for (c)  $d_{50} = 0.095\text{mm}$ , (d)  $d_{50} = 0.238\text{mm}$

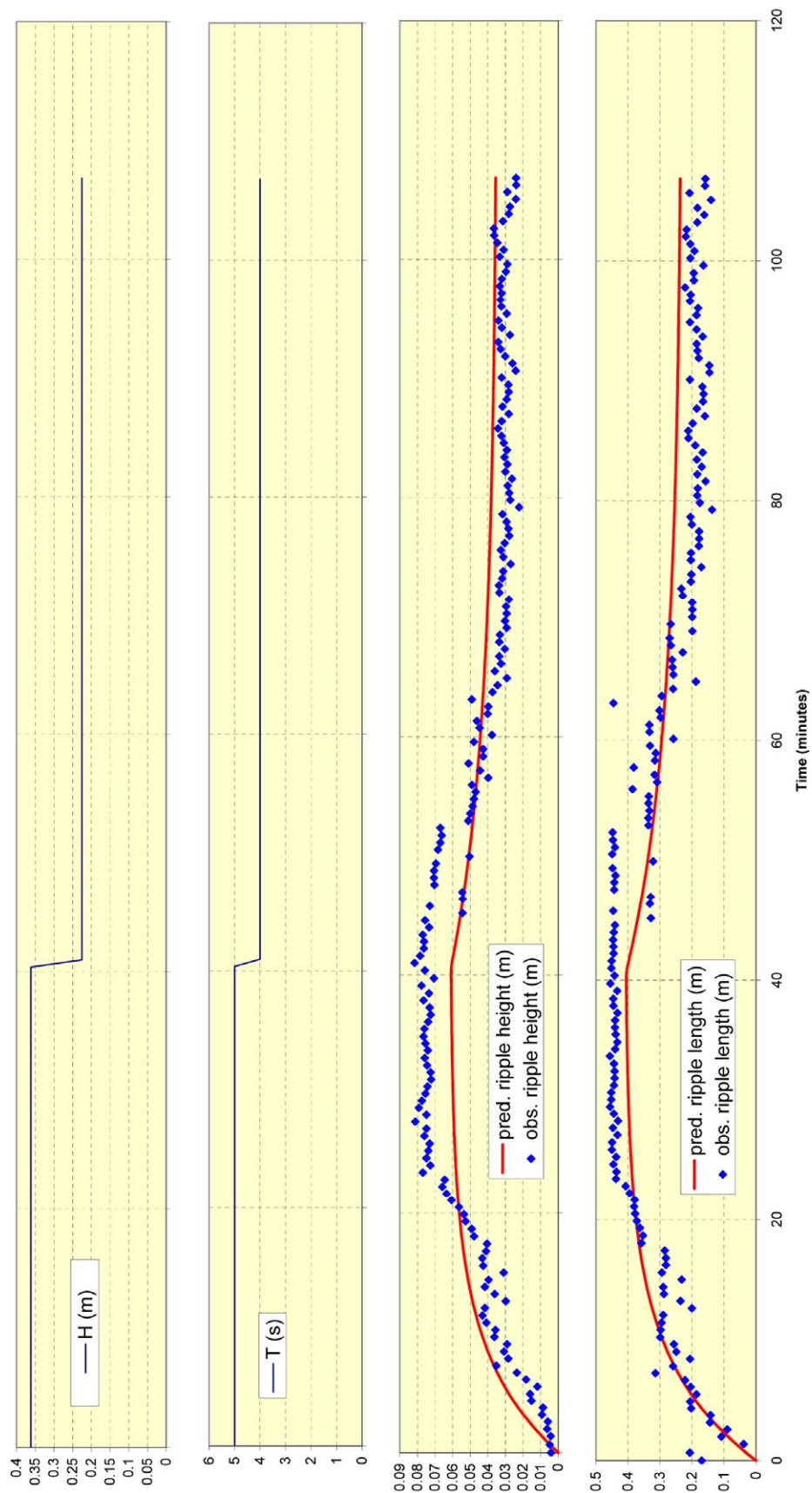


**Figure 12** Test of wave-ripple predictor against Doucette and O'Donoghue (2005) experiments – ripple growth and decay



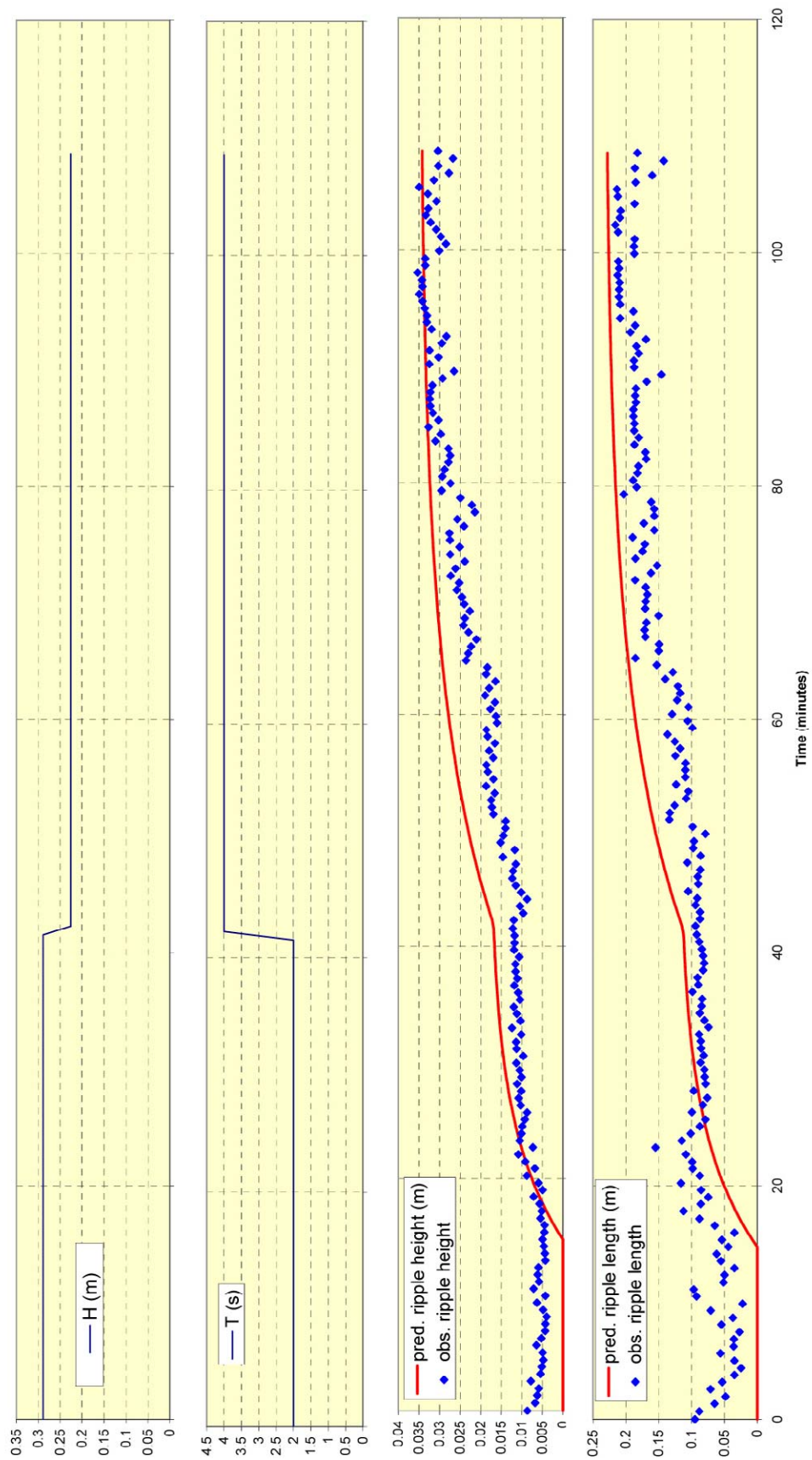


**Figure 13** *Test of wave-ripple predictor against Doucette and O'Donoghue (2005) experiments – ripple growth and further growth*

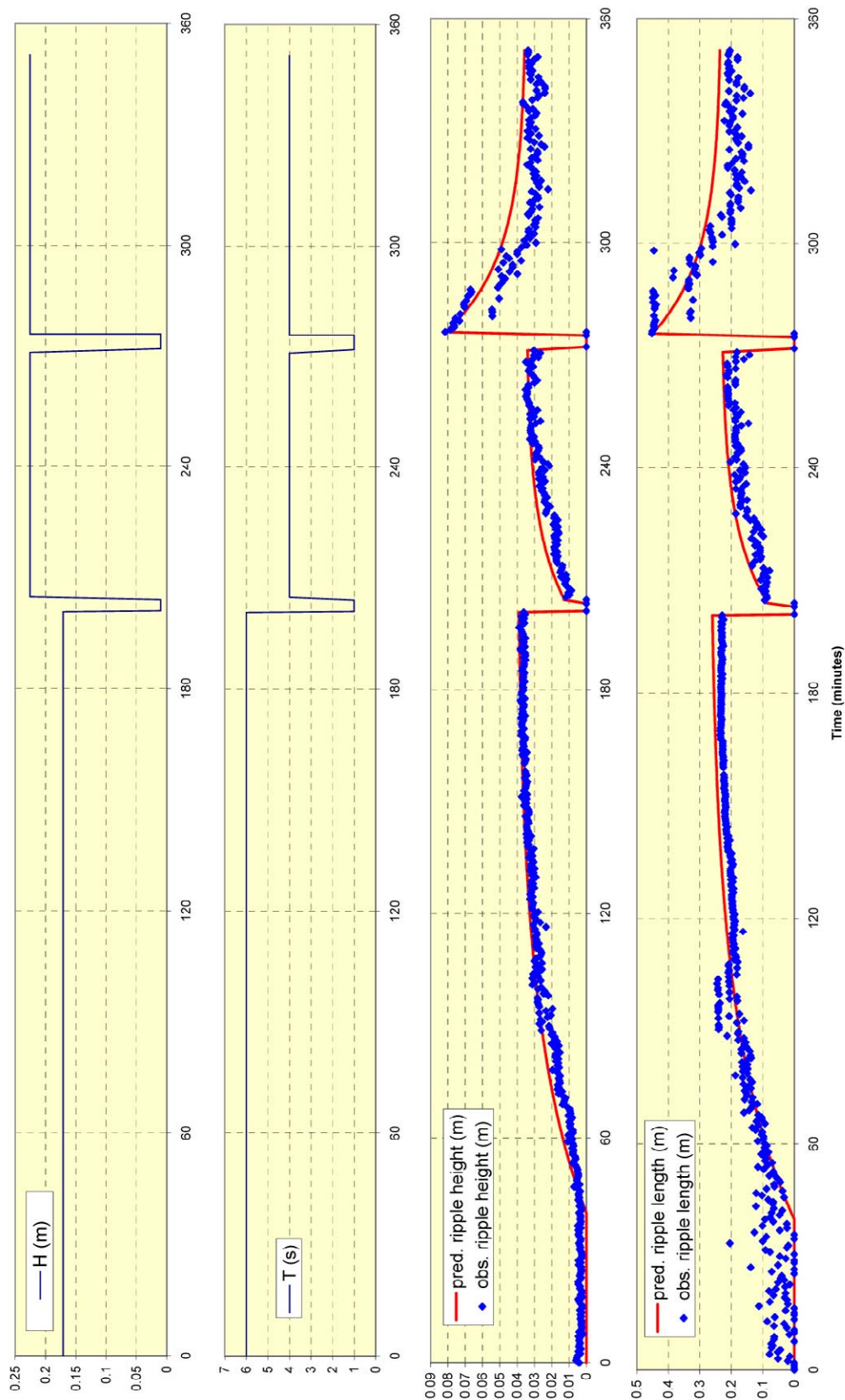


**Figure 14** *Test of wave-ripple predictor against three (non-consecutive) Doucette and O'Donoghue (2005) experiments – slow growth; growth from specified initial height, length; decay from specified height, length*

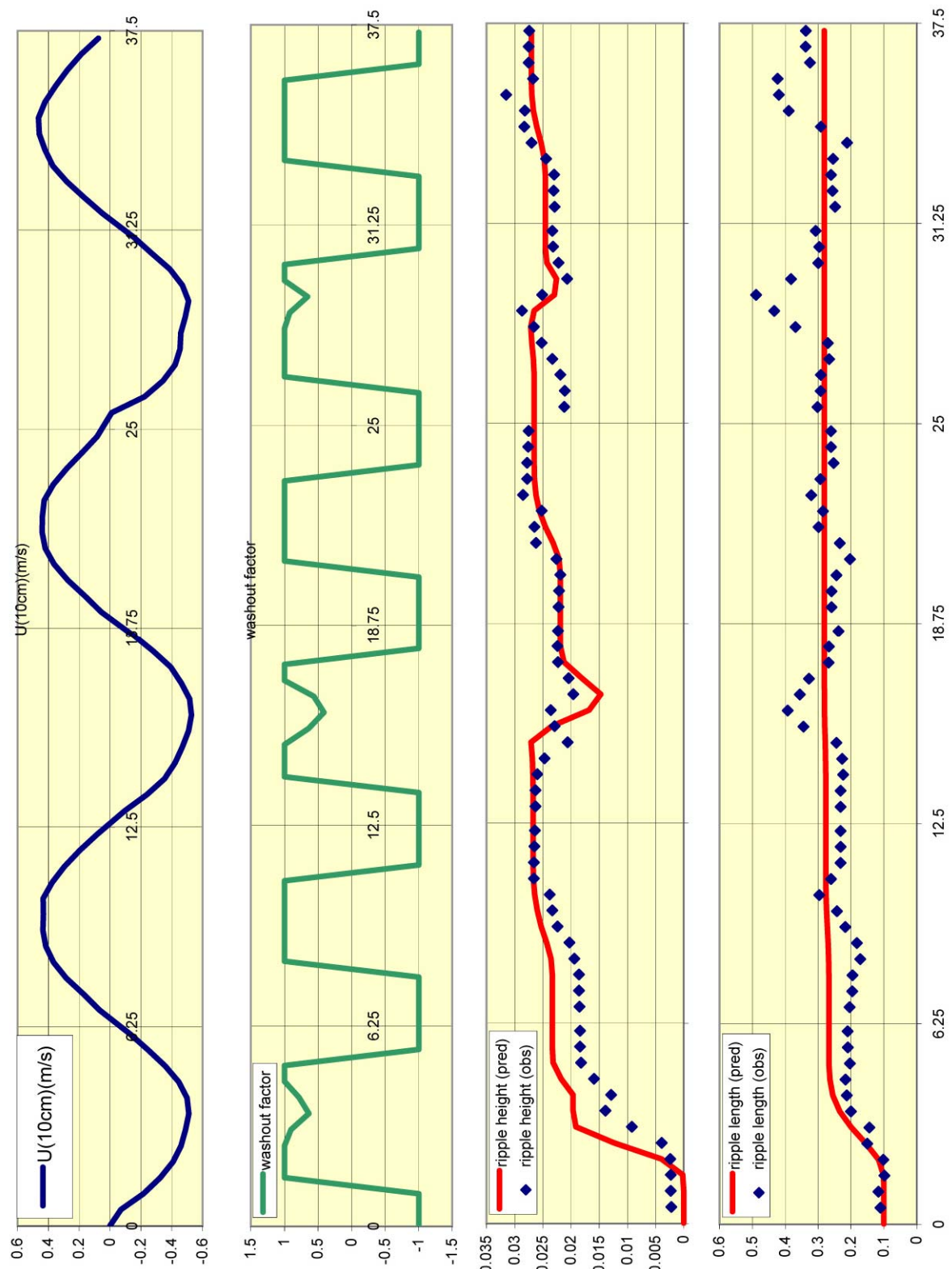


**Figure 15** *Test of current-ripple predictor against Whitehouse et al (1998) reversing-flume tidal experiments*



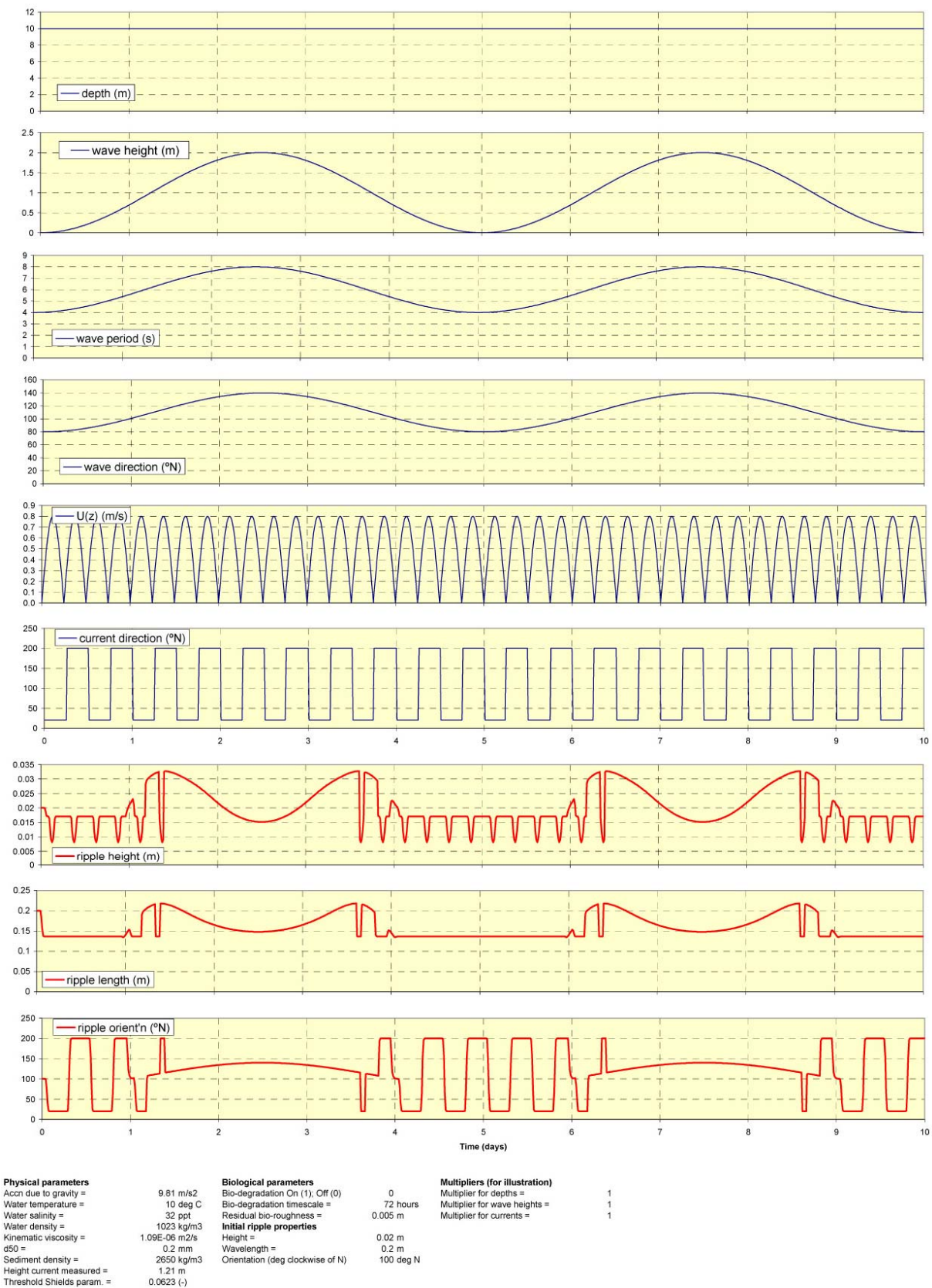
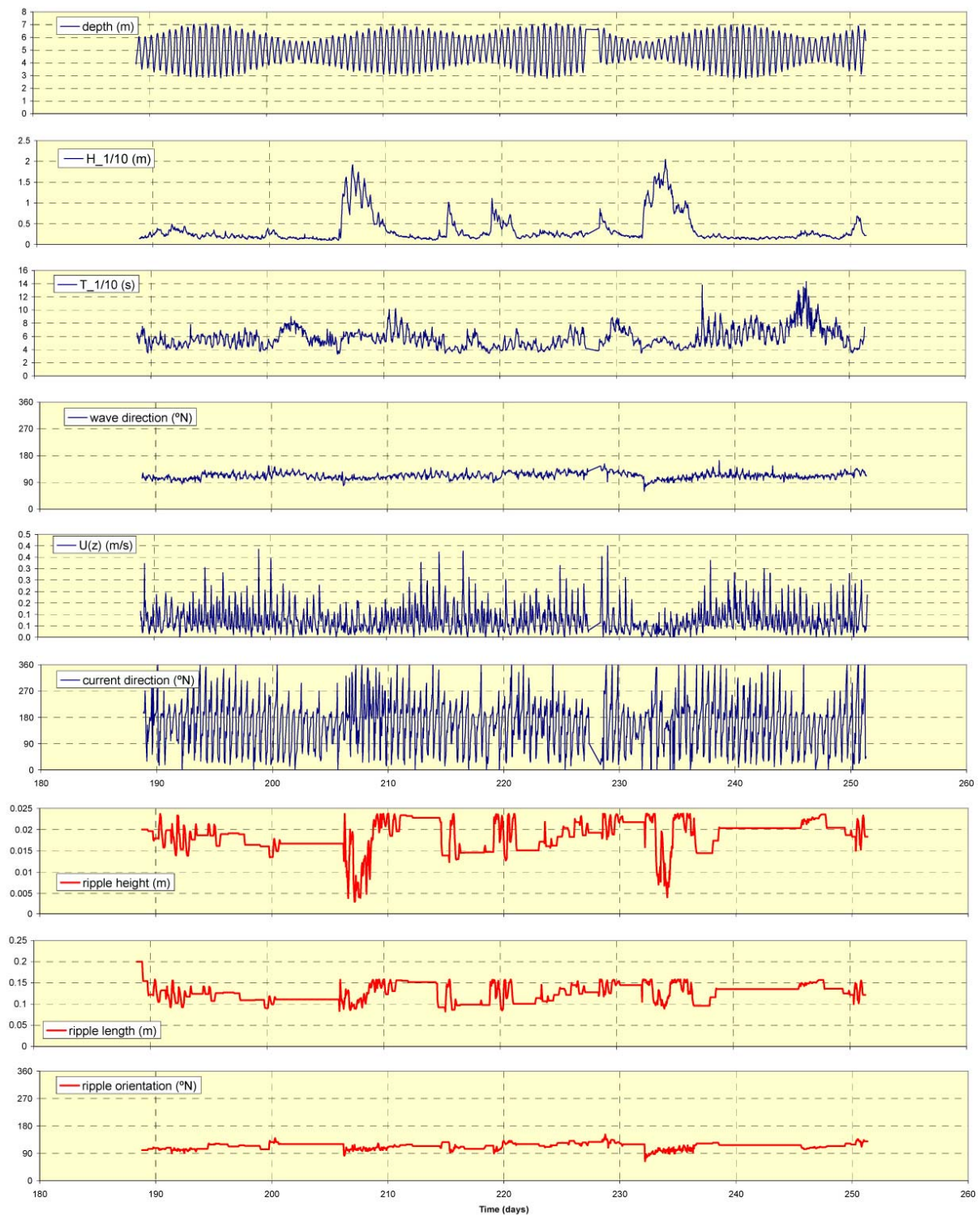


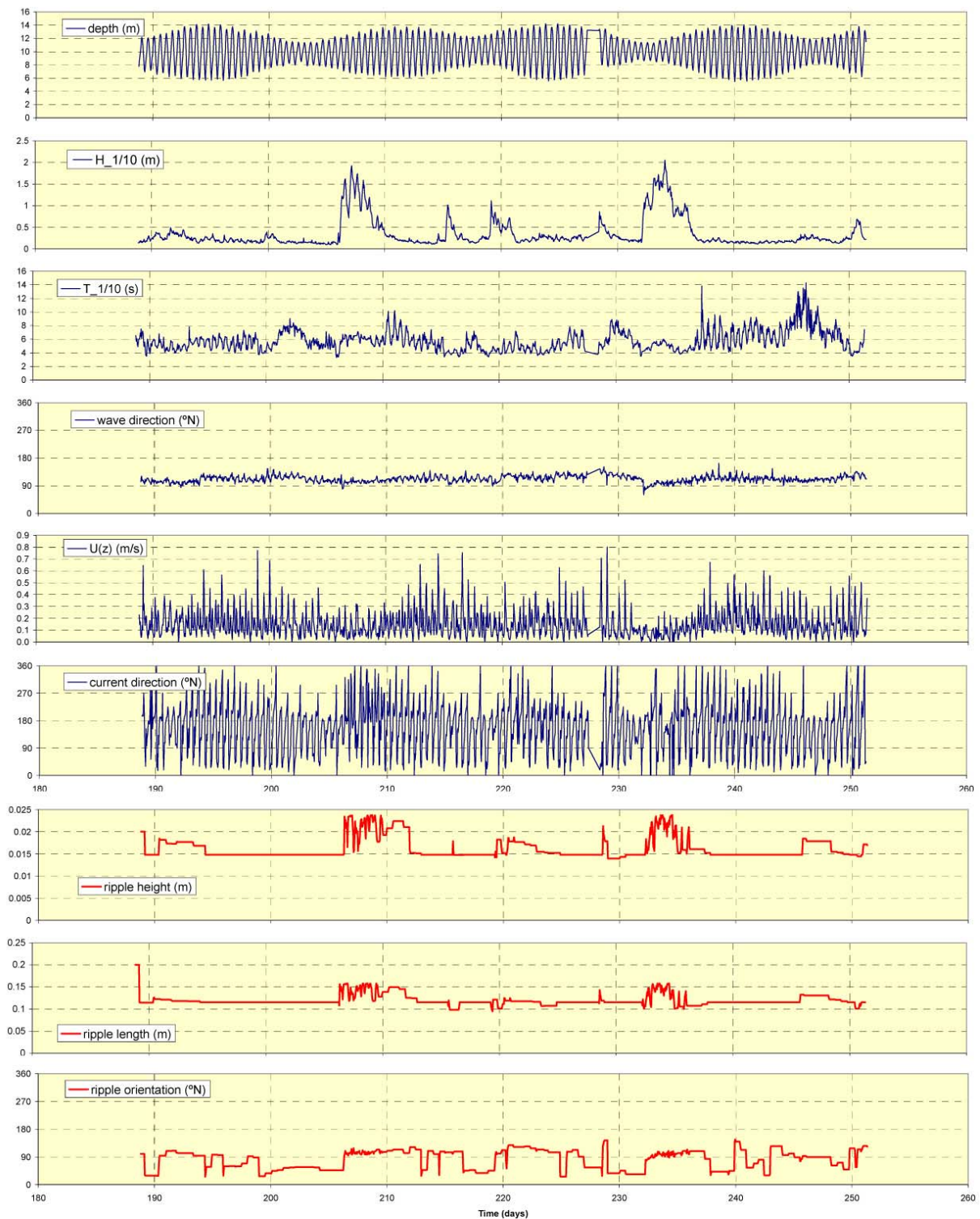
**Figure 16** *Test of wave-plus-current ripple predictor driven by synthetic wave and current data*



Physical parameters		Biological parameters		Multipliers (for illustration)	
Acn due to gravity =	9.81 m/s <sup>2</sup>	Bio-degradation On (1), Off (0)	0	Multiplier for depths =	1
Water temperature =	18.6 deg C	Bio-degradation timescale =	72.13475 hours	Multiplier for wave heights =	1
Water salinity =	32 ppt	Residual bio-roughness =	0.005 m	Multiplier for currents =	1
Water density =	1023 kg/m <sup>3</sup>	<b>Initial ripple properties</b>			
Kinematic viscosity =	1.09E-06 m <sup>2</sup> /s	Height =	0.02 m		
d50 (0.06 - 0.7mm) =	0.145	Wavelength =	0.2 m		
Sediment density =	2650 kg/m <sup>3</sup>	Orientation (deg clockwise of N)	100 deg N		
Height current measured =	1.21 m				
Threshold Shields param. =	0.062295				

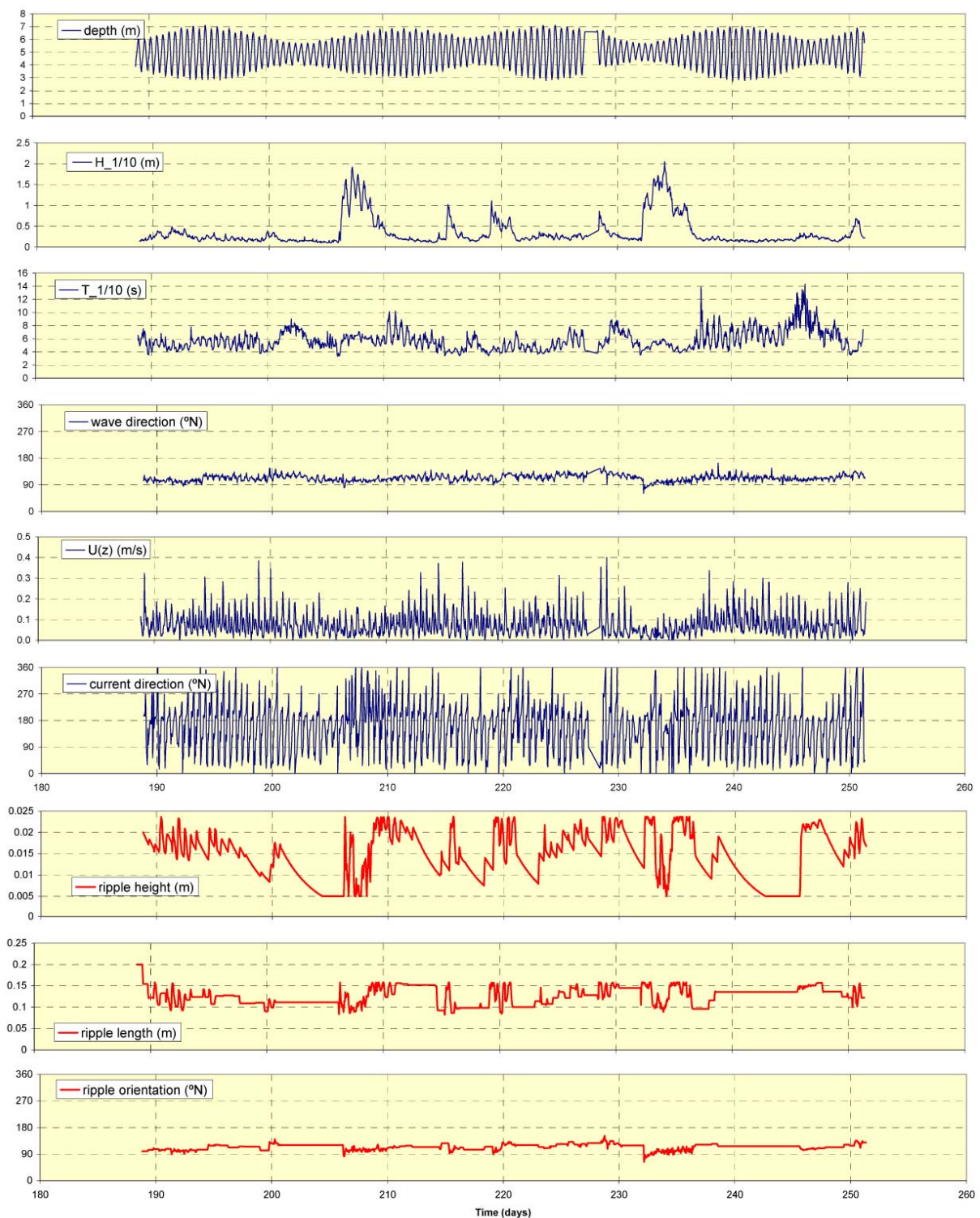
**Figure 17** *Test of wave-plus-current ripple predictor driven by field data from Teignmouth (Whitehouse, 2005)*





Physical parameters		Biological parameters		Multipliers (for illustration)	
Acn due to gravity =	9.81 m/s2	Bio-degradation On (1): Off (0)	0	Multiplier for depths =	2
Water temperature =	18.6 deg C	Bio-degradation timescale =	72.13475 hours	Multiplier for wave heights =	1
Water salinity =	32 ppt	Residual bio-roughness =	0.005 m	Multiplier for currents =	2
Water density =	1023 kg/m3	<b>Initial ripple properties</b>			
Kinematic viscosity =	1.09E-06 m2/s	Height =	0.02 m		
d50 (0.06 - 0.7mm) =	0.145	Wavelength =	0.2 m		
Sediment density =	2650 kg/m3	Orientation (deg clockwise of N)	100 deg N		
Height current measured =	1.21 m				
Threshold Shields param. =	0.062295				

**Figure 18** *Test of wave-plus-current ripple predictor driven by Teignmouth data with doubled depths and doubled current speeds*



Physical parameters		Biological parameters		Multipliers (for illustration)	
Accn due to gravity =	9.81 m/s <sup>2</sup>	Bio-degradation On (1), Off (0)	1	Multiplier for depths =	1
Water temperature =	18.6 deg C	Bio-degradation timescale =	72.13475 hours	Multiplier for wave heights =	1
Water salinity =	32 ppt	Residual bio-roughness =	0.005 m	Multiplier for currents =	1
Water density =	1023 kg/m <sup>3</sup>	<b>Initial ripple properties</b>			
Kinematic viscosity =	1.09E-06 m <sup>2</sup> /s	Height =	0.02 m		
d50 (0.06 - 0.7mm) =	0.145	Wavelength =	0.2 m		
Sediment density =	2650 kg/m <sup>3</sup>	Orientation (deg clockwise of N)	100 deg N		
Height current measured =	1.21 m				
Threshold Shields param. =	0.062295				

**Figure 19** *Test of wave-plus-current ripple predictor driven by Teignmouth data with bio-degradation switched ON*





## *Appendices*



## *Appendix A Algorithm for predicting the time-evolution of ripple height, wavelength and orientation in sandy sea-bed sediments under the influence of waves and currents*

### **A.1 Description of prediction algorithm**

The purpose of the algorithm is to predict: time-varying ripple heights, lengths and orientations, for any sandy sediment, driven by time-series of: water depths, wave heights, periods and directions, and current speeds and directions. It takes account of: evolution (“history”), threshold-of-motion, and wash-out effects, and bio-degradation of ripples. It covers both wave-generated and current-generated ripples, switching between them (in an evolving sense) depending on which forcing is dominant.

### **A.2 Inputs**

#### *Steady inputs*

$d_{50}$  = median grain diameter of sediment (m)  
 $\rho_s$  = density of sediment (= 2650 kg m<sup>-3</sup>)  
 $\rho$  = density of water (kg m<sup>-3</sup>)  
 $\nu$  = kinematic viscosity of water (m<sup>2</sup> s<sup>-1</sup>)  
 $g$  = acceleration due to gravity (= 9.81 m s<sup>-2</sup>)  
 $[z]$  = height above bed of current measurements  
 $Sw_b$  = switch for bio-degradation (= 0 for OFF, = 1 for ON)  
 $T_{1/2,b}$  = half-life for biological ripple height decay (hours)  
 $\eta_b$  = residual bio-roughness (m). (The average “trough to crest” height of biologically induced bed features.)

#### *Time-varying inputs – time-series of:*

$h$  = water depth (m)  
 $U_w$  = amplitude of near-bed wave-induced orbital velocity (ms<sup>-1</sup>)  
 $T$  = wave period (s)  
 $\phi_w$  = direction waves *come from* (degrees clockwise of North)  
 $\bar{U}$  [or  $U(z)$ ] = depth-averaged current speed [or measured value at height  $z$ ] (m s<sup>-1</sup>)  
 $\phi_c$  = direction currents *go towards* (degrees clockwise of North)

$U_w$  and  $T$  are representative of regular, sinusoidal waves. O’Donoghue et al (2005) showed from comparative laboratory tests that in regular, asymmetric waves the best representation for  $U_w$  is given by  $U_{max}$ , the maximum (usually onshore-directed) velocity (under the wave crest), and for irregular, asymmetric or symmetric waves the best representation for  $U_w$  is given by  $U_{1/10}$ , the mean of the highest one-tenth velocities. In irregular waves, the peak-period  $T_p$  gives the best representation of  $T$ .

The wave can alternatively be input as time-series of wave height and period, where (for the above reasons) the best choice is  $H_{1/10}$  and  $T_{1/10}$  (mean height of the highest 1/10 of waves, and their corresponding mean period). In this case, the orbital velocities are calculated from the depths, heights and periods, using linear wave theory or an approximation to it.

The current speeds can either be input as depth-averaged values (assumed in Sections A.4 and A.6 below), or as measurements at a fixed height  $z$  above bed. In the latter

case, a small modification to the algorithm is made (the latter version is implemented in the spreadsheet).

Initial values of the ripple height, wavelength and orientation are needed as inputs.

$\eta_0$  = initial ripple height (m)  
 $\lambda_0$  = initial ripple wavelength (m)  
 $\phi_{r,0}$  = initial ripple orientation (degrees clockwise of North)

In most cases, the choice of initial values will not be important, after an initial transient period. However, in the case of sub-threshold wave and current conditions the initial ripples will remain “frozen”, and in conditions slightly above threshold the values will change only slowly. Typical input values are  $\eta_0 = 0.02\text{m}$ ,  $\lambda_0 = 0.2\text{m}$ ,  $\phi_{r,0}$  = shore-normal direction (wave-dominated) or shore parallel direction (current-dominated).

### A.3 Outputs

*Time-series of:*

$\eta$  = ripple height (m)  
 $\lambda$  = ripple wavelength (m)  
 $\phi_r$  = ripple orientation (degrees clockwise of North)

### A.4 Calculate derived parameters

*Steady parameters*

$s = \rho_s/\rho$  = density ratio (A.1)

$D^* = \left[ \frac{g(s-1)}{v^2} \right]^{1/3} d_{50}$  = dimensionless grain-size (A.2)

Check  $D^*$  is in the range of validity of the algorithm,  $1.2 < D^* < 14$ , (approx  $d_{50}$  in range 0.06mm to 0.7mm). If not, the algorithm is not applicable.

$z_0 = d_{50} / 12$  (A.3)

$\theta_{cr} = 0.3/(1+1.2D^*) + 0.055[1 - \exp(-0.02D^*)]$  = threshold Shields parameter (Soulsby & Whitehouse formula) (A.4)

$T_b = 3600T_{1/2,b}/\ln(2)$  = exponential time-scale for bio-degradation (s) (A.5)

*Time-varying parameters (calculated at each time-step)*

If necessary, calculate  $U_w$  from  $H$  and  $T$  (or  $H_{1/10}$  and  $T_{1/10}$ ) using linear wave theory, or an approximation to it. Then calculate:

$A = U_w T / (2\pi)$  = amplitude of near-bed wave excursion (A.6)

$\Delta = A/d_{50}$  (A.7)

$\Psi = \frac{U_w^2}{g(s-1)d_{50}}$  = wave mobility parameter (A.8)

$f_w$  = grain-related wave friction factor (Swart formula)

$f_w = 0.3$  for  $\Delta \leq 3.93$  (A.9a)

$f_w = 0.00251 \exp [5.21(0.4\Delta)^{-0.19}]$  for  $\Delta > 3.93$  (A.9b)

$$\theta'_w = \frac{\frac{1}{2} f_w U_w^2}{g(s-1)d_{50}} \quad \begin{array}{l} \text{= amplitude of oscillatory skin-friction Shields parameter} \\ \text{due to waves} \end{array} \quad (\text{A.10})$$

$$C_D = \left[ \frac{0.40}{\ln(h/z_0) - 1} \right]^2 \quad \text{= drag coefficient for depth-averaged current} \quad (\text{A.11})$$

$$\theta'_c = \frac{C_D \bar{U}^2}{g(s-1)d_{50}} \quad \text{= skin-friction Shields parameter due to current} \quad (\text{A.12})$$

Or [for currents measured at height z]:

$$C_z = \left[ \frac{0.40}{\ln(z/z_0)} \right]^2 \quad (\text{A.13})$$

$$\theta'_c = \frac{C_z U(z)^2}{g(s-1)d_{50}} \quad (\text{A.14})$$

### **A.5 Calculate equilibrium ripple height, wavelength and orientation due to wave forcing, and rate-of-change parameter $\beta$**

*Time-varying parameters (calculated at each time-step)*

Check if waves are above threshold:

If  $\theta'_w \leq \theta_{cr}$ , ripples take pre-existing values of  $\eta$  and  $\lambda$

If  $\theta'_w > \theta_{cr}$ , equilibrium values of  $\eta$  and  $\lambda$  are given by Eqs (A.15), (A.16) and (A.17).

Calculate equilibrium quantities:

$$\frac{\lambda_{eq}}{A} = \left[ 1 + 1.87 \times 10^{-3} \Delta \left( 1 - \exp \left\{ - \left( 2.0 \times 10^{-4} \Delta \right)^{1.5} \right\} \right) \right]^{-1} \quad (\text{A.15})$$

$$\frac{\eta_{eq}}{\lambda_{eq}} = 0.15 \left[ 1 - \exp \left\{ - \left( 5000 / \Delta \right)^{3.5} \right\} \right] \quad (\text{A.16})$$

$$\frac{\eta_{eq}}{A} = \frac{\lambda_{eq}}{A} \cdot \frac{\eta_{eq}}{\lambda_{eq}} \quad (\text{A.17})$$

$$\phi_{r,eq} = \phi_w \quad (\text{A.18})$$

Calculate rate-of-change parameter:

$$\beta = 2.996 \psi^{1.07} / (21700 + \psi^{1.07}) \quad (\text{A.19})$$

### **A.6 Calculate equilibrium ripple height, wavelength and orientation due to current forcing, together with $\beta_\eta$ and $\beta_\lambda$**

*Time-varying parameters (calculated at each time-step)*

Check if current is above threshold:

If  $\theta'_c \leq \theta_{cr}$ , ripples take pre-existing values of  $\eta$  and  $\lambda$

If  $\theta'_c > \theta_{cr}$ , equilibrium values of  $\eta$  and  $\lambda$  are given by Eqs (A.20) and (A.21).

Calculate:

$$\eta_{\max} = d_{50} \cdot 202 D_*^{-0.554} \quad \text{for } 1.2 < D_* < 14 \quad (\text{A.20})$$

$$\lambda_{\max} = d_{50} (500 + 1881 D_*^{-1.5}) \quad \text{for } 1.2 < D_* < 14 \quad (\text{A.21})$$

$$\theta'_{wo} = 1.66 D_*^{-1.3} \quad \text{for } D_* > 1.58 \quad (\text{A.22})$$

$$\theta'_{sf} = 2.26 D_*^{-1.3} \quad \text{for } D_* > 1.58 \quad (\text{A.23})$$

$$\theta'_{wo} = 0.916 \text{ and } \theta'_{sf} = 1.25 \quad \text{for } D_* \leq 1.58 \quad (\text{A.24})$$

Then calculate equilibrium quantities:

$$\eta_{eq} = \text{pre-existing value} \quad \text{for } 0 \leq \theta'_c \leq \theta_{cr} \quad (\text{A.25})$$

$$\eta_{eq} = \eta_{\max} \quad \text{for } \theta_{cr} < \theta'_c \leq \theta'_{wo} \quad (\text{A.25a})$$

$$\eta_{eq} = \eta_{\max} \left( \frac{\theta'_{sf} - \theta'_c}{\theta'_{sf} - \theta'_{wo}} \right) \quad \text{for } \theta'_{wo} < \theta'_c \leq \theta'_{sf} \quad (\text{A.26})$$

$$\eta_{eq} = 0 \quad \text{for } \theta'_c > \theta'_{sf} \quad (\text{A.27})$$

$$\lambda_{eq} = \lambda_{\max} \quad (\text{A.28})$$

$$\varphi_{r,eq} = \varphi_c \quad (\text{A.29})$$

Calculate rate-of-change parameters:

$$T_c = \frac{\eta_{\max} \lambda_{\max}}{[g(s-1)d_{50}^3]^{1/2}} \quad (\text{A.30})$$

$$\beta_\eta = \frac{20(\theta'_c - \theta_{cr})^{1.5}}{2.5 + (\theta'_c - \theta_{cr})^{1.5}} \quad (\text{A.31})$$

$$\beta_\lambda = \frac{12(\theta'_c - \theta_{cr})^{1.5}}{2.5 + (\theta'_c - \theta_{cr})^{1.5}} \quad (\text{A.32})$$

## A.7 Set values of coefficients of $a_i$ and $b_i$ for time-step $t_i$ , based on wave or current dominance

*Time-varying parameters (calculated at each time-step)*

For ripple height:

- if  $\theta'_w \geq \theta'_c$ , then:

$$a(t) = \frac{\beta}{T} \cdot \eta_{eq} \quad (A.33)$$

$$b(t) = \frac{\beta}{T} + \frac{1}{T_b} \cdot Sw_b \quad (A.34)$$

- but if  $\theta'_c > \theta'_w$ , then:

$$a(t) = \frac{\beta_\eta}{T_c} \cdot \eta_{eq} \quad (A.35)$$

$$b(t) = \frac{\beta_\eta}{T_c} + \frac{1}{T_b} \cdot Sw_b \quad (A.36)$$

For ripple wavelength:

- if  $\theta'_w \geq \theta'_c$ , then:

$$a(t) = \frac{\beta}{T} \cdot \lambda_{eq} \quad (A.37)$$

$$b(t) = \frac{\beta}{T} \quad (A.38)$$

- but if  $\theta'_c > \theta'_w$ , then:

$$a(t) = \frac{\beta_\lambda}{T_c} \cdot \lambda_{eq} \quad (A.39)$$

$$b(t) = \frac{\beta_\lambda}{T_c} \quad (A.40)$$

For ripple orientation:

- if  $\theta'_w \geq \theta'_c$ , then:

$$a(t) = \frac{\beta}{T} \cdot \phi_{eq} \quad (A.41)$$

$$b(t) = \frac{\beta}{T} \quad (A.42)$$

- but if  $\theta'_c > \theta'_w$ , then:

$$a(t) = \frac{\beta_\lambda}{T_c} \cdot \phi_{eq} \quad (A.43)$$

$$b(t) = \frac{\beta_\lambda}{T_c} \quad (A.44)$$

Set  $a_i = a(t_i)$  and  $b_i = b(t_i)$  at the  $i$ 'th time-step.

### A.8 Calculate $x_{i+1}$ using Runge-Kutta integration (with over-ride) for each of ripple height, wavelength and orientation

The general equation to be solved is:

$$\frac{dx}{dt} = a(t) - b(t) \cdot x(t) \quad (\text{A.45})$$

where  $x$  represents either height, wavelength or orientation. The time-varying coefficients  $a(t)$  and  $b(t)$  are given in discrete form by  $a_i = a(t_i)$  and  $b_i = b(t_i)$  at the  $i$ 'th time-step.

Fourth-order Runge-Kutta integration is used to solve Eq (A.45) for each parameter in turn (height, wavelength, orientation) by the following steps:

$$\text{Calculate time-step } \Delta t = t_{i+1} - t_i \text{ (does not have to be constant for all } t_i). \quad (\text{A.46})$$

- If  $(b \cdot \Delta t) < 1.6$ , calculate in turn:

$$k_1 = \Delta t \cdot (a_i - b_i \cdot x_i) \quad (\text{A.47a})$$

$$k_2 = \Delta t \cdot \left( \frac{1}{2} (a_i + a_{i+1}) - \frac{1}{2} (b_i + b_{i+1}) \left( x_i + \frac{1}{2} k_1 \right) \right) \quad (\text{A.47b})$$

$$k_3 = \Delta t \cdot \left( \frac{1}{2} (a_i + a_{i+1}) - \frac{1}{2} (b_i + b_{i+1}) \left( x_i + \frac{1}{2} k_2 \right) \right) \quad (\text{A.47c})$$

$$k_4 = \Delta t \cdot (a_{i+1} - b_{i+1} \cdot (x_i + k_3)) \quad (\text{A.47d})$$

$$k = \frac{1}{6} (k_1 + 2k_2 + 2k_3 + k_4) \quad (\text{A.47e})$$

$$x_{i+1} = x_i + k \quad (\text{A.47f})$$

- But if  $(b \cdot \Delta t) \geq 1.6$ , instead calculate:

$$x_{i+1} = x_i + \left( \frac{a_i}{b_i} - x_i \right) (1 - \exp(-b_i \Delta t)) \quad (\text{A.48})$$

The values of  $x_{i+1}$  correspond to the predicted time-series of (physical) ripple heights  $\eta$ , wavelengths  $\lambda$ , and orientation  $\phi_r$ .

Finally, if  $Sw_b = 1$  (bio-degradation ON), then:

$$\text{height } \eta = \max (\text{physical height } \eta, \text{ biological roughness } \eta_b). \quad (\text{A.49})$$

The predicted wavelengths  $\lambda$ , and orientation  $\phi_r$ , are assumed to be unchanged by the biological activity.



## Appendix B Example input pages to Spreadsheet

### INPUT PARAMETERS

Enter values in yellow cells only	Computed values in green cells	Fixed values in orange cells
<b>Name of study</b>	Teignmouth continuous monitoring Bursts 15500 - 17000	
<b>Pre-set parameters</b>		
Accn due to gravity =	9.81	m/s <sup>2</sup>
Sediment density =	2650	kg/m <sup>3</sup>
<b>Physical parameters</b>		
Water temperature =	18.6	deg C
Water salinity =	32	ppt
Water density =	1023	kg/m <sup>3</sup> (using SandCalc)
Kinematic viscosity =	1.09E-06	m <sup>2</sup> /s (using SandCalc)
d50 (0.06 - 0.7mm) =	0.145	mm
Height current measured =	1.21	m
<b>Biological parameters</b>		
Bio-degradation On (1); Off (0)	0	
Bio-degradation half-life =	50	hours
Residual bio-roughness =	0.005	m
<b>Initial ripple properties</b>		
Height =	0.02	m
Wavelength =	0.2	m
Orientation (deg clockwise of N)	100	deg N
D* =	3.429323279	(-)
g(s-1)d50 =	0.002262293	m <sup>2</sup> /s <sup>2</sup>
[g(s-1)d50 <sup>3</sup> ] <sup>0.5</sup> =	6.89672E-06	m <sup>2</sup> /s
C_D for current at height z	0.001206826	(-)
Threshold Shields param. =	0.062294672	(-) (using SandCalc Soulsby & Whitehouse method)
d50(m) =	0.000145	m
Bio-degradation timescale (s) =	259685.1074	s
Bio-degradation timescale =	72.13475204	hours

**For illustration purposes only**

Set multipliers to 1 for normal use

Multiplier for depths =	1
Multiplier for wave heights =	1
Multiplier for currents =	1



